

DTIC FILE COPY

AFWAL-TR-88-4242

3-DIMENSIONAL RESPONSE OF COMPOSITES

S.R. Soni
S. Chandrashekara
G.P. Tandon
U. Santhosh
Ten-Lu Hsiao

ADTECH SYSTEMS RESEARCH INC.
1342, N. FAIRFIELD ROAD
DAYTON, OHIO 45432



DTIC
SELECTED
JAN 10 1989
S D

JANUARY 1989

FINAL REPORT FOR THE PERIOD 1 JUNE 1985 - 31 MAY 1988

Approved for public release; distribution is unlimited.

MATERIALS LABORATORY
AIR FORCE WRIGHT AERONAUTICAL LABORATORIES
AIR FORCE SYSTEMS COMMAND
WRIGHT-PATTERSON AIR FORCE BASE, OHIO 45433

89 1 10 023

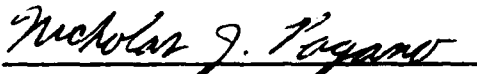
AD-A204 623

NOTICE

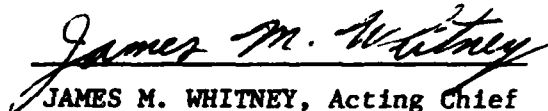
WHEN GOVERNMENT DRAWINGS, SPECIFICATIONS, OR OTHER DATA ARE USED FOR ANY PURPOSE OTHER THAN IN CONNECTION WITH A DEFINITELY GOVERNMENT-RELATED PROCUREMENT, THE UNITED STATES GOVERNMENT INCURS NO RESPONSIBILITY OR ANY OBLIGATION WHATSOEVER. THE FACT THAT THE GOVERNMENT MAY HAVE FORMULATED OR IN ANY WAY SUPPLIED THE SAID DRAWINGS, SPECIFICATIONS, OR OTHER DATA, IS NOT TO BE REGARDED BY IMPLICATION, OR OTHERWISE IN ANY MANNER CONSTRUED, AS LICENSING THE HOLDER, OR ANY OTHER PERSON OR CORPORATION; OR AS CONVEYING ANY RIGHTS OR PERMISSION TO MANUFACTURE, USE, OR SELL ANY PATENTED INVENTION THAT MAY IN ANY WAY BE RELATED THERETO.

THIS REPORT HAS BEEN REVIEWED BY THE OFFICE OF PUBLIC AFFAIRS (ASD/CPA) AND IS RELEASABLE TO THE NATIONAL TECHNICAL INFORMATION SERVICE (NTIS). AT NTIS, IT WILL BE AVAILABLE TO THE GENERAL PUBLIC, INCLUDING FOREIGN NATIONS.

THIS TECHNICAL REPORT HAS BEEN REVIEWED AND IS APPROVED FOR PUBLICATION.



NICHOLAS J. PAGANO, Matls Rsch Engr
Mechanics & Surface Interactions Br
Nonmetallic Materials Division



JAMES M. WHITNEY, Acting Chief
Mechanics & Surface Interactions Br
Nonmetallic Materials Division

FOR THE COMMANDER



MERRILL L. MINGES, Director
Nonmetallic Materials Division

IF YOUR ADDRESS HAS CHANGED, IF YOU WISH TO BE REMOVED FROM OUR MAILING LIST, OR IF THE ADDRESSEE IS NO LONGER EMPLOYED BY YOUR ORGANIZATION PLEASE NOTIFY AFWAL/MLBM, WRIGHT-PATTERSON AFB, OH 45433-6533 TO HELP US MAINTAIN A CURRENT MAILING LIST.

COPIES OF THIS REPORT SHOULD NOT BE RETURNED UNLESS RETURN IS REQUIRED BY SECURITY CONSIDERATIONS, CONTRACTUAL OBLIGATIONS, OR NOTICE ON A SPECIFIC DOCUMENT.

REPORT DOCUMENTATION PAGE				Form Approved OMB No. 0704-0188	
1a. REPORT SECURITY CLASSIFICATION Unclassified			1b. RESTRICTIVE MARKINGS		
2a. SECURITY CLASSIFICATION AUTHORITY			3. DISTRIBUTION/AVAILABILITY OF REPORT		
2b. DECLASSIFICATION/DOWNGRADING SCHEDULE			Approved for public release; distribution is unlimited.		
4. PERFORMING ORGANIZATION REPORT NUMBER(S) N/A			5. MONITORING ORGANIZATION REPORT NUMBER(S) AFWAL-TR-88-4242		
6a. NAME OF PERFORMING ORGANIZATION AdTech Systems Research, Inc.		6b. OFFICE SYMBOL (if applicable)	7a. NAME OF MONITORING ORGANIZATION Air Force Wright Aeronautical Laboratories Materials Laboratory (AFWAL/MLBM)		
6c. ADDRESS (City, State, and ZIP Code) 1342 N. Fairfield Road Dayton OH 45432			7b. ADDRESS (City, State, and ZIP Code) Wright-Patterson AFB OH 45433-6533		
8a. NAME OF FUNDING/SPONSORING ORGANIZATION		8b. OFFICE SYMBOL (if applicable)	9. PROCUREMENT INSTRUMENT IDENTIFICATION NUMBER F33615-85-C-5034		
8c. ADDRESS (City, State, and ZIP Code)			10. SOURCE OF FUNDING NUMBERS		
			PROGRAM ELEMENT NO. 62102F	PROJECT NO. 2419	TASK NO. 01
			WORK UNIT ACCESSION NO. 93		
11. TITLE (Include Security Classification) 3-Dimensional Response of Composites					
12. PERSONAL AUTHOR(S) S. R. Soni, S. Chandrashekara, G. P. Tandon, U. Santhosh, T. Hsiao					
13a. TYPE OF REPORT Final		13b. TIME COVERED FROM 1Jun85 TO 31May88		14. DATE OF REPORT (Year, Month, Day) January 1989	
15. PAGE COUNT 137					
16. SUPPLEMENTARY NOTATION					
17. COSATI CODES			18. SUBJECT TERMS (Continue on reverse if necessary and identify by block number)		
FIELD 11	GROUP 4	SUB-GROUP 1	Analytical Models, Finite Element 3-Dimensional Composite Laminates, Failure Analysis Stress Analysis - T25		
19. ABSTRACT (Continue on reverse if necessary and identify by block number) This report contains analytical models developed for the prediction of three-dimensional response of composites. Two aspects of the problem of stress and failure analysis are considered. One pertains to a macromechanical model in which the development of a global-local finite element method for stress analysis of composite laminates is given. The other aspect incorporates a micromechanics approach leading to a model, termed NDSANDS, for the stress and failure analysis of carbon-carbon composites. Again, the global-local formulation for the laminate stress analysis is numerically solved by two different finite element techniques. The NDSANDS model incorporates the effects of processing by evaluating the residual stresses due to hygrothermal effects. A number of problems has been solved for illustrating the effectiveness of all the above mentioned models. It is believed that these models are of extreme importance in studying the optimum design parameters in structural composites.					
20. DISTRIBUTION/AVAILABILITY OF ABSTRACT <input type="checkbox"/> UNCLASSIFIED/LIMITED <input type="checkbox"/> SAME AS RPT. <input checked="" type="checkbox"/> DTIC USERS				21. ABSTRACT SECURITY CLASSIFICATION UNCLASSIFIED	
22a. NAME OF RESPONSIBLE INDIVIDUAL Nicholas J. Pagano			22b. TELEPHONE (Include Area Code) (513) 255-6762		22c. OFFICE SYMBOL AFWAL/MLBM

FOREWORD

The 3-Dimensional Response of Composites Program (F33615-85-C-5034) was sponsored by the Air Force Wright Aeronautical Laboratories (AFWAL) Materials Laboratory, Wright-Patterson Air Force Base, Ohio 45433. The Air Force Project Engineer was first Dr. J.M. Whitney and later Dr. N.J. Pagano, AFWAL/MLBM.

The program was performed by AdTech Systems Research Inc., Dayton, Ohio. The research was conducted by Drs. S.R. Soni, S. Chandrashekara, G.P. Tandon; Mr. U. Santhosh and Mr. Ten-Lu Hsiao.



Accession For	
NTIS CRA&I	<input checked="checked" type="checkbox"/>
DTIC TAB	<input type="checkbox"/>
Unannounced	<input type="checkbox"/>
Justification	
By	
Distribution /	
Availability Codes	
Dist	Avail. and/or Special
A-1	

TABLE OF CONTENTS

	Page
1. INTRODUCTION	1
1.1 Literature Review	3
1.2 Project Summary	8
2. SOLUTION TO LOCAL MODEL	9
2.1 Direct Solution	10
2.2 Finite Difference Solution	15
3. STIFFNESS FINITE ELEMENT METHOD FOR GLOBAL-LOCAL MODEL	17
3.1 Element Modeling for Global Region	18
3.2 Discretization Procedure for Global Region	23
3.3 Element Modeling for Local Region	29
3.4 Discretization Procedure for Local Region	32
3.5 Surface Integrals involving Local and Global Regions	34
3.6 Numerical Solution Procedures	36
3.7 Results and Discussion	40
4. GLOBAL-LOCAL FINITE ELEMENT METHOD: FRONTAL SOLUTION TECHNIQUE	43
4.1 Local Domain	43
4.2 Global-Local Model	51
4.3 Example Problems and Numerical Results	58
4.4 Summary and Concluding Remarks	63
5. STIFFNESS AND STRENGTH DETERMINATION OF MULTI-ORIENTED, COATED FIBER COMPOSITES	65
5.1 The Composite Model	65
5.2 Model Assumptions and Method of Analysis	66
5.3 Determination of Stress and Displacement Fields	68
5.4 The Composite Response	69
5.5 Initial Failure Criterion	70
5.6 Verification of the Theoretical Model	72
5.7 Summary	76

	<u>Page</u>
5.8 The NDSANDS Program	77
5.9 Numerical Results and Discussion	79
5.10 Illustrative Problem	89
5.11 Concluding Remarks	95
REFERENCES	96
APPENDIX A	100

LIST OF FIGURES

<u>No.</u>	<u>Page</u>
1. Global and Local Regions of Laminate	108
2. Triangular (Area) Coordinates	109
3. Composite Element with Global and Local Layers	110
4. Flow Chart for Stiffness Finite Element Method with Global and Local Layers	111
5. Finite Element Grid Pattern for Square Plate	112
6. Finite Element Grid Pattern for Rectangular Plate	113
7. Convergence Study for Stiffness Finite Element Method	114
8. Laminate Geometry for Free Edge Problem	115
9. Convergence Study of Transverse Displacement for Rectangular Plate	116
10. Convergence Study of Transverse Displacement for Square Plate	117
11. Convergence Study of Normal Stress at Mid-surface for Tensile Load	118
12. Convergence Study of Normal Stress at 0/90 Interface for Tensile Load	119
13. Convergence Study of Shear Stress in z-y Plane at 0/90 Interface for Tensile Load . .	120
14. Convergence Study of Shear Stress in z-x Plane at 0/90 Interface for Tensile Load . .	121
15. Convergence Study of Weighted Displacement across Top Surface for Tensile Load . .	122
16. Convergence Study of Weighted Displacement across Top Surface for Tensile Load . .	123
17. Comparing Normal Stress (Mid-surface) of Different Geometry Parameter for Tensile Load	124

<u>No.</u>	<u>Page</u>
18. Convergence Study of Normal Stress at Mid-surface for Stretch Load	125
19. Convergence Study of Normal Stress at 0/90 Interface for Stretch Load	126
20. Convergence Study of Shear Stress in z-y Plane at 0/90 Interface for Stretch Load . .	127
21. Convergence Study of Shear Stress in z-x Plane at 0/90 Interface for Stretch Load . .	128
22. Convergence Study of Weighted Displacement across Top Surface for Stretch Load . .	129
23. Comparing Normal Stress (at Mid-surface) of Different Geometry Parameter for Stretch Load	130
24. Comparing Normal Stress (at 0/90 Interface) of Different Geometry Parameter for Stretch Load	131
25. Comparing Shear Stress (at 0/90 Interface) of Different Geometry Parameter for Stretch Load	132
26. Theoretical Micro-mechanics Model	133
27. Composite and Equivalent Body Characterization	134
28. Case of Uniaxial Tension	135
29. Four Phase Model	136
30. Flow Chart for Micro-mechanics Calculations	137

LIST OF TABLES

No.		Page
4.1	Rectangular Plate Solution	60
4.2	Square Plate Solution	60
5.1	Comparison of Elastic Moduli	73
5.2	Comparison of Stress Components at The Equator	74
5.3	Comparison of σ_z / σ_0 at Point A within the Coating	75
5.4	Stress Comparison for a Uniform Temperature Change	76
5.5	Property Tables	81
5.6	Three-dimensional 'Isotropic' Composite, Effective Moduli	91
5.7 (a)	Stress Component σ_r in The Fiber-coating and Coating-Matrix Interface at $\Delta T = -1^\circ\text{C}$	92
5.7 (b)	Stress Component σ_θ (algebraic maximum) in the Fiber, Coating and Matrix for $\Delta T = -1^\circ\text{C}$	93
5.7 (c)	Stress Component σ_z in the Fiber, Coating and Matrix for $\Delta T = -1^\circ\text{C}$	94

1. INTRODUCTION

The need to develop a technology base for producing damage tolerant composite materials is viewed as a key issue in obtaining wide acceptance of advanced composites for aircraft and aerospace structural applications. This need is further emphasized by the damage tolerant requirements set forth which must be met with if the material is to be used in primary structures. Research work in recent years has demonstrated that failure processes associated with delamination are of primary concern in structural composite materials. In order to predict the onset of delamination and/or propagation of delamination in complex geometries (e.g. around a crack or circular hole), a three-dimensional stress analysis model is required which can be applied to thick laminates (i.e., laminates containing more than six plies). Although finite element codes based on three-dimensional codes are available, they are very complex, time consuming and costly. In addition, many of these codes are not capable of analyzing thick laminates. The global-local model described in this report has that capability. To date, however, the solutions have been limited to simple straight edges of laminates. In order to fully utilize this approach, numerical procedures are required to solve problems with curved boundaries and sharp discontinuities.

Another key issue in today's composite technology, particularly in the utilization of carbon-carbon composites in exit cone applications, is the processing. There is a history of failures in three-dimensional carbon-carbon exit cones during processing. Such failures are not predictable by current models. Two classes of models are required in the analytical treatment of composite bodies under processing conditions. The first involves the study of transport phenomena. The second is a mechanical model which can examine the stress, strain and displacement fields within the body and forms the basis for failure prediction. Both these models are critical in determining the effect of processing parameters on resulting residual stresses and developing failure criteria.

In this report, a description of research efforts towards the objective of developing three-dimensional models capable of describing the behavior of thick laminated composites as well as

the residual stresses in carbon-carbon composites, is given. On a broader level, both macro- and micro-mechanics approaches have been considered. The macro-mechanics approach deals with the problem of stress analysis in composite laminates under different loading conditions with various types of boundary conditions (including complex ones such as stress-free edges). The solutions to these problems are attempted by using numerical techniques such as finite difference and finite element methods. The micro-mechanics approach deals with the determination of effective thermoelastic properties and the stress distribution under three-dimensional mechanical and/or hygrothermal loading.

The macro-mechanics study in this report includes an analytical procedure leading to a qualitative understanding of the nature of stress field near the regions of steep stress gradients. One aspect of this study is the free edge problem in a multi-layered composite laminate. The potentially high stress gradients near the free edges may limit the load carrying capability of the structure. It may also become a source of laminate failure. The presence of complex stress fields near the free edges of laminates has been established experimentally. However, the analytical investigation of the nature and magnitude of the free edge stresses by various researchers has lead to disparate conclusions. As an extension, a reliable analytical procedure for solving the free edge problem may also lead to an understanding of the various failure modes that have been shown to occur in composite laminates [1,2,3,4]. Also, in practical applications of composite materials, a large number of anisotropic layers are usually present. Consequently, an exact, three-dimensional analysis of such a laminate becomes extremely complicated. The references mentioned before indicate the importance of defining the stress fields in various layers of multi-layered laminate. Hence it becomes important to establish an analytical procedure to consider all these aspects of laminate behavior. In order to obtain an understanding regarding the procedures that are available for solving free edge problems of laminates, a brief review of literature pertaining to general laminate stress analysis is given.

The basis for the micro-mechanics study in this report is the fact that the mechanical properties of a fiber-reinforced material, including the failure modes and mechanisms, are governed

in part by the transfer of stress between fiber and the matrix. This transfer occurs across the interface between the components, and the properties of this interface, therefore, will affect the properties of the composite. For example the strength of the interface in tension has a direct bearing on the composite transverse and compressive strengths and delamination parallel to the fibers; whereas, the interface shear strength principally affects the load transfer length; composite fracture under conditions of fiber pullout and the deformation of the matrix. Recently, there has been an increasing use of coated fibers as a reinforcement in some new application areas such as carbon-carbon composites, electric composites, metal-matrix composites or ceramic composites intended for high temperature applications. The coating applied on the fiber serves to enhance the electrical conductivity, or the elastic stiffness or strength, or simply to serve as a chemical reaction barrier. From this point of view, it is essential to understand the interaction between the coating, fiber and matrix in order to arrive at conclusions regarding the nature of stress distribution and the consequent failure mechanisms under mechanical and hygrothermal loads. This report includes a model to study this aspect of composite behavior.

1.1 LITERATURE REVIEW

There exist in literature approximate theories for achieving reasonably accurate laminate stress analysis. The most popular of these is the classical laminate theory which is an extension of the well-known classical plate theory. This procedure [5], which included the bending-stretching coupling, later incorporated laminate shear deformation thus resulting in a generalized Reissner-Mindlin plate theory [6]. In these theories, the laminate was assumed to be in a state of plane stress. The assumptions involved in these theories were found to be too restrictive for general application [7,8]. They lead to inaccurate prediction of interlaminar stresses at the free edges, although they yield reasonably accurate results for regions away from the free edges. A higher order plate theory [9] in which the displacements no longer vary linearly, was applied [10] to evaluate the interlaminar normal stress distribution in a free edge boundary value problem, but only on a plane of symmetry. In the above mentioned theories, a displacement field is generally assumed that is continuous across the entire thickness of the laminate. This, however, does not guarantee continuity

of tractions at the interfaces between layers. Also, the traction boundary conditions for these approaches are, in general, shown to be insufficient to guarantee the equilibrium of edge boundary subregions [10].

The study of delamination phenomenon in structural composite laminates began with analytical and experimental observations of the response of such bodies in the vicinity of a free edge. In 1967, Hayashi [11] presented the first analytical model treating interlaminar stresses in what has come to be known as the "free edge problem". Characteristically, this work focused on the computation of interlaminar shear stress, as in the early stages of composite research interlaminar and delamination effects were viewed as being synonymous with interlaminar shear. The presence of interlaminar normal stress, being of a more subtle origin and also seemingly defying common intuition, was not appreciated until many years after the pioneering work of Hayashi. The development of the Hayashi model was based upon the implicit assumption that the in-plane stresses within a given layer did not depend upon the thickness coordinate. The magnitude of the maximum interlaminar shear stress was calculated to be a relatively large value in a glass epoxy $[0/90]_s$ laminate. Unfortunately, however, owing to the omission of the interlaminar normal stress, the computed stress field within each layer does not satisfy moment equilibrium.

The first reported experimental observations involving free edge delamination were made by Foye and Baker [12]. In that work, tremendous differences in fatigue life of boron-epoxy composite laminates as a function of layer stacking sequence were reported. Severe delaminations were witnessed in that work and were identified as the primary source of strength degradation in fatigue.

With regard to free edge problems, a finite width laminate under uniform extensional strain was first analyzed by Pipes and Pagano [13]. A finite difference scheme was used based on a formulation assuming isotropic elasticity. Subsequently, various authors have conducted investigations on this problem by using various techniques such as finite difference, finite element and series solutions. References [2, 3, 4, 14] lead to an understanding of various failure modes that

have been shown to occur in composite laminates. The bending and stretching of laminate deformation and Reissner-Mindlin plate theory have been incorporated [5, 6] and higher order classical laminate theory [9, 10] was applied to evaluate the interlaminar normal stress distribution, but only at a plane of symmetry. When a large number of layers is present in the laminate construction, contemporary models are incapable of providing precise solution of the local stress fields in the vicinity of free edge. In an effective moduli global model [14], only the extensional response of the regions was conducted, i.e. the flexural and flexural-extension coupling characteristics of laminated bodies were ignored. A global representation of a three dimensional laminate model [15] is a generalization and improvement of the material model given in reference 14. In the literature on the finite element solutions [14, 16], the traction free edge conditions are satisfied in weighted integrated sense or lead to oscillating solutions near the edges. Singular hybrid stress finite element models are also employed [17, 18, 19]. The free edge stresses in layered plates have also been evaluated by using eight nodes isoparametric elements [20]. It was shown [19, 20] that the laminate idealization for a reasonably accurate finite element analysis had to be very fine, i.e. a quarter of the laminate was divided into about 600 elements. No more than six layers would be considered for numerical calculations. For moderately large number of plies, these approaches will lead to computer storage/economic difficulties. In other studies a singular hybrid finite element model [21] is employed. The finite difference method reported [13] leads to difficulties in calculating transverse shear stresses at the free edges. More recently, a three-dimensional finite difference scheme has also been developed [22]. In addition, a perturbation technique [23] and a series solution [24] have also been presented for obtaining the solution to the free edge problem.

In order to circumvent the complexity of an exact three dimensional elastic analysis, while at the same time being a reasonably precise method of studying the stress fields in laminate with moderately large number of layers, a unified tractable model for the elastic response of the individual plies of the laminate has been introduced [24]. But this model, termed the local model, in which each layer is represented as a homogeneous, anisotropic continuum, becomes intractable as the number of layers becomes large. To overcome this difficulty, the local model has been recently extended into a formulation of global-local variational model [25]. In this model, a predetermined

area, termed local region, of interest is represented by Reissner's functional that involves both stresses and displacements. In this local model, the interface continuity, including three displacement components and the normal and shear stress components associated with the thickness direction are satisfied. For a large number of layers (exceeding 6), the exponential parameter becomes very large and consequently causes computer overflow.

On the other hand, for the rest of the region other than the local region, termed global region, the principle of potential energy is applied following an assumed, elementary displacement field and a consideration of effective or smeared laminate moduli. While the local model employs the theory presented in [24], the global model is based on higher order laminate theory given in [9]. The present report addresses the problem encountered by the previous methods of reasonably accurate analysis of composite laminates [26]. In references 25 and 26, a class of boundary value problems with free edges has been solved and the results are presented. This numerical problem pertains to the case of a laminate of finite width, similar to that of the case of plane strain, in which the stresses depend only on the width and thickness coordinates. The laminate is subjected to a uniform axial strain in the length direction. The solution was sought in the form of an exponential series for the field variables. It was found [25] that for a large number of layers, the exponential parameter becomes very large with a consequent exceeding of the computer limits. In other words, the number of layers in the laminate had to be restricted. The largest number of layers that could be considered by this numerical solution technique was 6.

This report describes some attempts at alternative solution techniques to circumvent the above mentioned difficulty. One of the techniques is based on the use of an available computer library subroutine to solve a set of linear differential equations with an appropriate number of boundary conditions. Yet another method involves the finite difference modeling of the one-dimensional problem mentioned before. All these methods are applicable to the local model only when each layer of the laminate is considered individually with regard to the satisfaction of the layer equilibrium and the interlayer continuity conditions. All these are satisfied exactly once the set of in-plane stress components are assumed and Reissner's variational functional invoked.

The present report also describes a numerical method of analysis which is applicable to the global-local model of the laminate. This method involves a discretization process using finite element technique. A current research literature survey was conducted with particular reference to the finite element models based on mixed variational principles (Reissner's principle, in this case). The purpose of this literature review was to establish the guidelines for the application of present finite element technique to the global-local model of the laminate.

It has been established that the failure mechanisms and the mechanical properties of fiber-reinforced composites are controlled in part by the transfer of stress between the fiber and the matrix [27]. For theoretical analysis (a micro-mechanics approach), the interphase region between the fiber and the matrix can be modeled as a coating [28]. A single fiber test [29] has frequently been used to characterize the fiber-matrix interface (or rather 'interphase' since the region adjacent to the fiber has its unique properties). Quite often, the interphase region is a product of the processing conditions involved in the manufacture of the composite.

In the case of continuous fiber composite, a number of works [30 -34] have been made to compute the stress field in a composite subjected to thermo-mechanical loadings, or to predict its stiffness. The model used in the above works is either a two-phase model consisting of inner cylinder with fiber properties and an outer cylinder with the properties of the matrix, or a three-phase model in which one more cylinder is added to the outside of the two-phase model with the composite properties. Recently, Mikata and Taya [35] have studied the stress field in a coated continuous fiber composite which requires a four-phase model that consists of fiber, coating, matrix and surrounding composite body. The material properties of the surrounding body (composite) were obtained by using a rule of mixtures. The solution to the stress distribution was determined with the composite subjected to three independent boundary conditions, namely, axisymmetric temperature change, uniaxial applied stress and biaxial applied stress.

1.2 PROJECT SUMMARY

This report contains analytical models developed for the prediction of three-dimensional response of composites. Two aspects of the problem of stress and failure analysis are considered. One pertains to a macromechanical model in which the development of a global-local finite element method for stress analysis of composite laminates is given. The other aspect incorporates a micro-mechanics approach leading to a model, termed NDSANDS, for the stress and failure analysis of carbon-carbon composites. Again, the global-local formulation for the laminate stress analysis is numerically solved by two different finite element techniques. The NDSANDS model incorporates the effects of processing by evaluating the residual stresses due to hygrothermal effects. A number of problems has been solved for illustrating the effectiveness of all the above mentioned models. It is believed that these models are of extreme importance in studying the optimum design parameters in structural composites.

2. SOLUTION TO LOCAL MODEL

This section refers to the attempts for obtaining solution to the local model [24]. Specifically, the first part of this section deals with an attempt to obtain a direct solution by using a library subroutine to solve a set of linear equations. The second part refers to a one-dimensional finite difference scheme to solve the problem of an infinitely long laminate subjected to uniform axial strain. As mentioned in the previous section, the exponential series solution to the field equations for the local model of the laminate encountered difficulties when implemented on the computer. This has been reported in reference 26 where a class of boundary value problems with free edges has been solved and the results presented. This numerical problem pertains to the case of a laminate of finite width, similar to that of the case of plane strain, in which the stresses depend only on the width coordinate y and the thickness coordinate z . The laminate is subjected to a uniform axial strain in the x -direction. The solution was sought in the form of an exponential series as

$$f^k = F^k e^{\lambda y} \quad (2.1)$$

where f^k represents the dependent variables for the k th layer and F^k denotes the coefficients for the corresponding layer. After substituting eq. (2.1) into the appropriate field equations obtained from theoretical developments for the local model [24] the values of λ were obtained by setting the determinant of the coefficients to zero. It was found [24] that for a large number of layers, λ became so very large as to exceed the computer limits. In other words, the number of layers in the laminate had to be restricted. The largest number of layers that could be considered by this numerical solution technique was six. The present section discusses an alternative mathematical approach to the solution to circumvent the above mentioned difficulty. This method involves the use of an available computer library subroutine to solve a set of linear differential equations.

2.1 DIRECT SOLUTION

One of the alternative solution procedures (direct solution) considered makes use of an IMSL subroutine, DVCPR, to solve a set of equations. The purpose of this subroutine is to solve a system of ordinary differential equations with boundary conditions defined at two points. The particular subroutine DVCPR, for example, is based on a variable step size finite difference method. The fundamental idea was to cast the set of second order linear differential equations governing the behavior of each layer of the laminate into a set of single order equations. This process would result in a set of additional equations and all the equations could then be solved simultaneously by using the computer subroutine.

The variables in the set of governing equations are the weighted displacement functions and the interlaminar stress components. For any layer, these are $U, V, W, \Omega, \psi, \chi, \phi, p_1, p_2, s_1, s_2, t_1, t_2$ where the first six refer to the weighted displacement functions and the three pairs of the last six refer to the interlaminar stresses associated with the thickness direction. The numerical problem for solution consists of a finite width laminate subjected to a uniform axial strain $\epsilon_x = \epsilon$. By virtue of the geometry, the stress components and the displacements depend only on y and z coordinates. Consequently, all the derivatives in the governing equations are with respect to y only, thus reducing the solution procedure to that of a one-dimensional problem. It can be seen from equations (6) through (9) of reference 26 that there exist single order derivatives in the interlayer continuity conditions and the boundary conditions on the upper and lower surfaces. However, in the layer equilibrium equations (5) of reference 26, the highest order of derivative is 2. Hence, a new set of variables was first written as, for example,

$$\begin{aligned}\bar{U} &= U' \\ \bar{V} &= V' \text{ etc.}\end{aligned}\tag{2.1.1}$$

where prime refers to differentiation with respect to y . The new variables with bars on them were

also considered as unknowns in further formulation. Thus, the layer equilibrium equations were written as single order differential equations in terms of variables U, U etc.

In accordance with the requirements of the computer subroutine, the next step was to derive a set of equations of the form:

$$(U^k)' = f(U^k, V^k, W^k, \Omega^k, \psi^k, \chi^k, \phi^k, \bar{U}^k, \bar{V}^k, \bar{W}^k, \bar{\Omega}^k, \bar{\psi}^k, \bar{\chi}^k, \bar{\phi}^k, p_1^k, p_2^k, s_1^k, s_2^k, t_1^k, t_2^k) \quad (2.2)$$

where superscript k refers to the layer.

It is to be noted that the right hand side function in (2.2) does not contain any derivative. Similar equations can be written for each of the dependent variable appearing with function parantheses in the above equation. It was found during the course of such a procedure that one of the weighted displacement functions, viz., ϕ could be eliminated by using the lower surface condition (for obtaining ϕ^1) and a judicious combination of intersurface continuity conditions and the particular layer equilibrium equation that involves ϕ^k (for obtaining ϕ^k , $k > 1$). Thus, only six of the seven layer equilibrium equations needed to be considered for final solution. The ϕ^k 's obtained in this manner were used elsewhere.

Also, two more sets of equations were obtained, one by equating the expression for $(\phi^k)'$ from the interlayer continuity conditions between layers k and $k-1$ and the other from one interlayer continuity condition between k and $k-1$ and a layer equilibrium equation involving ϕ^k . Hence, a set of linear simultaneous equations was obtained for derivative functions $(U^k)', (V^k)', (U^k)', (V^k)',$ etc. in terms of the variables $U^k, V^k, U^k, V^k,$ etc. These functions could be easily established by means of a simple simultaneous equation solver on the computer. The IMSL library subroutine DVCPR, was thus utilized for obtaining the solution for $\bar{U}^k, \bar{V}^k,$ etc.

At this juncture, it is important to note how the boundary conditions at the free edge were

used in the solution procedure. Again the weighted displacement parameter ϕ was eliminated from the appropriate expressions (the expressions for N_y and N_{xy} in this case). This was done by obtaining one equation (for each layer) by considering simultaneously N_y and N_{xy} at $y = +b$ and again at $y = -b$. The final boundary equations obtained by setting $y = \pm b$ in various expressions such as V_y , M_y , M_{xy} , etc. contained the weighted displacement parameters and the interlaminar stress components specified at the edges $y = \pm b$.

Finally, there were $(9N-2)$ equations obtained by the layer equilibrium equations and intersurface continuity and top and bottom surface conditions. To these were added $6N$ equations of the type (2.1), thus adding to $(15N-2)$ equations. The unknown parameters were given as follows:

$$\begin{array}{ll}
 t^1 = s^1 = 0 ; \quad p_2^N = s_2^N = t_2^N = 0 \quad s_i \text{ and } t_i \dots & 2(N-1) \\
 U, V, W, \Omega, \psi, \chi & \dots \dots \dots 6N \\
 \bar{U}, \bar{V}, \bar{W}, \bar{\Omega}, \bar{\psi}, \bar{\chi} & \dots \dots \dots 6N \\
 p_i & \dots \dots \dots (N-1) + 1 \\
 \text{Total} & \dots \dots \dots (15N-2)
 \end{array} \tag{2.3}$$

In using the library subroutine, $(15N-2)$ single order linear differential equations were considered for solution. The number of boundary conditions are listed as follows:

$$\begin{array}{ll}
 V_y^k (\pm b) = 0 \\
 M_y^k (\pm b) = 0 & \dots \dots \dots k = 1, 2, 3, \dots, N \\
 M_{xy}^k (\pm b) = 0 \\
 s_2^k (\pm b) = 0 & \dots \dots k = 1, 2, 3, \dots, N-1 \\
 \text{combination of equations for } N_y^k \text{ and } N_{xy}^k \text{ at } \pm b & \dots \dots k = 1, 2, 3, \dots, N \\
 \text{equations of type } U^k - \bar{U}^k = 0 & \dots \dots k = 1, 2, 3, \dots, N \\
 & \dots \dots \dots (2.4)
 \end{array}$$

Thus, the total number of boundary conditions is $(15N-2)$.

In this method of solution however, two main difficulties were encountered:

- (i) The reduction of the number of equations to be solved by elimination made the method very complicated to code,
- (ii) The Gauss-Jordan computer subroutine that reduced the first order equations to the form given in (2.2) to be used later on in the differential equation solver DVCPR encountered problems of singularity.

Thus it was decided not to eliminate ϕ , but instead to retain the original set of equations because the effect of reducing the number of equations to be solved by eliminating ϕ was not found to be significant enough to offset the additional coding involved. The cause for the singularity arising in the computer subroutine was traced to be due to the coupling of the displacement parameters W^k and χ^k in the layer equilibrium equation 6 of reference 26. This necessitated the introduction of another variable

$$H^k = \bar{W}^k - \bar{\chi}^k = W^k - \chi^k \quad (2.5)$$

This substitution had an additional advantage of reducing the number of variables to be solved for in each layer by one. After carrying out the above substitution and judiciously manipulating the equations, a non-singular system of equations was obtained that could subsequently be reduced to the form illustrated by equation (2.2), using a Gauss-Jordan elimination algorithm.

If the interlaminar equations

$$\begin{aligned} p_2^k &= p_1^{k+1} \\ s_2^k &= s_1^{k+1} \quad \text{and} \\ t_2^k &= t_1^{k+1} \end{aligned} \quad (2.6)$$

were incorporated into the layer equilibrium equations and the interlaminar continuity conditions, then the number of unknowns in each layer could be reduced to 15, viz., $U, V, W, \Omega, \psi, \chi, \phi, \bar{U}, \bar{V}, H, \bar{\Omega}, \bar{\psi}, p_1, s_1$ and t_1 . Additionally there were three extra variables p_2^N, s_2^N and t_2^N in layer N (at the free surface of the laminate). Since the laminate was unstressed at its surface

$$p_2^N = s_2^N = t_2^N = 0 \quad (2.7)$$

Furthermore, in the first layer, due to the symmetry of the layer about the midplane

$$s_1^1 = t_1^1 = 0 \quad (2.8)$$

Hence the total number of variables to be solved for as well as the number of equations became $(15N-2)$.

The library subroutine DVCPR required that there be the same number of boundary conditions as the number of equations. These $(15N-2)$ boundary conditions were taken as

$$\begin{aligned} V_y^k(\pm b) &= M_y^k(\pm b) = M_{xy}^k(\pm b) = 0 \quad \dots k = 1, 2, \dots N \\ N_y^k(+b) - N_y^k(-b) &= 0 \\ N_{xy}^k(+b) - N_{xy}^k(-b) &= 0 \quad \dots k = 1, 2, 3, \dots N-1 \\ N_y^k(+b) &= N_{xy}^k(+b) = 0 \\ s_2^k(\pm b) &= 0 \quad \dots k = 1, 2, 3, \dots N \\ \text{and equations of type } U^{k'} - \bar{U}^k &= 0 \quad \dots k = 1, 2, 3, \dots N \end{aligned} \quad (2.9)$$

The above system of first order differential equations and boundary conditions could finally be solved by the previously mentioned library subroutine.

Even in this method, some difficulties were encountered due to the fact that some of the layer equilibrium equations and the interlaminar continuity conditions had to be differentiated in order to achieve a form similar to the one shown by equation (2.1.2). In doing so the original problem is weakened since the order of some of the equations is increased.

Hence in order to preserve the nature of the original problem and to avoid singularity situation, it was decided to construct a finite difference model for the problem.

2.2 FINITE DIFFERENCE SOLUTION

Since the free edge problem had been reduced to essentially a one-dimensional problem (in the width dimension y) [26], the finite difference model was based on formulas for the first and second derivatives derived from the quadratic Lagrange polynomials in one variable. Since these formulas are of order two, the errors vary as the square of the step size.

For the problem on hand, variable step size was chosen over fixed step size. This was done because the computations could then be made more efficient by making the step size at regions of high stress gradients very small and choosing step sizes for other regions according to the desired accuracy of the results desired. Furthermore, the need for fictitious nodes adjacent to but outside the boundaries are eliminated. This was accomplished by using forward and backward difference formulas at the left and right boundaries respectively. At all interior nodes central difference formula was used.

Finite difference solutions to similar problems have been given while studying the elastic response of involute bodies [27,28]. These methods are direct methods used to solve the resulting set of finite difference equations. Since the number of these equations was quite large, the limits of available computer memory was attained even while solving relatively small size problems. In order to reduce the storage burden on the computers and to make the calculations more efficient, the iterative Gauss-Siedel method was used in the current solution technique to solve the finite difference equations. Another attractive feature of using the iterative method was that by reducing the memory requirement of this procedure the maximum problem size could be increased. However, this method failed to yield good results.

The difficulty seems to be in the fact that the way the original problem is presented, the number of boundary conditions is less than the number of field equations available for solution. It has been found [27, 28] that this leads to inconsistencies in standard numerical methods. Thus

some of the field equations that normally are satisfied at all interior nodes may be enforced at the boundaries so that they supplement the boundary conditions. This has been shown in the above mentioned references to yield satisfactory results.

3. STIFFNESS FINITE ELEMENT METHOD FOR GLOBAL-LOCAL MODEL

The global-local variational approach has already been numerically solved by an exponential series solution [25] with limited success. One global-local interface had been considered in that procedure. In the present section, a discretization procedure using finite element method of solving the laminate problem is given based on the same global-local approach. In general, instead of considering the first variation of the energy functional representing the laminate, the stresses and displacements are written in terms of the nodal degrees of freedom of an element of chosen shape. The solution to the problem is then sought by making the functional stationary with respect to each of the nodal degrees of freedom. At first, a current literature survey was conducted pertaining to the finite element models based on mixed variational principles (Reissner's principle, in this case). The purpose of this literature review was to establish the guidelines for the application of the present finite element technique to the global-local model of the laminate. The variational functional for the entire laminate consists of two distinct energy functionals - one, a total potential energy functional characterizing the global region and the other, a Reissner variational functional for a predetermined local region of interest (figure 1). The finite element discretization based on these variational principles is individually well documented [38, 39, 40, 41]. The potential energy principle is very commonly used as the basis for a displacement -based compatible finite element model. The Reissner variational principle is intrinsically multifield in which the primary field variables characterizing the element behavior are both stresses and displacements.

Following the theoretical development for the global-local model, the variational functional for the entire laminate is written to represent both the global region and N layers of the local region as follows:

$$\pi = \int_{V_g} W_p(u_i, e_{ij}) dv + \sum_{k=1}^N \int_{V_k} [1/2 \sigma_{ij} (u_{i,j} + u_{j,i}) - W_c(\sigma_{ij}, e_{ij})]^k dv_k - \int \tau_i u_i ds \quad (3.1)$$

In the above expression, $W_p(u_i, e_{ij})$ is the potential energy of the global region and $W_c(\sigma_{ij}, e_{ij})$ is the complementary energy corresponding to the local region. The terms V_g and V_k refer to the volume domains of the global and local regions respectively. It should be noted that V_k in particular refers to a local layer k in the local domain which is assumed to have N local layers.

In the abbreviated form, the above expression can be written as

$$\pi = \pi_g + \pi_l + \pi_s \quad (3.2)$$

where π_g , referring to the first integral of (3.1), is the potential energy for the global region, and π_l is the Reissner variational functional for N layers in the local region. π_l is the summation term ($k = 1$ to N) in the equation (3.1). Finally, π_s , referring to the last term of (3.1) corresponds to the potential energy of the prescribed surface tractions.

3.1 ELEMENT MODELING FOR THE GLOBAL REGION

By defining the constitutive laws as

$$\begin{aligned} \sigma_i &= C_{ij} (\epsilon_j^0 + z \kappa_j^0 - e_j) \quad (i, j = 1, 2, 3, 6) \\ \sigma_i &= C_{ij} (\epsilon_j^0 + z \kappa_j + z^2/2 \beta_j^0) \quad (i, j = 4, 5) \end{aligned} \quad (3.3)$$

the potential energy for the global region is written as

$$\pi_g = \pi_{g\epsilon} + \pi_{g\kappa} \quad (3.4)$$

In the above expressions, ϵ^0 and e are midsurface and expansional strains respectively, and κ and β are curvature parameters characterizing strains at any distance z from the surface. These through-the-thickness variations of strains follow those for displacements on the global region (i.e., a linear variation for inplane displacements and a quadratic variation for the transverse

displacement). π_{ge} and π_{ge} in (3.4) refer to the volume integrals over volume domain V_g of the global region in terms of the mechanical and expansional strains respectively. Because of the polynomial variation with respect to z , of the displacements (and hence of strains), it is possible to write each of the integrals π_{ge} and π_{ge} as a sum of several integrals with various powers of z appearing as coefficients. In other words, it is possible to carry out the integration, with respect to z , of the stiffness terms C_{ij} in conjunction with various powers of z to obtain the moduli corresponding to the entire global domain. These moduli are defined as

$$(A_{ij}, B_{ij}, D_{ij}, F_{ij}, H_{ij}) = \int_{-H/2}^{H/2} (1, z, z^2, z^3, z^4) C_{ij} dz \quad (3.5)$$

where H , appearing in the integration limits, is the total thickness of global domain of layers. This process reduces the volume integral to an area integral in terms of the x and y coordinates. For this purpose, the various components of strains and curvatures are written in vector form as follows:

$$\begin{aligned} \{\epsilon^0\}^T &= \{\epsilon_1^0 \quad \epsilon_2^0 \quad \epsilon_3^0 \quad \epsilon_6^0\}^T \\ \{\bar{\epsilon}^0\}^T &= \{\epsilon_4^0 \quad \epsilon_5^0\}^T \\ \{\kappa\}^T &= \{\kappa_1 \quad \kappa_2 \quad \kappa_3 \quad \kappa_6\}^T \\ \{\bar{\kappa}\}^T &= \{\kappa_4 \quad \kappa_5\}^T \\ \{\beta\}^T &= \{\beta_4 \quad \beta_5\}^T \\ \{e\}^T &= \{e_1 \quad e_2 \quad e_3 \quad e_6\}^T \end{aligned} \quad (3.6)$$

Then the integral corresponding to the mechanical strains in the global region can be written as

$$\pi_{ge} = \frac{1}{2} \int_{V_g} (\pi_{ge}^1 + z \pi_{ge}^2 + z^2 \pi_{ge}^3 + z^3 \pi_{ge}^4 + z^4 \pi_{ge}^5) dv \quad (3.7)$$

where for example

$$\pi_{ge}^1 = \{ \epsilon^0 \}^T [\bar{C}_{11}] \{ \epsilon^0 \} + \{ \bar{\epsilon}^0 \}^T [\bar{C}_{22}] \{ \bar{\epsilon}^0 \} + 2 \{ \epsilon^0 \}^T [\bar{C}_{21}] \{ \bar{\epsilon}^0 \} \quad (3.8a)$$

$$\pi_{ge}^2 = 2 \{ \kappa \}^T [\bar{C}_{11}] \{ \epsilon^0 \} + 2 \{ \bar{\kappa} \}^T [\bar{C}_{22}] \{ \bar{\epsilon}^0 \} + 2 \{ \bar{\kappa} \}^T [\bar{C}_{21}] \{ \epsilon^0 \} + 2 \{ \epsilon^0 \}^T [\bar{C}_{21}] \{ \bar{\kappa} \} \quad (3.8b)$$

and so on.

The material stiffness matrix in the above expressions are defined as

$$[\bar{C}_{11}] = \begin{bmatrix} C_{11} & C_{12} & C_{13} & C_{16} \\ C_{12} & C_{22} & C_{23} & C_{26} \\ C_{13} & C_{23} & C_{33} & C_{36} \\ C_{16} & C_{26} & C_{36} & C_{66} \end{bmatrix}$$

$$[\bar{C}_{22}] = \begin{bmatrix} C_{14} & C_{45} \\ C_{45} & C_{55} \end{bmatrix}$$

$$[\bar{C}_{21}] = \begin{bmatrix} C_{14} & C_{24} & C_{34} & C_{46} \\ C_{15} & C_{25} & C_{35} & C_{56} \end{bmatrix}$$

In a similar way, the expression for π_{ge} can also be written as

$$\pi_{ge} = \int_{V_g} (\pi_{ge}^1 + z \pi_{ge}^2 + z^2 \pi_{ge}^3) dv \quad (3.9)$$

where for example,

$$\pi_{ge}^1 = \{ \epsilon^0 \}^T [\bar{C}_{11}] \{ e \} + \{ \epsilon^0 \}^T [\bar{C}_{21}] \{ e \} \quad (3.9a)$$

$$\pi_{ge}^2 = \{ \kappa \}^T [\bar{C}_{11}] \{ e \} + \{ \kappa \}^T [\bar{C}_{21}] \{ e \} \quad (3.9b)$$

For the finite element description, the vector of variables for the global region is

$$\{ \mathbf{u} \}^T = \{ \bar{u}, \bar{v}, u^*, v^*, \bar{w}, w^*, \hat{w} \}^T \quad (3.10)$$

where \bar{u}, \bar{v} , etc. are the weighted displacement parameters that are related to the midsurface displacements and curvature terms [24] by the following relations:

$$\begin{aligned} u^0 &= 1/2 \bar{u} \\ v^0 &= 1/2 \bar{v} \quad \text{etc.} \end{aligned} \quad (3.11)$$

and by definition,

$$(\bar{w}, w^*, \hat{w}) = \int_{-H/2}^{H/2} w (1, 2z/H^2, 4z/H^2) 2/H \, dz$$

It is now possible to write each of the vector quantities in (3.6) in terms of the vector of variables $\{ \mathbf{u} \}$. For example,

$$\{ \epsilon^0 \} = [L_1][L_2]\{ \mathbf{u} \} \quad (3.11a)$$

$$\{ \bar{\epsilon}^0 \} = [L_1][L_2]\{ \mathbf{u} \} \quad (3.11b)$$

$$\{ \kappa \} = [L_3][L_4]\{ \bar{\mathbf{u}} \} \quad (3.11c)$$

$$\{ \bar{\kappa} \} = [L_3] w^* \quad (3.11d)$$

$$\{ \beta \} = [L_5][L_6]\{ \bar{\bar{\mathbf{u}}} \} \quad (3.11e)$$

In the above expressions, there are two other vectors $\{ \bar{\mathbf{u}} \}$ and $\{ \bar{\bar{\mathbf{u}}} \}$ on the right hand side (in addition to a single weighted displacement parameter w^*) which are but parts of the vector of complete variables. That is,

$$\{ \bar{\mathbf{u}} \}^T = \{ u^* \, v^* \, \bar{w} \, \hat{w} \}^T \quad (3.12a)$$

$$\{ \bar{\bar{\mathbf{u}}} \}^T = \{ \bar{w} \, \hat{w} \}^T \quad (3.12b)$$

All the other matrices appearing in the set of equations (3.11) are given below.

$$[L_1] = \begin{bmatrix} \partial/\partial x & 0 & 0 \\ 0 & \partial/\partial y & 0 \\ 0 & 0 & 1 \\ \partial/\partial y & \partial/\partial x & 0 \end{bmatrix} \quad (3.13a)$$

$$[L_2] = \begin{bmatrix} 1/2 & 0 & 0 & 0 & 0 & 0 & 0 \\ 0 & 1/2 & 0 & 0 & 0 & 0 & 0 \\ 0 & 0 & 0 & 0 & 0 & 3/H & 0 \end{bmatrix} \quad (3.13b)$$

$$[L_1] = \begin{bmatrix} \partial/\partial y & 0 & 1 \\ \partial/\partial x & 1 & 0 \end{bmatrix} \quad (3.13c)$$

$$[L_2] = \begin{bmatrix} 0 & 0 & 0 & 0 & 9/8 & 0 & -15/8 \\ 0 & 0 & 3/H & 0 & 0 & 0 & 0 \\ 0 & 0 & 0 & 3/H & 0 & 0 & 0 \end{bmatrix} \quad (3.13d)$$

$$[L_3] = [L_1] \quad (3.13e)$$

$$[L_4] = \begin{bmatrix} 3/H & 0 & 0 & 0 \\ 0 & 3/H & 0 & 0 \\ 0 & 0 & -15/H^2 & 45/H^2 \end{bmatrix} \quad (3.13f)$$

$$\{L_3\} = 3/H \{ \partial/\partial y \quad \partial/\partial x \}^T \quad (3.13g)$$

$$\{L_5\} = \{ \partial/\partial y \quad \partial/\partial x \}^T \quad (3.13h)$$

$$[L_6] = \begin{bmatrix} -15/H^2 & 0 \\ 0 & 45/H^2 \end{bmatrix} \quad (3.13i)$$

3.2 DISCRETIZATION PROCEDURE FOR THE GLOBAL REGION

The nature of the interpolation functions, which describe the mapping of the variables chosen for the element, is derived from the governing equations for the global domain. The variables are given in (3.10). From the stress - strain relations (3.3), it is possible to obtain the stress - displacement relations by using the kinematic relationships [25] given below:

$$\begin{aligned} \epsilon_1^0 &= \partial u^0 / \partial x \\ \epsilon_2^0 &= \partial v^0 / \partial y \\ \epsilon_3^0 &= \psi_z \\ \epsilon_4^0 &= \psi_z + \partial w^0 / \partial y \quad \text{etc.} \end{aligned} \quad (3.14)$$

Then, it can be seen that for the stresses to be linear in the spatial coordinates x and y , the displacements and the curvature terms u^0 , v^0 , w^0 , ψ_x , ψ_y , ψ_z and ϕ have to be quadratic in x and y . Consequently, from the relationships (3.11), the weighted displacement parameters (3.10) should vary quadratically with respect to x and y .

In the present formulation, triangular elements are chosen for discretization purposes. It has been established [38,39] that it is convenient to work with area coordinates or natural coordinates when dealing with triangular elements. If ζ_1 , ζ_2 and ζ_3 are the area coordinates, then the

relationships between these and the cartesian coordinates are given by (figure 2.) the following set of equations. The last of the following expressions is an identity associated with the area coordinates. This identity is used to obtain a unique relationship between the two sets of coordinates:

$$\begin{aligned}x &= x_1 \zeta_1 + x_2 \zeta_2 + x_3 \zeta_3 \\y &= y_1 \zeta_1 + y_2 \zeta_2 + y_3 \zeta_3 \\1 &= \zeta_1 + \zeta_2 + \zeta_3\end{aligned}\tag{3.15a}$$

Following the above equations, it should be noted that the edge 1-3 of the triangle is defined by only two area coordinates ζ_1 and ζ_2 , while the third area coordinate $\zeta_3 = 0$. Similarly, the boundary 3-5 has $\zeta_1 = 0$ and on boundary 5-1, the coordinate $\zeta_2 = 0$. Also, the numerical integration of functions on the rectangular boundary 1-3 is carried with respect to ζ_1 and ζ_2 only. Similar reasoning follows for the other two rectangular boundaries and the integration is carried out with respect to all the three coordinates for the upper and lower triangular boundaries of the element.

By inversion of equations (3.15a), one can get

$$\begin{Bmatrix} \zeta_1 \\ \zeta_2 \\ \zeta_3 \end{Bmatrix} = \frac{1}{2A} \begin{bmatrix} y_{23} & x_{32} & x_2 y_3 - x_3 y_2 \\ y_{31} & x_{13} & x_3 y_1 - x_1 y_3 \\ y_{12} & x_{21} & x_1 y_2 - x_2 y_1 \end{bmatrix} \begin{Bmatrix} x \\ y \\ 1 \end{Bmatrix}\tag{3.15b}$$

In the above equations, x_i, y_i ($i = 1,2,3$) are the cartesian coordinates of the node i and

$$y_{23} = y_2 - y_3$$

$$x_{32} = x_3 - x_2$$

$$x_{21} = x_2 - x_1 \quad \text{etc.} \quad \text{and}$$

$$2A = (x_1 - x_3)(y_2 - y_3) - (x_2 - x_3)(y_1 - y_3)$$

For the purpose of establishing rules for differentiation and integration, only ζ_1 and ζ_2 are considered as independent variables. Thus $\partial/\partial\zeta_1$ implies that ζ_2 is held constant and $\partial/\partial\zeta_2$ implies that ζ_1 is held constant. The differentiation rule is given by

$$\begin{Bmatrix} \partial/\partial\zeta_1 \\ \partial/\partial\zeta_2 \end{Bmatrix} = [J] \begin{Bmatrix} \partial/\partial x \\ \partial/\partial y \end{Bmatrix} \quad (3.16a)$$

where $[J]$ is the Jacobian matrix. Its determinant is equal to $2A$. In other words

$$[J] = \begin{bmatrix} x_{13} & y_{13} \\ x_{23} & y_{23} \end{bmatrix} \quad (3.16b)$$

Thus the differential area $dx dy$ is replaced in all integrations by

$$dx dy = |J| d\zeta_1 d\zeta_2 \quad (3.16c)$$

where $|J|$ symbolizes the determinant of the Jacobian Matrix $[J]$.

In the final analysis, it is necessary to maintain continuity of displacements u , v and w between the layers of the laminate. For this purpose, we choose as the nodal degrees of freedom the displacements at the top and the bottom of the layer. Denoting by the subscripts t and b the top and the bottom displacements respectively (such as u_t and u_b etc.), it is possible to use the relationships such as, for example,

$$u = 1/2 \bar{u} + 3z/H u^*$$

and write

$$\begin{aligned}
 u_t &= 1/2 \bar{u} + 3/2 u^* \\
 u_b &= 1/2 \bar{u} - 3/2 u^* \\
 v_t &= 1/2 \bar{v} - 3/2 v^* \\
 v_b &= 1/2 \bar{v} - 3/2 v^* \\
 w_t &= -3/4 \bar{w} + 3/2 w^* + 15/4 \hat{w} \\
 w_b &= -3/4 \bar{w} - 3/2 w^* + 15/4 \hat{w}
 \end{aligned} \tag{3.17a}$$

Another relationship for w is added so that the seven unknown displacements are related to the seven weighted displacement parameters. This last relationship refers to the middle surface displacement w_0 . That is,

$$w_0 = 9/8 \bar{w} - 15/8 \hat{w} \tag{3.17b}$$

The displacements u_t , u_b , v_t , v_b , w_t , w_b , w_0 are graphically shown for different nodes of a layer in Figure 2.

In the matrix form, the equations (3.17) can be written as

$$\{ u_{tb} \} = [L_{u\bar{u}}] \{ u \} \tag{3.18}$$

where $\{ u_{tb} \} = \{ u_t, u_b, v_t, v_b, w_t, w_b, w_0 \}^T$ and the elements of the matrix $[L_{u\bar{u}}]$ are given by

$$[L_{uu}] = \begin{bmatrix} 1/2 & 0 & 3/2 & 0 & 0 & 0 & 0 \\ 0 & 1/2 & 0 & 3/2 & 0 & 0 & 0 \\ 1/2 & 0 & -3/2 & 0 & 0 & 0 & 0 \\ 0 & 1/2 & 0 & -3/2 & 0 & 0 & 0 \\ 0 & 0 & 0 & 0 & -3/4 & 3/2 & 15/4 \\ 0 & 0 & 0 & 0 & -3/4 & -3/2 & 15/4 \\ 0 & 0 & 0 & 0 & 9/8 & 0 & -15/8 \end{bmatrix}$$

The inverse relationships of (3.18) can be written as

$$\{u\} = [L_{uu}]^{-1} \{u_{tb}\} \quad (3.19)$$

As per earlier discussion, the interpolation representation for the displacements $\{u_{tb}\}$ is written as, for example,

$$u_t = u_t^1 N_1 + u_t^2 N_2 + u_t^3 N_3 + u_t^4 N_4 + u_t^5 N_5 + u_t^6 N_6 \quad (3.20)$$

Similar quadratic representations are written for $u_b, v_t, v_b, w_t, w_b, w_o$ also. In the above expression (3.20), N_i ($i=1,6$) represent the shape functions and u_t^i and u_b^i etc. refer to the corresponding quantities at the node i . The same shape functions are used to characterize all the displacements. These shape functions are given by the following expressions [38]:

$$\begin{aligned} N_1 &= \zeta_i (2 \zeta_i - 1) \quad (i = 1, 2, 3) \\ N_4 &= 4 \zeta_1 \zeta_2 \\ N_5 &= 4 \zeta_2 \zeta_3 \\ N_6 &= 4 \zeta_1 \zeta_3 \end{aligned} \quad (3.21)$$

It is now possible to use equations (3.18) through (3.21) in conjunction with equations (3.11) to obtain the various stiffness matrix terms for the global region. As an illustration, the

following development is given.

$$\text{From (3.11a), } \{ \epsilon^0 \} = [L_1] [L_2] \{ u \}$$

$$\text{With (3.19), } \{ \epsilon^0 \} = [L_1] [L_2] [L_{u\bar{u}}]^{-1} \{ u_{tb} \}$$

With the set of interpolation functions (following the type given in (3.20)) given as

$$\{ u_{tb} \} = [N_S] \{ u_e^N \} \quad (3.22)$$

in which the vector $\{ u_e^N \}$ includes all the nodal degrees of freedom for the element. Then,

$$\begin{aligned} \{ \epsilon^0 \} &= [L_1] [L_2] [L_{u\bar{u}}]^{-1} [N_S] \{ u_e^N \} \\ &= [L_{12}^N] \{ u_e^N \} \end{aligned} \quad (3.23)$$

Hence the first expression on the right hand side of equation (3.8a) is written as

$$\{ \epsilon^0 \}^T [\bar{C}_{11}] \{ \epsilon^0 \} = \{ u_e^N \}^T [L_{12}^N]^T [\bar{C}_{11}] [L_{12}^N] \{ u_e^N \} \quad (3.24)$$

The corresponding stiffness matrix is

$$\int_{V_g} [L_{12}^N] [\bar{C}_{11}] [L_{12}^N] dv$$

In the above expression, the integration with respect to z can be done independently. The remaining terms in the integrand are now functions of x and y only. These area integrals are numerically evaluated by using the Gauss quadrature formulas. Similar expressions as (3.24) are written for various quantities given in equations (3.7) and (3.8) and element stiffness matrices are individually written for each expression of these equations. In each case, the integration with respect to z is appropriately done by considering the various powers of z appearing in (3.7).

3.3 ELEMENT MODELING FOR THE LOCAL REGION

The functional characterizing the behavior of the entire laminate also consists of a Reissner's functional π_R that represents the local region of the laminate. For a local region consisting of N layers, this functional is given as

$$\pi_R = \sum_{k=1}^N \pi_l^k - \int_{S_\sigma} \tau u \, ds \quad (3.25)$$

where π_l^k is the volume integral expression given by

$$\pi_l^k = \int_{V_l^k} [1/2 \, \sigma_{ij} (u_{i,j} + u_{j,i}) - U^* (\sigma_{ij}, e_{ij})]^k \, dv_k \quad (3.26)$$

Here, $U^* (\sigma_{ij}, e_{ij})$ is the complementary energy density and V_l^k refers to the volume enclosed by the k^{th} layer in the local region. The volume integral expression is written as (without the superscript k for convenience),

$$\pi_l = \int_{V_l} [\sigma (\epsilon - e) - U^*] \, dv \quad (3.27)$$

Writing $\epsilon = (S \sigma + e)$ and the appropriate expression for U^* , the equation (3.27) can be rewritten as

$$\pi_l = 1/2 \int_{V_l} \sigma^T S \sigma \, dv + \int_{V_l} \sigma^T e \, dv \quad (3.28)$$

where S represents the compliance matrix. It should be noted that σ , ϵ and e are vector quantities. For the local region, the in-plane stress components are assumed to be linear functions of z and the remaining stresses are either quadratic or cubic in z as a consequence of substitution in the layer equilibrium equations. These stresses are functions of the interlaminar stress components p_1, p_2 ,

t_1, t_2, s_1 and s_2 [24]. These latter terms, therefore appear as the nodal degrees of freedom for the layer in the local region in addition to the displacement degrees of freedom as in the global region.

As in the case of strain components for the global region, the stress components here are split up into two vectors for mathematical convenience. These are

$$\{ \sigma^1 \}^T = \{ \sigma_1 \quad \sigma_2 \quad \sigma_3 \quad \sigma_6 \}^T \quad \text{and} \quad \{ \sigma^2 \}^T = \{ \sigma_4 \quad \sigma_5 \}^T \quad (3.29)$$

By using relations (3.25) of reference 24, these vectors can be written in terms of the force and moment components and the interlaminar stress components. These are

$$\{ \sigma^1 \} = [M_1^*] \{ N_R \} \quad \text{and} \quad \{ \sigma^2 \} = [M_2^*] \{ V \} \quad (3.30)$$

where

$$\begin{aligned} \{ N_R \}^T &= \{ N_x/h^2 \quad N_y/h^2 \quad N_z/h^2 \quad M_x/h^2 \quad M_y/h^2 \quad M_z/h^2 \quad M_{xy}/h^2 \quad p_1 \quad p_2 \}^T, \\ \{ V \}^T &= \{ V_x/h \quad V_y/h \quad s_1 \quad s_2 \quad t_1 \quad t_2 \} \quad \text{and} \end{aligned}$$

$$[M_1^*] = \begin{bmatrix} 1 & 0 & 0 & 0 & 12z/h & 0 & 0 & 0 & 0 & 0 \\ 0 & 1 & 0 & 0 & 0 & 12z/h & 0 & 0 & 0 & 0 \\ 0 & 0 & F_1 & 0 & 0 & 0 & F_2 & 0 & F_3 & F_4 \\ 0 & 0 & 0 & 1 & 0 & 0 & 0 & 12z/h & 0 & 0 \end{bmatrix}$$

$$[M_2^*] = \begin{bmatrix} 0 & F_1 & F_5 & F_6 & 0 & 0 \\ F_1 & 0 & 0 & 0 & F_5 & F_6 \end{bmatrix}$$

In the above expressions, quantities V_x, V_y, N_z, M_z are defined in reference 24, h is the thickness of the layer under consideration and F_1 through F_6 are defined as follows:

$$F_1 = 3/2 - 6 z^2/h^2$$

$$F_2 = 30 z/h - 120 z^2/h^2$$

$$F_3 = -1/4 + 3 z/2h + 3 z^2/h^2 - 10 z^3/h^3$$

$$F_4 = -1/4 - 3 z/2h + 3 z^2/h^2 + 10 z^3/h^3$$

$$F_5 = -1/4 - z/h + 3 z^2/h^2 \quad \text{and}$$

$$F_6 = -1/4 + z/h + 3 z^2/h^2$$

Corresponding to the stress components (3.21), the compliance matrix for the layer is split up as follows:

$$[\bar{S}_{11}] = \begin{bmatrix} S_{11} & S_{12} & S_{13} & S_{16} \\ S_{12} & S_{22} & S_{23} & S_{26} \\ S_{13} & S_{23} & S_{26} & S_{36} \\ S_{16} & S_{26} & S_{36} & S_{66} \end{bmatrix}$$

$$[\bar{S}_{22}] = \begin{bmatrix} S_{44} & S_{45} \\ S_{45} & S_{55} \end{bmatrix}$$

$$[\bar{S}_{21}] = \begin{bmatrix} S_{14} & S_{24} & S_{34} & S_{46} \\ S_{15} & S_{25} & S_{35} & S_{56} \end{bmatrix}$$

Again as before,

$$\pi_l = \pi_l^1 + \pi_l^2 + \pi_l^3 + \pi_l^4 + \pi_l^5 \quad (3.31)$$

where

$$\pi_l^1 = 1/2 \int \{ \sigma^1 \}^T [\bar{S}_{11}] \{ \sigma^1 \} dv \quad \text{and}$$

$$\pi_l^2 = 1/2 \int \{ \sigma^2 \}^T [\bar{S}_{21}] \{ \sigma^1 \} dv \quad \text{and so on.}$$

Upon substitution of expressions (3.30) for $\{ \sigma^1 \}$ and $\{ \sigma^2 \}$ into equations of type (3.32), one gets, for example,

$$\pi_l^1 = 1/2 \int_{V_l} \{ N_R \}^T [M_1^*]^T [\bar{S}_{11}] [M_1^*] \{ N_R \} dv$$

It should be noted that in the above expression, the z -terms appear only in the matrix $[M_1^*]$. As such, the above expression can be rewritten as

$$\pi_l^1 = 1/2 \int_{A_l} \{ N_R \}^T [\bar{S}_{11}^*] \{ N_R \} dA \quad (3.33)$$

where, now,

$$[\bar{S}_{11}^*] = \int_{A_l} [M_1^*]^T [\bar{S}_{11}] [M_1^*] dz$$

The other expressions in (3.32) can be similarly written as, for example ,

$$\pi_l^2 = 1/2 \int_{A_l} \{ V \}^T [\bar{S}_{21}^*] \{ N_R \} dA \quad \text{etc.} \quad (3.34)$$

Thus it is possible to write each integral expression in equation (3.31) in terms of the force and moment components as well as the interlaminar stress components.

3.4 DISCRETIZATION PROCEDURE FOR LOCAL REGION

It is now possible to invoke the layer constitutive relations to write (3.34) in terms of the displacement functions and the interlaminar stress components. These can be symbolically written as

$$\{ N_R \} = [R_1] \{ u_1 \} + [R_3] \{ e \} \quad (3.35a)$$

$$\{ V \} = [R_2] \{ u_2 \} \quad (3.35b)$$

where

$$\{ u_1 \} = \{ \bar{u} \quad \bar{v} \quad u^* \quad v^* \quad \bar{w} \quad w^* \quad \hat{w} \quad p_1 \quad p_2 \}$$

$$\{ u_2 \} = \{ u^* \quad v^* \quad \bar{w} \quad \hat{w} \quad s_1 \quad s_2 \quad t_1 \quad t_2 \}$$

The matrices $[R_1]$, $[R_2]$ and $[R_3]$ express the relations of the force and moment components with the above mentioned vectors of the weighted displacement parameters and the interlaminar stress components. Substitution of expressions (3.35) into expressions of type (3.33) and (3.34) results in the variational functional π_I of (3.31) to be written as

$$\begin{aligned} \pi_I = 1/2 \int [& \{ u_1 \}^T [R_{11}] \{ u_1 \} + \{ u_1 \}^T [R_{13}] \{ e \} + \\ & \{ e \}^T [R_{13}]^T \{ u_1 \} + \{ e \}^T [R_{33}] \{ e \} + \\ & \{ u_2 \}^T [R_{22}] \{ u_2 \} + \{ u_1 \}^T [R_{12}] \{ u_2 \} + \\ & \{ u_2 \}^T [R_{12}]^T \{ u_1 \} + \{ u_2 \}^T [R_{23}] \{ e \} + \\ & \{ e \}^T [R_{23}]^T \{ u_2 \}] dA \end{aligned} \quad (3.36)$$

The various matrices $[R_{11}]$, $[R_{12}]$ etc. are defined as follows:

$$[R_{11}] = [R_1] [\bar{S}_{11}^*] [R_1]$$

$$[R_{12}] = [R_1]^T [\bar{S}_{21}^*]^T [R_2]$$

$$[R_{23}] = [R_2]^T [\bar{S}_{21}^*] [R_3] \quad \text{and so on.}$$

Again, as in the case of global region, it is necessary to maintain displacement and stress continuity between any two layers of the local region. Thus, we revert to actual set of degrees of freedom which are now the actual displacements at the top and bottom of each layer (u_t , u_b etc.) along with the interlaminar stress components.

The relationships between the actual displacements and the weighted displacement parameters are similar to equations (3.17) [24] and the steps for further development of element stiffness matrices for the local region follow those for the global region. The major differences between these two developments are that:

(i) in the matrix expression in equation (3.18), there are additional terms referring to the interlaminar stress components,

(ii) while the interpolation functions for the displacements follow the same pattern of quadratic variation, the new degrees of freedom for the local region referring to the interlaminar stress components are linearly interpolated. That is,

$$\begin{aligned}
 p_1 &= p_1^1 N_1 + p_1^2 N_2 + p_1^3 N_3 \\
 p_2 &= p_2^1 N_1 + p_2^2 N_2 + p_2^3 N_3 \\
 t_1 &= t_1^1 N_1 + t_1^2 N_2 + t_1^3 N_3 \\
 t_2 &= t_2^1 N_1 + t_2^2 N_2 + t_2^3 N_3 \\
 s_1 &= s_1^1 N_1 + s_1^2 N_2 + s_1^3 N_3 \\
 s_2 &= s_2^1 N_1 + s_2^2 N_2 + s_2^3 N_3
 \end{aligned} \tag{3.37}$$

These expressions are incorporated into the equation (3.36) and the variation of π_l with respect to the chosen degrees of freedom generates the stiffness matrix for the element of the local layer under consideration.

3.5 SURFACE INTEGRALS INVOLVING LOCAL AND GLOBAL REGIONS

The surface integrals to be considered in the present variational formulation for the global-local model are

$$\int_{S_{\sigma l1}} \bar{\tau} u \, dS + \int_{S_{\sigma g1}} \bar{\tau} u \, dS + \sum_{k=1}^N \int_{S_{\sigma l2}} (\bar{\tau}^k u^k + \bar{\tau}^{k+1} u^{k+1}) \, dS_k + \int_{S_{\sigma g2}} (\bar{\tau}_l + \bar{\tau}_g) u \, dS \tag{3.38}$$

In the above expression, $S_{\sigma l}$ and $S_{\sigma g}$ represent in general the external boundaries of the local and global regions, respectively where the tractions are prescribed. These include the top and bottom surfaces of the laminate (where an external loading may or may not be prescribed). In (3.38), the additional subscript 2 represents the interlaminar surfaces between the local layers and the common surface between the global and local regions. Since there are no prescribed tractions on $S_{\sigma l2}$ and $S_{\sigma g2}$ (the continuity of stresses and displacements being taken care of by common nodal parameters), the last two integral terms of (3.38) are zero. Any of the two remaining integrals can be generally written as

$$\int_{S_{\sigma}} \bar{\tau} u \, dS \quad (3.39)$$

where $\{\bar{\tau}\}$ is the traction vector of boundary tractions on the boundary S_{σ} and $\{u\}$ is the vector of corresponding displacement components. These displacement components can be written in terms of the appropriate nodal degrees of freedom pertaining to the boundary under consideration. The equation (3.39) can include a general type of loading that can be represented by the vector $\{\bar{\tau}\}$. The traction components in the surface integral expression need to be specified on every boundary of the element. By a knowledge of the state of stress at any location, the traction components on boundary surfaces are readily obtained by the following general relationships.

$$\begin{Bmatrix} \tau_x \\ \tau_y \\ \tau_z \end{Bmatrix} = \begin{bmatrix} \sigma_x & \tau_{xy} & \tau_{xz} \\ \tau_{xy} & \sigma_y & \tau_{yz} \\ \tau_{xz} & \tau_{yz} & \sigma_z \end{bmatrix} \begin{Bmatrix} n_x \\ n_y \\ n_z \end{Bmatrix} \quad (3.40)$$

In the above equations n_x , n_y , n_z are the direction cosines of the normal to the boundary surface under consideration.

In the present mathematical formulation, a uniformly distributed load is considered for checking the validity of the present approach. In such a case of transverse loading, only the z -

component of the traction vector is non-zero and is equal to the magnitude of the applied load ($n_z = 1$ and $n_x = n_y = 0$). The surface integral (3.39) then becomes

$$q \int_{S_\sigma} \{N\}_b^T \{u\}_b dS \quad (3.41)$$

where $\{N\}_b$ refers to the vector of shape functions associated with the displacement w and $\{u\}_b$ is the vector of the degrees of freedom pertaining to the boundary. This expression now involves integration with respect to x and y of the boundary. As in the previous cases this integration is written in terms of the area coordinates and the numerical integration is done by Gaussian quadrature constants as described in the next section. This results in a consistent load vector as the right hand side of the final equations to be solved.

3.6 NUMERICAL SOLUTION PROCEDURES

By considering the mathematical developments of discretization as in the previous sections, a numerical solution scheme was evolved and the corresponding computer algorithm written. This corresponds to the various stages such as evaluation of volume integrals for global and local regions, assembly procedures at the element level and later at the structure level for the triangular mesh pattern chosen and the appropriate inclusion of boundary conditions and finally solution of algebraic equations. As mentioned before, the initial cases considered for the numerical work pertain to the checking of the validity of the present model. As such, numerical problems for which solutions are established are chosen for this purpose.

The final form of variational functional governing the behavior of the laminate can be written as

$$\pi = 1/2 f^T K f - f^T Q \quad (3.42)$$

In this expression, the stiffness matrix K is obtained by assembling the corresponding

stiffness matrices for all the elements. Thus \mathbf{K} can be referred to as the structure stiffness matrix. Similarly, the consistent load vector \mathbf{Q} also corresponds to the structure. \mathbf{f} in the above expression is the vector of the nodal degrees of freedom for the structure. The variation of the above functional with respect to each of the nodal degrees of freedom gives rise to a set of linear, simultaneous equations. It is then necessary to apply the boundary conditions applicable to the problem under consideration. This process reduces the number of simultaneous equations to be solved finally.

The various analytical developments given in the previous sections have been transformed into computer codes in order to solve numerical problems pertaining to laminate stress analysis. The computer program written for this purpose covers the following topics. The corresponding subroutines performing these operations are also given.

(1) Input element description, nodal coordinates and properties of individual layers (thickness, fiber orientation, material constants etc.). The nodal number generation and the corresponding coordinate evaluation are done by the subroutine ELGEN after the dimensions of the plate and the mesh/grid patterns are read.

(2) Calculation of global moduli for the layers comprising of the global region. This is achieved by the subroutine GLOBQ, the output of which are the quantities of the layer moduli integrated appropriately through the thicknesses of the layers.

(3) Calculation of shape function parameters and Jacobian of transformation which are applicable to both global and local regions.

(4) Evaluation of the various stiffness matrix elements for global region using the global moduli. This is done in a subroutine VOGLOB which essentially converts volume integral terms to area integral terms. The numerical integration is effected by the 5-point Gauss-Radau formula for which the constants are read as input in the beginning.

(5) Assembly of the matrix elements at the element level for the global region using subroutine ELSTG.

(6) Evaluation of compliance elements for a local layer based on the individual layer properties for that layer. This evaluation is done in the main program. Calculation of stiffness matrix elements for a local layer following the analytical descriptions is also done here.

(7) Assembly of stiffness matrix elements at the element level for the local layer under consideration (subroutine ELSTL).

(8) Repetition of the calculations for all the local layers so that the stiffness matrix for the element now includes all the local layers as well as the global region. Repetition of calculations of the above steps to cover all the elements of the structure.

(9) Calculation of the consistent load vector corresponding to the element under consideration (subroutine LOAD).

(10) Assembly of element stiffness matrix and load vector elements to obtain the corresponding structure stiffness matrix and load vector using the subroutine ASSMB.

(11) The boundary conditions read in step (1) are now invoked (subroutine BCOND) and the necessary rows and columns are set to zero corresponding to zero boundary conditions.

(12) Solution of the resulting set of simultaneous equations to obtain the required nodal degrees of freedom. This is done by means of library subroutine LEQT1P. The results - both stresses and displacements - are listed.

These steps are shown in the form of a flow chart in Figure 4.

As described in the previous sections, area integrals involving cartesian coordinates are encountered during the present discretization process. Since the area coordinates (or the natural coordinates) are chosen for the numerical work, the computations are also done with the latter as the variables. Specifically, a typical integral in cartesian coordinates is transformed to one in area coordinates as follows.

$$I = \iint F \, dx \, dy = \iint F \det [J] \, d\zeta_1 \, d\zeta_2$$

The numerical evaluation of the above integral is carried out by means of the Gauss-Radau integration constants involving 5 points [38]. In other words, the integral is numerically written as

$$I = \sum_{i=1}^5 \sum_{j=1}^5 W F(\zeta_1, \zeta_2, \zeta_3) \det [J]$$

where

$$\begin{aligned} \zeta_1 &= AI(i) \\ \zeta_2 &= AJ(j) [1 - AI(i)] \\ \zeta_3 &= 1 - \zeta_1 - \zeta_2 \quad \text{and} \\ W &= AS(i) H(j) [1 - AI(i)] \end{aligned}$$

The five sets of values (corresponding to the five point integration formula) for the constants $AI(i)$, $AJ(j)$ etc. are chosen from reference 38.

For the purpose of numerical computations for obtaining the stiffness matrix elements from the present approach, a laminate as shown in Figure 5 is considered. Figure 5a shows an element arrangement for a quarter plate with an assumed symmetry about the x and y coordinate axes. Figure 5b shows a set of more refined finite element mesh patterns to be used later on in the investigation. This is a typical mesh pattern associated with triangular finite elements. A scheme of nodal numbering is also shown in these figures to obtain an economical storage capacity in the

computer. These numbers refer to the nodes which have all the layers incorporated in them and thus the stiffness matrix for any element here would have already incorporated the stiffness matrix contributions from all the layers of the laminate.

3.7 RESULTS AND DISCUSSION

To start with, consideration is given to laminates with isotropic layer properties. This is intended to check the validity of the present approach by comparison with known results. In all the following calculations one global layer and one local layer are considered. From the mathematical developments described before, this gives an element 84 degrees of freedom (the element containing both the local and global region as shown in figure 3). The material properties chosen are: $E = 30 \times 10^6$ psi and $G = 11.54 \times 10^6$ psi. The geometry chosen is represented by $a = 1''$ and total thickness = 0.01".

First, a square plate is chosen with only two elements in the quarter plate as shown in figure-4. This is done primarily to check the various stages of calculations in the procedure such as symmetry of stiffness matrix, appropriate assembly technique etc. At the element level, an eigenvalue check is done for the stiffness matrix which, in mathematical terms, is given by the equation

$$K - \lambda I = 0$$

where K is the element stiffness matrix, I is identity matrix, and λ 's are the eigenvalues. The f 's (see equation 3.42) associated with λ 's are the corresponding eigenvectors. The above solution must have at least six zero eigenvalues corresponding to the six rigid body modes for the structure. It was found that for one element in the grid shown in figure 5a, there were six eigenvalues very close to zero compared to the rest of the eigenvalues. It was also found that the diagonal elements of the stiffness matrix were nonzero, positive and relatively dominant. A check was also done on the assembly procedure for the two elements shown in figure 5a. Since the plate is chosen to be square, geometric symmetry tests were also applied. For example, the stiffness associated with displacement

u at node 2 is identical with that associated with displacement v at node 4. The stiffnesses associated with w at nodes 2 and 4 were found to be identical. Similar checks were applied for symmetric nodes such as 3 and 7 and 6 and 8.

The next stage of calculation involved the actual solution to the problem of a plate transversely loaded by a uniformly distributed load. The boundary conditions were chosen to be simply supported on the edges $x = a$ and $y = a$. This implies that at the bottom of the laminate w is set to zero at nodes 7, 8, 9, 6 and 3. Also, the shear stresses τ_{xz} and τ_{yz} are set to zero on the edges $x = a$ and $y = a$ respectively. Because of the isotropic laminate construction and the chosen symmetry of geometry, the following conditions were also applied.

$$\begin{aligned} u &= 0 & \text{at} & \quad x = 0, \quad y = y \\ v &= 0 & \text{at} & \quad y = 0, \quad x = x \end{aligned}$$

All the above mentioned conditions were applied to the assembled stiffness matrix representing the entire quarter plate and the resulting equations were solved by a library subroutine. The maximum value of the vertical deflection was found to be $0.0287 q_1$ where q_1 is the intensity of the applied load. The exact value as given in standard text books is

$$w_{\max} = 0.00406 q_1 a^4 / D$$

where a is the side of the plate and D is the flexural rigidity. For the geometry and the material properties chosen, this deflection is given as $0.02365 q_1$. This shows an error of about 21% with the finite element result. This is expected for the grid that has been chosen.

The next two cases refer to the laminates that are rectangular in planform. For this purpose, several grid patterns are chosen as shown in figure 6. In the first case here, a rectangular laminate with $b/a = 2$ is chosen. For this case, the exact solution for the maximum deflection is given as

$$w_{\max} = 0.01013 q_1 a^4 / D = 0.00369 q_1$$

With the grids (a) and (b) in figure 6 (i.e., 2 and 4 elements respectively), the finite element results for w_{\max} were found to be $0.0046 q_1$ and $0.00323 q_1$ representing errors of 24.7% and 12.4% respectively.

The next case of rectangular laminate has an aspect ratio of 4. The same grid patterns as shown in figure 6 are chosen here. However, for studying the convergence of results, higher number of elements in the quarter plate is chosen. These grid patterns are shown in figures 6c through 6f in which the number of elements are respectively 6, 8, 10 and 12. The exact solution for this case is

$$w_{\max} = 0.01282 q_1 a^4 / D = 0.000292 q_1$$

With 4, 6, 8, 10 and 12 elements in the quarter laminate, the corresponding values for maximum deflection were found to be $0.000345 q_1$, $0.000325 q_1$, $0.000316 q_1$, $0.000300 q_1$ and $0.000294 q_1$ respectively. It can be seen that the results from the finite element formulation converge very well to the exact result. In order to obtain a graphical idea about this, the percentage errors of the finite element results are plotted against the number of elements for this specific case with aspect ratio equal to 4. This is shown in figure 7. It can be seen that for the last case where the number of elements is 12, the error is about 0.7%. These results establish an acceptable standard of convergence rate for the finite element stiffness model considered in this section.

4. GLOBAL-LOCAL FINITE ELEMENT METHOD: FRONTAL SOLUTION TECHNIQUE

In this section a set of problems (bending, uniform tensile and stretch) have been studied by using global-local and local models. An important aspect of this part is the use of frontal method of finite element solution. This is done in order to reduce the size of the structure matrix so that more plies and more refined mesh can be studied. Currently, the program can solve 3500 degrees of freedom or more on IBM RT PC without having any memory problem. The present illustrative study includes: (1) The analysis of bending effects in laminates under prescribed uniform transverse load and (2) The analysis of edge effects in laminates under applied uni-axial uniform tensile stress or strain. The basic formulation of the variational problem using the global-local approach has already been described in the previous section. The aspects of computer programs incorporating the frontal solution technique [42] and the consequent numerical results are delineated and discussed in this section.

4.1 LOCAL DOMAIN (MODEL 1)

Based on the reference 24, the simplest assumption consistent with a realistic stress analysis for the in-plane stress component are assumed to vary linearly through the thickness of each ply. The substitution of these stress components into the differential equations of equilibrium yields the interlaminar stress components in terms of tractions p_i , s_i , t_i ($i=1,2$), stress and moment resultants. Finally the weighted displacements are expressed in terms of stress resultants through constitutive relations. For the sake of clarity, some of the expressions are reproduced here. The energy functional is first written as [24]

$$\pi_I = \int_V \sum_{k=1}^N \{ \sigma^T \epsilon - 1/2 \sigma^T S \sigma - \sigma^T e \} dV_k$$

The simplest assumption consistent with realistic stress analysis for the in-plane stress

component can be expressed as

$$\sigma_x = \frac{N_x}{h} + \frac{12 M_x z}{h^3}$$

$$\sigma_y = \frac{N_y}{h} + \frac{12 M_y z}{h^3}$$

$$\tau_{xy} = \frac{N_{xy}}{h} + \frac{12 M_{xy} z}{h^3}$$

where N_x , N_y , N_{xy} , M_x , M_y , M_{xy} are functions of x and y . Obviously, these functions represent the force and moment resultants arising in plate theory. As in reference 24, we introduce the following stress and moment resultants.

$$N_i = \int_{-h/2}^{h/2} \sigma_i dz \quad i = 1, 2, 3, 6$$

$$M_i = \int_{-h/2}^{h/2} z \sigma_i dz$$

where h is the thickness of each layer and N_3 and M_3 are mathematical, not physical, quantities. We first consider a single layer of thickness h within the laminate. We let x and y represent the coordinates in the midplane of the layer, which is bounded by the planes $z=\pm h/2$. The interlaminar stresses σ_z , τ_{zx} , τ_{zy} at the top of the layer are denoted by p_2 , s_2 , t_2 respectively, while the corresponding stresses at the bottom of the layer are designated as p_1 , s_1 , t_1 .

In plate theory, the equations of equilibrium or balance of linear momentum, in terms of special description within whole local region R_l are in general expressed as

$$\rho a_i = \sigma_{ij,j} + \rho b_i$$

where σ_{ij} are stress components, a_i is the acceleration of deformed body, b_i are body force per unit mass, and ρ is the density per unit volume. By neglecting body force and considering steady state only, we now substitute in-plane stresses along the values of the interlaminar stress at $z = \pm h/2$, into the equilibrium equations, which leads to the following distributions

$$\begin{aligned} \sigma_z = & \frac{(p_1 + p_2)}{4} \frac{(12 z^2 - 1)}{h^2} + \frac{(p_2 - p_1)}{4} \frac{(40 z^3 - 6z)}{h^3} \\ & + \frac{3N_z}{2h} \left(1 - \frac{4z^2}{h^2} \right) + \frac{15M_z}{h^2} \left(\frac{2z}{h} - \frac{8z^3}{h^3} \right) \end{aligned}$$

$$\tau_{zy} = (s_2 - s_1) \frac{z}{h} + \frac{(s_1 + s_2)}{4} \frac{(12 z^2 - 1)}{h^2} + \frac{3V_y}{2h} \left(1 - \frac{4z^2}{h^2} \right)$$

$$\tau_{zx} = (t_2 - t_1) \frac{z}{h} + \frac{(t_1 + t_2)}{4} \frac{(12 z^2 - 1)}{h^2} + \frac{3V_x}{2h} \left(1 - \frac{4z^2}{h^2} \right)$$

where the shear resultants V_x and V_y given by

$$\begin{aligned} V_x &= \int_{-h/2}^{h/2} \tau_{xz} dz \\ V_y &= \int_{-h/2}^{h/2} \tau_{yz} dz \end{aligned}$$

and are functions of x and y only.

Following theoretical development in 24 and simplifying, the Reissner's energy can be expressed as

$$\pi = \pi_I - \pi_S$$

where

$$\begin{aligned} \pi_I = & \iint \{ [V_2]^T [R_2]^T [RS]^T [RND] [R_2] [V_2] + [V_3]^T [R_3]^T [RS]^T \\ & \times [RND] [R_2] [V_2] + [V_3]^T [R_9] [V_2] + [V_3]^T [R_{10}] [U^*] \\ & - 1/2 \{ [V_2]^T [R_2] [RS]^T [RQ] [RS] [R_2] [V_2] + [V_3]^T [R_3] [RS] \\ & \times [RQ]^T [R_2] [V_2] + [V_3]^T [RT] [RS] [R_2] [V_2] \\ & + [V_2]^T [R_2]^T [RS] [RS] [R_3]^T [V_2] + [V_3]^T [R_3] [RS] \\ & \times [RQ]^T [R_2] [V_3] + [V_2]^T [RT] [RS] [R_3] [V_3] \\ & + [V_2]^T [R_2]^T [RS^{-1}]^T [RT]^T [V_3] + [V_3]^T + [R_3]^T [RS]^T [RT] \times [V_2] + [V_3]^T [RP] [V_3] \} dx dy \end{aligned}$$

and

$$\pi_S = \int \sigma_i u ds$$

where

$$[V_2]^T = [\bar{u} \ \bar{v} \ \bar{w} \ u^* \ v^* \ w^* \ \hat{w}] \quad [u^*]^T = [u^t \ v^t \ w^t \ u^b \ v^b \ w^b]$$

$$[V_3]^T = [p_2 \ s_2 \ s_2 \ p_1 \ s_1 \ t_1] \quad [V_5]^T = [N_x \ N_y \ N_z \ N_{xy} \ M_x \ M_y \ M_z \ M_{xy} \ V_y \ V_x]$$

$$RND = \begin{bmatrix} 1/h & 0 & 0 & 0 & 0 & 0 & 0 & 0 & 0 & 0 \\ 0 & 1/h & 0 & 0 & 0 & 0 & 0 & 0 & 0 & 0 \\ 0 & 0 & 1/h & 0 & 0 & 0 & 0 & 0 & 0 & 0 \\ 0 & 0 & 0 & 1/h & 0 & 0 & 0 & 0 & 0 & 0 \\ 0 & 0 & 0 & 0 & 12/h^3 & 0 & 0 & 0 & 0 & 0 \\ 0 & 0 & 0 & 0 & 0 & 12/h^3 & 0 & 0 & 0 & 0 \\ 0 & 0 & 0 & 0 & 0 & 0 & 12/h^3 & 0 & 0 & 0 \\ 0 & 0 & 0 & 0 & 0 & 0 & 0 & 12/h^3 & 0 & 0 \\ 0 & 0 & 0 & 0 & 0 & 0 & 0 & 0 & 1 & 0 \\ 0 & 0 & 0 & 0 & 0 & 0 & 0 & 0 & 0 & 1 \end{bmatrix}$$

$$R_2 = \begin{bmatrix} \frac{h}{2} \frac{\partial}{\partial x} & 0 & 0 & 0 & 0 & 0 & 0 \\ 0 & \frac{h}{2} \frac{\partial}{\partial y} & 0 & 0 & 0 & 0 & 0 \\ 0 & 0 & 0 & 0 & 0 & 3 & 0 \\ \frac{h}{2} \frac{\partial}{\partial y} & \frac{h}{2} \frac{\partial}{\partial x} & 0 & 0 & 0 & 0 & 0 \\ 0 & 0 & 0 & \frac{h^2}{4} \frac{\partial}{\partial x} & 0 & 0 & 0 \\ 0 & 0 & 0 & 0 & \frac{h^2}{4} \frac{\partial}{\partial y} & 0 & 0 \\ 0 & 0 & \frac{-5h}{4} & 0 & 0 & 0 & \frac{15h}{4} \\ 0 & 0 & 0 & \frac{h^2}{4} \frac{\partial}{\partial y} & \frac{h^2}{4} \frac{\partial}{\partial x} & 0 & 0 \\ 0 & 0 & \frac{3}{4} \frac{\partial}{\partial y} & 0 & \frac{3}{h} & 0 & \frac{-3\partial}{4\partial y} \\ 0 & 0 & \frac{3\partial}{4\partial x} & \frac{3}{h} & 0 & 0 & \frac{-3\partial}{4\partial x} \end{bmatrix}$$

$$RS = \begin{bmatrix} S_{11} & S_{12} & S_{13} & S_{16} & 0 & 0 & 0 & 0 & 0 & 0 \\ S_{21} & S_{22} & S_{23} & S_{26} & 0 & 0 & 0 & 0 & 0 & 0 \\ S_{31} & S_{32} & \frac{6S_{33}}{5} & S_{16} & 0 & 0 & 0 & 0 & 0 & 0 \\ S_{61} & S_{62} & S_{63} & S_{66} & 0 & 0 & 0 & 0 & 0 & 0 \\ 0 & 0 & 0 & 0 & S_{11} & S_{12} & S_{13} & S_{16} & 0 & 0 \\ 0 & 0 & 0 & 0 & S_{21} & S_{22} & S_{23} & S_{26} & 0 & 0 \\ 0 & 0 & 0 & 0 & S_{31} & S_{32} & \frac{10S_{33}}{7} & S_{36} & 0 & 0 \\ 0 & 0 & 0 & 0 & S_{61} & S_{62} & S_{63} & S_{66} & 0 & 0 \\ 0 & 0 & 0 & 0 & 0 & 0 & 0 & 0 & \frac{6S_{44}}{5h} & \frac{6S_{45}}{5h} \\ 0 & 0 & 0 & 0 & 0 & 0 & 0 & 0 & \frac{6S_{45}}{5h} & \frac{6S_{55}}{5h} \end{bmatrix}$$

$$R_3 = \begin{bmatrix} 0 & 0 & 0 & 0 & 0 & 0 \\ 0 & 0 & 0 & 0 & 0 & 0 \\ \frac{S_{33}h}{10} & 0 & 0 & \frac{S_{33}h}{10} & 0 & 0 \\ 0 & 0 & 0 & 0 & 0 & 0 \\ 0 & 0 & 0 & 0 & 0 & 0 \\ 0 & 0 & 0 & 0 & 0 & 0 \\ \frac{S_{33}h^2}{28} & 0 & 0 & \frac{-S_{33}h^2}{28} & 0 & 0 \\ 0 & 0 & 0 & 0 & 0 & 0 \\ 0 & \frac{S_{44}}{10} & \frac{S_{45}}{10} & 0 & \frac{S_{44}}{10} & \frac{S_{45}}{10} \\ 0 & \frac{S_{45}}{10} & \frac{S_{55}}{10} & 0 & \frac{S_{45}}{10} & \frac{S_{55}}{10} \end{bmatrix}$$

$$R_4 = \begin{bmatrix} 0 & 0 & \frac{3}{4} & 0 & 0 & -\frac{3}{2} & -\frac{15}{4} \\ 0 & -\frac{1}{2} & \frac{-h \partial}{8 \partial y} & 0 & -\frac{3}{2} & \frac{h \partial}{4 \partial y} & \frac{3 h \partial}{8 \partial y} \\ -\frac{1}{2} & 0 & \frac{-h \partial}{8 \partial x} & -\frac{3}{2} & 0 & \frac{h \partial}{4 \partial x} & \frac{3 h \partial}{8 \partial x} \\ 0 & 0 & -\frac{3}{4} & 0 & 0 & -\frac{3}{2} & \frac{15}{4} \\ 0 & \frac{1}{2} & \frac{-h \partial}{8 \partial y} & 0 & -\frac{3}{2} & \frac{-h \partial}{4 \partial y} & \frac{2 h \partial}{8 \partial y} \\ \frac{1}{2} & 0 & \frac{-h \partial}{8 \partial x} & -\frac{3}{2} & 0 & \frac{-h \partial}{4 \partial x} & \frac{3 h \partial}{8 \partial x} \end{bmatrix}$$

$$R_{10} = \begin{bmatrix} 0 & 0 & 1 & 0 & 0 & 0 \\ 0 & 1 & 0 & 0 & 0 & 0 \\ 1 & 0 & 0 & 0 & 0 & 0 \\ 0 & 0 & 0 & 0 & 0 & -1 \\ 0 & 0 & 0 & 0 & -1 & 0 \\ 0 & 0 & 0 & -1 & 0 & 0 \end{bmatrix}$$

$$RP = \begin{bmatrix} S_{33}F_4^2 & S_{35}F_4F_6 & S_{36}F_4F_6 & S_{33}F_3F_4 & S_{35}F_4F_6 & S_{36}F_4F_5 \\ S_{53}F_4F_6 & S_{55}F_6F_6 & S_{56}F_6F_6 & S_{53}F_3F_6 & S_{55}F_5F_6 & S_{56}F_5F_6 \\ S_{63}F_4F_6 & S_{65}F_6F_6 & S_{66}F_6F_6 & S_{63}F_3F_6 & S_{65}F_5F_6 & S_{66}F_5F_6 \\ S_{33}F_3F_4 & S_{35}F_3F_6 & S_{33}F_3F_6 & S_{33}F_3F_3 & S_{35}F_3F_5 & S_{33}F_3F_5 \\ S_{53}F_3F_5 & S_{55}F_5F_6 & S_{56}F_5F_6 & S_{53}F_3F_5 & S_{55}F_5F_5 & S_{56}F_5F_5 \\ S_{63}F_3F_5 & S_{65}F_5F_6 & S_{66}F_5F_6 & S_{63}F_3F_5 & S_{65}F_5F_5 & S_{66}F_5F_5 \end{bmatrix}$$

$$F_1 = \frac{3}{2} - \frac{6z^2}{h^2}$$

$$F_2 = \frac{30z}{h} - \frac{120z^3}{h^3}$$

$$F_3 = -\frac{1}{4} + \frac{3}{2} \frac{z}{h} + \frac{3z^2}{h^2} - \frac{10z^3}{h^3}$$

$$F_4 = -\frac{1}{4} + \frac{3}{2} \frac{z}{h} + \frac{3z^2}{h^2} - \frac{10z^3}{h^3}$$

$$F_5 = -\frac{1}{4} + \frac{z}{h} + \frac{3z^2}{h^2}$$

$$F_6 = -\frac{1}{4} + \frac{z}{h} + \frac{3z^2}{h^2}$$

$$I_3 = \frac{12z}{h^3}$$

$$I_4 = \frac{12z}{h^4}$$

$$I_5 = \frac{12z}{h^5}$$

From above equations, the functional, π , has been defined. Therefore the problem becomes to find the stationary value of V_2 and $V_3 \in H_1$ and H_3 respectively such that

$$\pi = \pi_I - \pi_s + \int MV_2 ds_1 + \int NV_3 ds_2$$

where

$$H_1 = \{ V_2 \mid V_2 \in H^m(R^3), MV_2 = q_1, \text{ on } \partial s_1 \}$$

$$H_2 = \{ V_3 \mid V_3 \in H^m(R^3), NV = q_2, \text{ on } \partial s_2 \}$$

H^m is infinite dimensional space ∂s_1 and ∂s_2 are the boundary section in which V_2 and V_3 are prescribed.

Equilibrium requires that π be stationary, i.e., $\delta\pi = 0$ where it must be recognized that V_2 and V_3 are independent variables. Hence, in the finite element analysis of an assemblage of elements we only need to enforce interelement continuity on V_2 and V_3 , which can readily be achieved in the same way as in the isoparametric finite element analysis of solid. Following the standard finite element analysis we use

$$V_2 = \sum_{i=1}^q \phi_i V_i, \quad V_3 = \sum_{j=1}^r \chi_j V_j$$

where the ϕ_i and χ_j are the interpolation functions and q and r are the number of nodes of the element with respect to weighted displacement and interlaminar stresses. Using the fact that the total Reissner energy must be stationary and taking account of the discretization, the final algebraic equations can be expressed as

$$[K] \begin{Bmatrix} V_2 \\ V_3 \end{Bmatrix} = \begin{Bmatrix} F \\ U^a \end{Bmatrix}$$

where the K is the stiffness matrix obtained from the volume integrals of the energy equations for the entire region. V_2 and V_3 are the discretizing weighted displacements, normal and shear stress at the top and bottom of layers. F is load vector obtained from the area integral of the external tractions of whole boundary. U^a is displacement equivalent vector derived from the interlayer

continuity.

4.2 GLOBAL-LOCAL MODEL (MODEL 2)

The global-local model was formulated in order to solve the actual displacement and interlaminar stresses at the same time. The energy equation for the global regions and local layer can be expressed as

$$\pi = \int_V \widetilde{W} dV + \int_V [1/2 \sigma_{ij} (U_{i,j} + U_{j,i}) - W] dV - \int_S \tau_i U_i ds$$

where $\widetilde{W} = \widetilde{W}(U_i, e_{ij})$, $W = W(\sigma_{ij}, e_{ij})$ and \widetilde{W} and W are strain energy density functions, the first in terms of displacements U_i and e_{ij} , the expansional strain components, and the second in terms of stresses σ_{ij} and e_{ij} .

The energy equation can be written as

$$\pi = \pi_g + \pi_l - \pi_s$$

where

$$\pi_g = \int_{A_g} [U] \left\{ q^T A q_1 + q^T B q_1 + q^T B q_2 + q^T E q_2 + q^T E q_3 + q^T F_1 q_3 + q^T E_1 q_1 + q^T F_1 q_2 + q^T H_1 q_3 \right\} [V] dx dy$$

$$\pi_l = \int_{A_l} \sum_{k=1}^N \left\{ [U]^T [D_6]^T [RS] [RQ] [RS] [D_6] [V] + [U_3]^T [R_3]^T [RS]^T [RQ] [D_6] [V] + [V]^T [D_6] [RS]^T [RQ] [RS] [R_3] [U_3] + [U_3] [R_3] [RS] [RQ] [RS] [R_3] [V_3] + [U_3]^T [RT] [RS] [R_3] [V_3] + [V_3]^T [R_3]^T [RS]^T [RT] [U_3] + [U]^T [D_6]^T [RS]^T [RT] [V_3] + [V_3] [RT] [RS] [D_6] [U] + [U_3]^T [RP] [V_3] \right\}^k dx dy$$

$$\pi_s = \int_{S_g} f_g u d S_g + \int_{S_l} f_l u d S_l$$

where the A_g and A_l represent the area of the global and local region in the x - y plane respectively. The S_g and S_l indicate the external boundaries of the global and local regions respectively. The f_g and f_l stand for the external forces acting at the global and local regions and

$$q_1 = D_1 D_4 D_5^{-1}$$

$$q_2 = D_2 D_4 D_5^{-1}$$

$$q_3 = D_3 D_4 D_5^{-1}$$

$$D_6 = R_2 D_5^{-1}$$

$$D_1 = \begin{bmatrix} \frac{\partial}{\partial x} & 0 & 0 & 0 & 0 & 0 & 0 \\ 0 & \frac{\partial}{\partial y} & 0 & 0 & 0 & 1 & 0 \\ 0 & 0 & 0 & 0 & 0 & 0 & 0 \\ \frac{\partial}{\partial y} & \frac{\partial}{\partial x} & 0 & 0 & 0 & 0 & 0 \\ 0 & \frac{\partial}{\partial y} & \frac{\partial}{\partial x} & 0 & 1 & 0 & 0 \\ 0 & 0 & \frac{\partial}{\partial x} & 1 & 0 & 0 & 0 \end{bmatrix}$$

$$D_2 = \begin{bmatrix} 0 & 0 & 0 & \frac{\partial}{\partial x} & 0 & 0 & 0 \\ 0 & 0 & 0 & 0 & \frac{\partial}{\partial y} & 0 & 0 \\ 0 & 0 & 0 & 0 & 0 & 0 & 1 \\ 0 & 0 & 0 & \frac{\partial}{\partial y} & \frac{\partial}{\partial x} & 0 & 0 \\ 0 & 0 & 0 & 0 & 0 & \frac{\partial}{\partial y} & 0 \\ 0 & 0 & 0 & 0 & 0 & \frac{\partial}{\partial x} & 0 \end{bmatrix}$$

$$D_3 = \begin{bmatrix} 0 & 0 & 0 & 0 & 0 & 0 & 0 \\ 0 & 0 & 0 & 0 & 0 & 0 & 0 \\ 0 & 0 & 0 & 0 & 0 & 0 & 0 \\ 0 & 0 & 0 & 0 & 0 & 0 & 0 \\ 0 & 0 & 0 & 0 & 0 & 0 & \frac{\partial}{\partial y} \\ 0 & 0 & 0 & 0 & 0 & 0 & \frac{\partial}{\partial y} \end{bmatrix}$$

$$D_4 = \begin{bmatrix} \frac{1}{2} & 0 & 0 & 0 & 0 & 0 & 0 \\ 0 & \frac{1}{2} & 0 & 0 & 0 & 0 & \frac{-15}{h^2} \\ 0 & 0 & \frac{9}{8} & 0 & 0 & 0 & 0 \\ 0 & 0 & 0 & \frac{3}{h} & 0 & 0 & 0 \\ 0 & 0 & 0 & 0 & \frac{3}{h} & 0 & 0 \\ 0 & 0 & 0 & 0 & 0 & \frac{3}{h} & 0 \\ 0 & 0 & \frac{-15}{h^2} & 0 & 0 & 0 & \frac{45}{h^2} \end{bmatrix}$$

$$D_5 = \begin{bmatrix} \frac{1}{2} & 0 & 0 & \frac{3}{2} & 0 & 0 & 0 \\ 0 & \frac{1}{2} & 0 & 0 & \frac{3}{2} & 0 & 0 \\ 0 & 0 & -\frac{3}{4} & 0 & 0 & \frac{3}{2} & \frac{15}{4} \\ \frac{1}{2} & 0 & 0 & -\frac{3}{2} & 0 & 0 & 0 \\ 0 & 0 & 0 & 0 & -\frac{3}{2} & 0 & 0 \\ 0 & 0 & -\frac{3}{4} & 0 & 0 & -\frac{3}{2} & \frac{15}{4} \\ 0 & 0 & \frac{9}{8} & 0 & 0 & 0 & -\frac{15}{8} \end{bmatrix}$$

$$C^1 = \begin{bmatrix} M_{11} & M_{12} \\ M_{21} & M_{22} \end{bmatrix}$$

$$C^3 = \begin{bmatrix} M_{12} \\ M_{22} \end{bmatrix}$$

$$M_{11} = \begin{bmatrix} C_{11} & C_{12} & C_{13} & C_{16} \\ C_{21} & C_{22} & C_{23} & C_{26} \\ C_{31} & C_{32} & C_{33} & C_{36} \\ C_{41} & C_{42} & C_{43} & C_{46} \end{bmatrix}$$

$$M_{22} = \begin{bmatrix} C_{44} & C_{45} \\ C_{44} & C_{45} \end{bmatrix}$$

$$^T M_{12} = M_{21} = \begin{bmatrix} C_{41} & C_{42} & C_{43} & C_{46} \\ C_{51} & C_{52} & C_{53} & C_{56} \end{bmatrix}$$

$$\begin{aligned}
(A, B, E) &= \int_{-h/2}^{h/2} (1, z, z^2) C \, dz \\
(E_1, F_1) &= \int_{-h/2}^{h/2} (.5) (z^2, z^3) C^3 \, dz \\
H_1 &= \int_{-h/2}^{h/2} (.5) (z^4) M_{22} \, dz
\end{aligned}$$

and [R₂], [R₃], [R_S], [R_Q], [R_P], and [R_T] are defined as local model in the previous section.

From above equations, the functional π of π_g , π_l and π_s are defined. Therefore the problem becomes to find the stationary value of U , U_3 ϵ H_1 and H_2 respectively such that

$$\pi = \pi_g + \pi_l - \pi_s + \int_{\partial S_1} MV ds_1 + \int_{\partial S_2} NV_3 dS_2$$

where

$$\begin{aligned}
H_1 &= \left\{ V \mid V \in H^m(R^3), MV = q_1 \text{ on } \partial S_1 \right\} \\
H_2 &= \left\{ V_3 \mid V_3 \in H^m(R^3), MV_3 = q_2 \text{ on } \partial S_2 \right\}
\end{aligned}$$

H^m is infinite dimensional space, ∂S_1 and ∂S_2 are the boundary section in which U and U_3 are prescribed.

Equilibrium requires the π is stationary, i.e. $\partial\pi = 0$ where it must be recognized that U and U_3 are independent variables. Hence in the finite element analysis of an assemblage of elements we only need to enforce interelement continuity on U and U_3 , which can readily be achieved in the same way as in isoparametric finite element analysis of solid. Following by standard finite element analysis we choose

$$U = \sum_{i=1}^q \phi_i U_i, \quad U_3 = \sum_{j=1}^r \chi_j U_j$$

where the ϕ_i and χ_j are the interpolation functions, and q and r are the number nodes of the element with respect to weighted displacement and interlaminar stresses.

Using the fact that the total energy must be stationary and taking account of the discretization, the final algebraic equation can be expressed as

$$[K] \begin{bmatrix} U \\ U_3 \end{bmatrix} = [F]$$

where the K is the stiffness matrix obtained from the volume integrals of the energy equations for the entire region. U , U_3 are the discretizing actual displacements, normal and shear stress at the top and bottom of layers. F is load vector obtained from the area integral of the external forces of whole boundary.

The computer code "GLFEM", based on the mixed variational finite element formulation with frontal solver have been successfully developed. A transverse loading (bending) of simple supported case have been studied to test the numerical solution and convergence. Also a unidirectional tension load applied at the edge of the plate have been studied. The flow chart of the program is given in Appendix A, and in a brief description of the program, "GLFEM", is as follows:

- i) Data files have been opened by the Index of NFIA, NFIB, NFDA, NFOB, NFOC, NFOD and MY, the first two Index are input files and others are output files. If number of variable is more than 3,000, then other output file is recommended to open. All

the data files are open at beginning of main program and close at end of main program, for more detail see appendix A.

ii) All the basic data is input or generated in the INPUT subroutine. The data include number of total element, node coordinates, node numbers, element connectivity, control index, material properties for each layer, integrating data, boundary condition data and control data of pre-frontal part.

iii) The element data based on two dimension model can be directly read from data files generated from pre-processor program. By using convert subroutine those data are converted into 3 dimensional data, The basic FRONTAL routine data are generated in INPUT subroutine.

iv) The smeared (or effective moduli) for both global and local region are calculated by GLOBAQ and LOCAQ subroutine respectively. The pre-data of global and local regions are obtained by SMAT, USBAR and ALLOT subroutine.

v) The shape functions and their derivatives for both linear and quadratic functions in triangular and rectangular elements are set up in SFR2, SHAPW, SHAPQ2 and SHAPL subroutine. The matrices of the transformation are evaluated in JACOB2 subroutine. The Gauss-Radau data is input in GAUSPT subroutine.

vi) The stiffness matrix of global region is calculated in ESTIFPS subroutine. The stiffness matrix of local region is evaluated from DBLOCA subroutine. The predata values are calculated by PREPBM, DISWET subroutine, the inverse of the matrix is executed by SOLVE subroutine.

vii) The load vector can be composed by concentrated and body forces, edge distribution

forces and distributed bending forces, which are coded by LOADPS, BODY, EDGEF and LOADPB subroutine respectively.

viii) The assembly of the stiffness matrix and elimination of the variables for the global and local domains are done by FRONTAL subroutine. The standard frontal procedure are followed (for more detail, see reference 42).

4.3 EXAMPLE PROBLEMS AND NUMERICAL RESULTS

The theoretical formulation is made for the analysis of composite structures with any geometric shape and size. Three cases of boundary value problems have been investigated. Case a deals with the bending of isotropic thick and thin rectangular plates with simply supported edges due to a uniformly distributed transverse load. Case b deals with the stress analysis of composite laminate under the influence of an applied in-plane unidirectional stress at the edges ($x=\text{constant}$) of the laminate. Case c deals with the stress analysis of a composite laminate under the influence of an applied in-plane strain at $x=\text{constant}$. The results are presented in graphical form. A comparison is made with existing results and show a good agreement.

Case a: Bending case

For testing the computer program written for the model 2, the solution to the problem of a plate transversely loaded by a uniformly distributed load with simply supported edges was obtained. The laminate geometry is shown in figure 8. Because of the isotropic laminate construction and the chosen symmetric geometry (see figure 6a), the following conditions were applied:

$$u = 0 \text{ at } x = 0 \qquad v = 0 \text{ at } y = 0$$

The boundary conditions were chosen to be simply supported on the edges where $x = a$, $y = b$. This implies that at the edge of the laminate the transverse deflection W is set to zero for all nodes. Also, the shear stress components τ_{zx} and τ_{zy} are set to zero on edge $x = a$ and $y = b$

respectively. All the above mentioned conditions were applied to the assembled stiffness matrix representing the actual structure plate. The above solution of square plate as given in standard text books is

$$W_{\max} = 0.00406 q a^4/D$$

where q is the intensity of the applied loads, a is the side of the plate and D is the flexural rigidity. Material properties in the plane of elastic symmetry of each layer are given by

$$E_L = E_T = E_Z = 30 \times 10^6 \text{ psi}, \quad G_{LT} = G_{LZ} = G_{TZ} = 1.154 \times 10^6 \text{ psi}$$

$$\nu_{LT} = \nu_{LZ} = \nu_{TZ} = 0.3,$$

where L , T and Z refer to fiber, transverse, and thickness directions respectively. The exact maximum deflection for square plate is given as $0.02365 q$ and $0.002956 q$ for plate thicknesses equal to .01 and .02 inch, respectively. The exact maximum deflection for rectangular plate with $a/b = 2$ is given as $0.00369 q$ and $0.000461 q$ for the plate thicknesses equal to 0.01 and 0.02 inch respectively.

The triangular elements and nodes are shown in figure 3. Figure 5 shows the grid patterns used in the model (for a square plan). With grid patterns 1,2, 3 and 4 in the quarter laminate, the corresponding values for maximum deflection listed in these tables. It can be seen that the results from the global local finite element model converge very well to the exact value. In order to obtain a graphical idea about this aspect, the displacement parameter W calculated by the finite element method and given in Tables 4.1 and 4.2 are plotted in figures 9 and 10 against the number of grids of the square and rectangular plates for both plate thicknesses.

1a Thickness = .01 INCH

grid number	W FEM RESULTS	EXACT SOLUTION
1	.0185 q	.02365 q
2	.0189 q	
3	.0196 q	
4	.0206 q	

1b. Thickness = .02 INCH

grid number	W FEM RESULTS	EXACT SOLUTION
1	.00232 q	.002956 q
2	.00240 q	
3	.00258 q	
4	.00274 q	

Table 4.1 Rectangular Plate Solution

2a Thickness = .01 INCH

grid number	W FEM RESULTS	EXACT SOLUTION
1	.00297 q	.00369 q
2	.00306 q	
3	.00324 q	
4	.00342 q	

2b. Thickness = .02 INCH

grid number	W FEM RESULTS	EXACT SOLUTION
1	.000373 q	.0004609 q
2	.000396 q	
3	.000427 q	
4	.000444 q	

Table 4.2 Square Plate Solution

By comparing the figures 9 and 10 in numerical sense, the error percentage change from 7.4% to 3.6% as the total plate thickness changes from .01 inch to .02 inch for the rectangular plate using grid 4. Similarly for square plate, the error percentage changes from 12.6% to 7.26%. The results in figures 9 and 10 show that the converging speed and error percentage of rectangular plate are better than those of square plate.

Case b: Applied Tensile Stress

This section shows the solution for the problem of a finite plate subjected to an in-plane tensile load $\sigma_x = 1$ at the edge, $x = a$ by using models 1 and 2. The laminate geometry is shown in figure 8. Two cases of geometric configurations, the ratio of a/b , are studied using the first and second model. Also, the solutions for the thin and thick finite plate are compared. A $[0/90]_S$ symmetric laminate with the stacking of layers as $0^\circ, 90^\circ, 90^\circ, 0^\circ$ will be examined in this study. Comprehensive results based on the reference 24 will be employed to compare specific results given by the present theory. The layers are of equal thickness h , the laminate width is $2b = 80h$ or $2b = 16h$ and material properties in the plane of elastic symmetry of each layer are given by

$$\begin{aligned} E_{11} &= 20 \times 10^6 \text{ psi} ; & E_{22} &= E_{33} = 2.1 \times 10^6 \text{ psi} \\ G_{12} &= G_{13} = G_{23} = .85 \times 10^6 \text{ psi} & \nu_{12} &= \nu_{13} = \nu_{23} = .21 \end{aligned}$$

where 1,2 and 3 refer to the fiber, transverse, and thickness directions respectively, and ν_{12} for example, is the Poisson ratio measuring strain in the transverse direction due to uniaxial tension in the fiber direction.

Because of the chosen symmetry of geometry in Figure 5a, the following conditions were applied

$$\text{For model 1: } \bar{u}, u^* = 0 \quad \text{at } x = 0 \qquad \bar{v}, v^* = 0 \quad \text{at } y = 0$$

$$\text{For model 2: } u^t, u^b = 0 \quad \text{at } x = 0 \qquad v^t, v^b = 0 \quad \text{at } y = 0$$

where parameters in model 1 are weighted displacements in x and y direction and are defined in references 24, 25 and the superscripts t and b denote the respective variable at top and bottom of the layer, respectively. For applied in-plane tensile load case, the boundary conditions of the finite plate for both formulations are as follows:

The shear stress components τ_{zx} and τ_{zy} are set to zero at $x = a$ and $y = b$ respectively. At mid-surface, the transverse deflection W and shear stress components τ_{zy} and τ_{zx} are set to zero everywhere. All the above mentioned conditions were applied to the assembled stiffness matrix representing the actual structure plate.

The triangular elements and nodes are shown in Fig. 3 and different grid patterns are shown in figure 5b. Figures 11 to 16 show the convergence study of both interlaminar stress components and weighted displacement for thick plates of aspect ratio $a/b=5$. The applied load is constant in-plane tensile stress at the edge of $x=\text{constant}$. The results obtained from model 1 have the same trend compared with reference 24, but magnitudes are slightly different. That is because the applied boundary condition in the present formulation is $\sigma_x = 1$ at $x = a$ while in reference 24 is $\epsilon_x = \epsilon$. The results of the stresses from the model 2 are almost equal to zero at free edge even though the actual displacements are reasonable. Figure 17 shows the comparing interlaminar stress of different geometric parameter for applied tensile load.

Case c: Uniform Applied Strain

In this section the response of the laminate under the influence of the unidirectional constant strain applied at the edge of the plate has been studied. This case is simulated by applying the equivalent biaxial stress obtained by lamination theory. The convergence study of both interlaminar stress and weighted displacement of the thin and thick plate is similar to the one with uniform tensile load applied at the edge. Figures 18 to 22 show the convergence pattern of interlaminar stresses and weighted displacement for thick/thin plate of aspect ratio $a/b=5$. The results of interlaminar stresses obtained from model 1 for constant strain case, have the same trend

but different magnitude as reference 24. Figures 23 to 25 show the comparison of interlaminar stress distribution between the existing and present results. The differences in magnitude between the current model and those of reference 24 may be explained by the following points:

1. The present is 3D model and solution is obtained for finite length plate.
2. The meshes are not fine enough near the edge and/or more sublayers should be used in order to get better accuracy in results.

Figures 23 to 25 also show the comparison of interlaminar stress of thick ($h=.25$ in.) and thin ($h=.05$ in.) plate for both strain load with respect to aspect ratio $a/b=5$.

4.4 SUMMARY AND CONCLUDING REMARKS

The convergence of current model is good as shown in the pictures. The results of interlaminar stress components and weighted displacement for both constant tensile and strain load from the Model 1 have the same trend but different magnitude compared with those of reference 24. The differences in magnitude between the current model and existing results may be explained as follows:

1. The present is 3D model and solution is obtained for finite length plate.
2. The meshes are not fine enough near the edge or more sublayers should be used in order to get accurate results especially for the thin plate.
3. Applied boundary conditions are different.
4. Geometric parameters are different.

The results of interlaminar stresses obtained from Model 2 are almost zero, even though the

displacement trend makes sense. The reason may be explained as follows:

1. The meshes are not fine enough near the edge. For more accurate results, more refined mesh and/or more sub-layers should be used.
2. The transformation used to convert the weighted displacements into actual displacements may introduce additional applied loads, even though the displacement makes sense.
3. The global region may be needed to include the interlaminar stresses as well as displacements.

For the thin plate, the results in figures 23 to 25 show that the shear stresses are more significant than the normal stress as compared to thick plate solution. It should be pointed out that because the mesh near the edge is not very fine, the models do not give prominent peak stresses in the presented thin plates solutions. This is because of the limited current hard disk space. A more refined mesh will be studied in future investigations. Convergence study, as shown in pictures, indicates that the results for constant strain applied load case are more stable than those for the constant tensile load case. The results by using the constant tensile load show slight oscillation. These oscillations reduce very significantly as the element number increases near the edge. The aspect ratio (a/b) may also have effect on the oscillation for the tensile load case.

The current code uses frontal solver and helps reduce memory space requirements. For example the program can handle 3500 degrees of freedom on IBM RT PC only using about 400 maximum frontal size, but the execution time is increased. The benefit of using frontal solution will increase with the solution of laminates with large number of layers. The future studies include, modification of the computational procedure and the application of this model for investigating laminates with flaws and through the thickness holes. Also the curing stress study will be included.

5. STIFFNESS AND STRENGTH DETERMINATION OF MULTI-ORIENTED, COATED FIBER COMPOSITES

In this part of the report, a coated continuous fiber composite has been analyzed using a three-phase concentric cylinder model. Effective thermoelastic properties have been determined and the solution for the stress distribution derived under a uniform three dimensional mechanical and/or hygrothermal loading. First, the theoretical model is described and the numerical results are compared with some of the closed form solutions already available in the literature. Next, details of the computer program, called NDSANDS, which was developed to implement the numerical algorithm, are discussed. Finally, some numerical results are presented for the effective thermoelastic moduli and the micro stress distribution under a uniform temperature change for a three-dimensional coated fibrous composite.

5.1 THE COMPOSITE MODEL

A coated , continuous fiber reinforced composite is modeled by a representative volume element composed of N concentric , circular cylinder elements, in which the innermost cylinder is the fiber, the next ring is the coating and the outer ring is the matrix as shown in figure 26. Let us further denote the composite volume in between the elements as the interstitial matrix region. Both the matrix in the composite cylinder as well as in the interstitial region, in turn, could be reinforced by particles.

Each element orientation , j , is defined via the two cylindrical angles $\Omega^{(j)}$ and $\Phi^{(j)}$ with respect to a fixed $x_1 - x_2 - x_3$ coordinate system. The local element cartesian coordinate system is represented by $X_1 - X_2 - X_3$. It should be further noted that the local fiber axis, X_1 , coincides with the z - coordinate in the local cylindrical system, whereas, $X_2 - X_3$ is the transverse $r - \theta$ plane.

If we denote $Q_{kl}^{(j)} = \cos(X_k^{(j)}, x_l)$, then from geometry in figure 26, we have

$$Q_{kl}^{(j)} = \begin{bmatrix} \cos \Omega & \sin \Omega \cos \phi & \sin \Omega \sin \phi \\ -\sin \Omega & \cos \Omega \cos \phi & \cos \Omega \sin \phi \\ 0 & -\sin \phi & \cos \phi \end{bmatrix} \quad (5.1)$$

5.2 MODEL ASSUMPTIONS AND METHOD OF ANALYSIS

The general definition of the effective elastic moduli of heterogeneous materials has been discussed in [43] and [44]. For the purpose of self-consistency, a short discussion, specific to the problem here treated, will now be given.

In fiber-reinforced materials, the ratio of length to fiber diameter is usually very large. Accordingly, fiber end conditions will only be considered here in the Saint Venant sense. The fiber, coating and the matrix are assumed to be linearly elastic, homogeneous and perfectly bonded. In general, the constituent materials may have transversely isotropic elastic and thermal expansion coefficients.

Let the composite material volume be subjected to a set of boundary conditions of the form

$$u_i(s) = \epsilon_{ij}^0 x_j \quad \text{or} \quad T_i(s) = \sigma_{ij}^0 n_j \quad (5.2a, 5.2b)$$

where n_j is the unit outward normal vector on the boundary surface S , x_j are the cartesian coordinates of that surface and ϵ_{ij}^0 and σ_{ij}^0 are constants.

For (5.2) prescribed, it can be shown that

$$\bar{\epsilon}_{ij} = \epsilon_{ij}^0 = \text{const.} \quad \text{or} \quad \bar{\sigma}_{ij} = \sigma_{ij}^0 = \text{const.} \quad (5.3a, 5.3b)$$

respectively, where an overbar denotes the average value over the whole volume. When displacements are prescribed, the average strains are $\bar{\epsilon}_{ij}^0$ and $\bar{\sigma}_{ij}$ have to be found and for prescribed traction, the average stresses are $\bar{\sigma}_{ij}^0$ and $\bar{\epsilon}_{ij}$ need to be determined.

The specimen is further assumed to be macroscopically homogeneous, by which is meant that for (5.2) prescribed, strain and stress averages taken over large enough subregions of the specimen are the same for any such subregion. Such a subregion will be referred to as a representative volume element (RVE).

To facilitate the analysis we next introduce an equivalent homogeneous medium (figure 27), having the effective composite properties, as a comparison material and assume that the

displacements or traction acting on the boundary of each composite cylinder element, $S_c^{(j)}$, can be approximated by those on the comparison material, i.e.,

$$u_i^{(j)} = \bar{\epsilon}_{ik}^0 x_k \quad \text{on } S_c^{(j)} \quad \text{or} \quad T_i^{(j)} = \bar{\sigma}_{ik}^0 n_k \quad \text{on } S_c^{(j)} \quad (5.4a, 5.4b)$$

according to whether (5.2a) or (5.2b) is prescribed and no summation on the superscripts is implied. Further, equation (5.4b) applies on the radial boundary of the composite cylinder elements while on the ends the following resultants need to be specified:

$$\begin{aligned} F_z &= \int_0^{2\pi} \int_0^{r_3} \sigma_{zz} r \, dr \, d\theta \quad ; \quad T = \int_0^{2\pi} \int_0^{r_3} \tau_{z\theta} r^2 \, dr \, d\theta \\ M_2 &= \int_0^{2\pi} \int_0^{r_3} \sigma_{zz} r^2 \sin \theta \, dr \, d\theta \quad M_3 = \int_0^{2\pi} \int_0^{r_3} \sigma_{zz} r^2 \cos \theta \, dr \, d\theta \end{aligned} \quad (5.5)$$

where F_z is the axial force, T the torque, and M_2 and M_3 the resultant moment about the X_2 and X_3 axis, respectively. The resultant forces in the X_2 and X_3 directions, F_2 and F_3 respectively, are non-zero but are not independent boundary conditions. Thus, under boundary conditions leading to a constant strain or stress field within a homogeneous body, the stress and the displacement inside the composite cylinder element, can now be evaluated as described in the following section.

5.3 DETERMINATION OF STRESS AND DISPLACEMENT FIELDS

If the composite volume is now subjected to boundary conditions given by (5.2a) or (5.2b), then, within each of the N elements, we have three displacement fields (in materials (1), (2) and (3) or fiber, coating and matrix, respectively). The form of the governing field equations and boundary conditions lead to a general solution of the type.

$$u_i^{(j,p)} = \sum_{n=0}^2 F_{in}^{(j,p)}(r, z) \begin{cases} \cos n\theta \\ \sin n\theta \end{cases} \quad (5.6)$$

where $j = 1, 2, \dots, N$; $p = 1, 2, 3$.

Using the strain displacement equations and the stress-strain relations for a transversely isotropic constituent, the stress field is expressed as

$$\sigma_i^{(j,p)} = \sum_{n=0}^2 H_{in}^{(j,p)}(r, z) \begin{cases} \cos n\theta \\ \sin n\theta \end{cases} \quad (5.7)$$

where the general form of the functions $F_{in}^{(j,p)}(r, z)$ and $H_{in}^{(j,p)}(r, z)$ in equations (5.6) and (5.7), respectively, are given in Ref [45] and the specific constants are to be evaluated by the following boundary / interface conditions:

- i) Displacements (eq 5.4a) or traction (eq 5.4b) and end resultants (eqs 5.5) are prescribed according to (5.2a) or (5.2b), respectively, at the boundary of the composite cylinder assemblage ; Equilibrium of the entire body, however, imposes certain implied

connections among the traction components [46];

ii) Traction and displacements must be continuous across the interfaces; and

iii) Stresses and displacements must be bounded at the origin, $r = 0$.

For convenience, the terms involving rigid body motion can be further neglected. The expressions for the constants are available in detail in Refs [46, 47].

5.4 THE COMPOSITE RESPONSE

The composite stress, $\bar{\sigma}_{kl}$ or strain $\bar{\epsilon}_{kl}$, can now be determined by volume averaging the stress or strain field over the constituents, namely, the composite cylinder elements and the interstitial matrix, respectively. The stress-strain relation for the composite now takes the form

$$\bar{\sigma}_{kl} = \bar{C}_{klmn} (\bar{\epsilon}_{mn} - \bar{e}_{mn}) \quad \text{or} \quad \bar{\epsilon}_{kl} = \bar{S}_{klmn} \bar{\sigma}_{mn} + \bar{e}_{kl}, \quad (5.8a, 5.8b)$$

where \bar{C}_{klmn} is the effective stiffness, \bar{S}_{klmn} is the effective compliance and \bar{e}_{kl} is the effective expansional (non-mechanical) strain of the composite.

To evaluate the effective elastic moduli, we set the expansional strain components identically equal to zero, i.e.,

$$\stackrel{(j, p)}{e_{kl}} = 0 \quad (\text{for all } j, p) \quad (5.9)$$

With (5.9), the stress-strain relation for the composite, eqs. (5.8), therefore reduce to (using contracted notation)

$$\bar{\sigma}_k = \bar{C}_{kl} \bar{\epsilon}_l \quad \text{or} \quad \bar{\epsilon}_k = \bar{S}_{kl} \bar{\sigma}_l \quad (\bar{k}, l = 1, 2, \dots, 6) \quad (5.10a, 5.10b)$$

By setting each strain (or stress) component equal to one individually, while all others are zero, we will respectively obtain the l^{th} column of the \bar{C}_{kl} (or \bar{S}_{kl}) matrix. The composite engineering constants can now be defined in terms of the elastic stiffnesses (or compliances). Finally, the effective expansional strains can be determined by substituting in eqs. (5.8).

5.5 INITIAL FAILURE CRITERION

The problem of the analysis of failure of composite materials is by an order of magnitude more difficult than the problem of physical property prediction which has been discussed until now. When a composite specimen is subjected to increasing load and/or temperature, microfailure will develop at some stage. These may be in the form of matrix cracks, fiber ruptures, interface separation and local plastification. As loading continues, they will multiply and ultimately merge to produce catastrophic failure.

The criteria for strength or failure are often expressed in terms of stresses, but such criteria do not necessarily refer only to a state of complete rupture of the materials. Failure criteria may, in fact, refer to the initial events, as evidenced in yielding, that are the precursors of ultimate failure.

One such simple criteria, which is widely used to predict the initial or first failure of composite materials, is the so called maximum stress criteria. This criteria is applied by calculating the strength/stress ratio for each stress component. The sign of the normal stress determines if tensile or compressive strength should be used (primed quantities mean compressive). The lowest strength ratio among the following three equations determines the ratio that controls the failure of the composite.

$$R_x = \frac{X}{\sigma_x} \text{ if } \sigma_x > 0, \quad \text{or} \quad R_x' = \frac{X'}{|\sigma_x|} \text{ if } \sigma_x < 0 \quad (5.11) \quad \text{contd.}$$

$$R_y = \frac{Y}{\sigma_y} \text{ if } \sigma_y > 0, \quad \text{or} \quad R_y' = \frac{Y'}{|\sigma_y|} \text{ if } \sigma_y < 0 \quad (5.11)$$

$$R_s = \frac{S}{|\sigma_s|}$$

where X = Longitudinal tensile strength
 X' = Longitudinal compressive strength
 Y = Transverse tensile strength
 Y' = Transverse compressive strength
 S = Longitudinal shear strength

When the applied stress component is unity, the resulting strength ratio is the strength.

Most of the other failure theories of isotropic materials are applied on the principal stresses (σ_1 , σ_2 and σ_3) within the structure. The state of stress at a point is first transformed (via Mohr's circle for instance) to obtain the principal stresses.

For ductile materials, Tresca proposed the following yield criteria

$$\max \{ 0.5 |\sigma_1 - \sigma_2|, 0.5 |\sigma_2 - \sigma_3|, 0.5 |\sigma_3 - \sigma_1| \} = \tau_y \quad (5.12)$$

where τ_y is the yield limit in simple shear, which is, for ductile materials, set equal to the shearing stress at yield in simple tension or compression.

According to the maximum normal stress theory, a brittle material fails when any of the principal stresses reaches the ultimate value, i.e.,

$$\max \{ |\sigma_1|, |\sigma_2|, |\sigma_3| \} = \sigma_u \quad (5.13)$$

The maximum stress criteria is often used because of its simplicity, but it has significance for one-dimensional state, and its use in multidimensional stress state must be made with caution. Again we should avoid extending the simplistic failure modes based on maximum stress components to fiber, matrix and interfacial failure modes because the micromechanics of failure is highly coupled and does not reduce to clearly defined modes of two or three types.

5.6 VERIFICATION OF THE THEORETICAL MODEL

To place the present theory in proper perspective and to test the validity of the analysis, we numerically simulated some trial cases and made comparisons with some of the already published exact solutions. The reported results are based upon displacement boundary formulation since this has traditionally led to better agreement with experimental measurements of composite moduli.

a. Effective Moduli

Expressions and bounds for the five effective elastic moduli of a unidirectional fiber composite, consisting of transversely isotropic fibers and matrix, had been derived by Hashin [48] on the basis of analogies between isotropic and transversely isotropic elasticity equations. Using the properties of a graphite/epoxy system, the bounds, along with the calculated results, at various fiber volume fraction, c , are listed in Table 5.1 below. (values within paranthesis indicate lower and upper bound respectively)

Table 5.1: Comparison of elastic moduli
(Hashin's results and present analysis)

c	$E_A \times 10^3 \text{ MPa}$	ν_A	$G_A \times 10^3 \text{ MPa}$	$K \times 10^3 \text{ MPa}$	$G_T \times 10^3 \text{ MPa}$
0.16	58.116	.32407	1.3804	4.5697	1.4931
	(58.116,	(.3217,	(1.3804,	(4.5684,	(1.4766,
	58.131)	.32407)	1.3855)	4.5972)	1.5141)
0.25	88.8597	.3098	1.4404	4.7619	1.6407
	(88.8597,	(.3067,	(1.4404,	(4.7530,	(1.6045,
	88.8807)	.3098)	1.4478)	4.7955)	1.6622)
0.36	126.433	.2927	1.5175	5.008	1.8465
	(126.433,	(.2891,	(1.5175,	(4.995,	(1.7817,
	126.458)	.2927)	1.5271)	5.051)	1.8622)

Four out of the five effective elastic constants, namely, E_A , ν_A , G_A and K coincide with the bounds, whereas, the fifth, which is the transverse shear modulus, G_T , lies in between.

b. Stress Field Around a Fibrous Inclusion

Edwards [49] has obtained exact closed solutions for the distribution of stress around a spheroidal inclusion in an elastic body, which is in a uniform state of stress infinitely far from the inclusion. For the special case of uniaxial tension applied perpendicular to the major axis of the inclusion, as shown in Fig. 28 below, the normal stress component, σ_x , has been evaluated at the

two equatorial points, B and C, as a function of the parameter H.

By definition,

$$H = \frac{G'}{G} - 1$$

where

G' = shear modulus of the inclusion

G = shear modulus of the matrix

e.g. $H = -1$, a cavity

$H = 0$, single homogeneous medium

$H \rightarrow \infty$, rigid inclusion

Table 5.2: Comparison of stress components at the equator
(Edward's solution and present analysis)

H	σ_x at B (calculated)	σ_x at B (exact result)	σ_x at C (calculated)	σ_x at C (exact result)
- 1.0	3.15E - 06	-	2.9999	3.0
-0.5	0.7573	0.743	1.5058	1.5
0.	1.0	1.0	1.0	1.0
10.0	1.4158	1.4	0.1034	0.089
∞	1.4770	1.471	-.0317	-.035

c. Stress Field Around a Coated Continuous Fiber

The stress field in a coated continuous fiber composite subjected to thermo-mechanical

loading has been calculated by Mikata and Taya [35] by use of four concentric circular cylinder model. The target material was Ni- or SiC- coated graphite fiber/6061 aluminium composite. From the material properties used, it is noted that the matrix and the coating are isotropic, but graphite fiber is transversely isotropic. The geometrical model used in their analysis is illustrated in Figure 29.

d. Uniaxial Tension

For a uniaxial applied stress, σ_{oz} , the maximum stresses which occur at point A, within the coating, have been evaluated by changing two parameters; V_f , the volume fraction of fiber, and c/d , which is the ratio of coating thickness to fiber diameter. Their results along with our theoretical predictions are listed in table 5.3.

Table 5.3: Comparison of σ_z/σ_o at point A within the coating
(Mikata and Taya's results and present analysis)

V_f	c/d	Ni coating		SiC coating	
		M & T	Our's	M & T	Our's
0.25	1/70	1.880	1.872	4.18	4.141
	5/70	1.750	1.739	3.41	3.403
0.36	3/70	1.550	1.537	3.14	3.122
	5/70	1.480	1.468	2.80	2.784
0.49	3/70	1.320	1.308	2.64	2.610
	5/70	1.260	1.241	2.31	2.300

e. Uniform temperature change ($\Delta T > 0$)

As a special case of the formulation, Mikata and Taya obtained an explicit closed form solution for a single inhomogeneity problem (i.e. a continuous fiber embedded in an infinite matrix). Using the material properties of graphite T300 fiber and Al 6061 matrix, the following stress field was obtained for the composite subjected to a uniform temperature change, ΔT .

Table 5.4 : Stress comparison for a uniform temperature change
(Mikata and Taya's results and present analysis)

Normalised stress	Fiber			Matrix (at interface)		
	$\sigma_r/\Delta T$	$\sigma_\theta/\Delta T$	$\sigma_z/\Delta T$	$\sigma_r/\Delta T$	σ_θ/Δ	$\sigma_z/\Delta T$
M & T	8.855	8.855	5.703	8.855	-8.855	5.084
	E + 4	E + 4	E + 6	E + 4	E + 4	E - 10
Present	8.855	8.855	5.703	8.855	-8.855	-1.425
	E + 4	E + 4	E + 6	E + 4	E + 4	E - 02

5.7 SUMMARY

Generally speaking, very good agreement has been obtained between our results and the analysis of other researchers in the field. What is specially to be noted is the fact that a model has been developed to predict the effective thermoelastic properties of multidirectional coated fiber composites and the solution to the stress distribution has been obtained under a uniform

three-dimensional mechanical and/or non-mechanical loading. It is therefore very encouraging to observe that the analysis does reduce down to the available exact solutions for some of the simpler cases. This has therefore given us reasonable confidence and we can proceed to use this program for the analysis and parametric study of fiber reinforced composite materials.

5.8 THE NDSANDS PROGRAM

Micromechanical considerations in composite materials may require the use of a practical tool that can handle different constituent materials, arbitrary fiber orientations and multi-axial loading conditions. To address these requirements, the computer code called NDSANDS (N Directional Stiffness A N DStrength) has been developed. A flow chart of the program is given in Figure 30. As seen from the diagram, the program can be used either to analyze a composite or to conduct parametric study. By parametric study what is meant is that the user can change either a material property or the geometry of the composite, one single variable at a time while the remainder are kept constant, and thereby examine the change in effective properties and stress distribution as a result of different input values of the parameter selected. When changing the material property, we must insure that both the stiffness and compliance matrices remain positive definite at all times [50].

Description of the Computer Program

The computer code NDSANDS was modified so that it could be implemented on a IBM PC and generalised so that it became more efficient, user friendly and easily menu driven. What follows is a brief description of some of the procedures that were incorporated in the original program.

i) Data files FIBRE, SHEATH, MATRIX and PARTICLE which enlisted the complete set of property characterization for each one of the constituents, were created. This data is intended to be of value primarily in the preliminary selection of materials to fulfill the requirements of anticipated aerospace applications. A comprehensive list of the constituent properties is given in the next section.

ii) By a suitable choice of constituent material from each one of the material libraries, and by specifying the geometric variables, such as radii, orientation angles etc., the user can create his/her own composite. At present, one can choose two different types of fibres and two different types of sheath materials and specify a maximum of ten different orientations of the fiber.

iii) A maximum of five different composites can be analyzed simultaneously. Their effective thermoelastic properties are calculated and presented in a tabular form so that direct comparisons can be made. The stress distribution under an externally applied general three-dimensional mechanical loading and/or non-mechanical loading (specify ΔT , the temperature difference, and thereby calculate the thermal load or specify ΔC , the concentration difference, and calculate the hygrothermal load) could then be determined.

iv) The stress analysis can be carried out either in cylindrical or cartesian coordinates depending upon the user input. The computed stress components can be listed in a table or can be plotted. It is upto the user to define the grid points for listing the stress components or give the plot specifications if he/she is interested in seeing the graphs. At present, one can plot either at a constant radius (with variable angle) or at a constant angle (with variable radius). The user can change the number of grid points for listing or the plot specifications at any time when needed. Using the optimization routine, COMPLEX (FUNK), the location where each one of the stress component (cylindrical or cartesian) exhibits a maximum or a minimum can be further determined.

v) The maximum stress criteria has been incorporated into the model to predict the initial or first failure of the composites. This criteria is applied by calculating the strength/stress ratio for each stress component. The lowest strength ratio controls the failure of the composite. Similar to the stress components, the user has the option to list, optimize or plot any or all of the strength ratios.

vi) Once the effective thermoelastic properties of the composite have been calculated, the

user has the option of changing mechanical, thermal or hygrothermal loads without having to recalculate the effective properties. The original program could handle only one loading condition applied to a single composite, whereas, now with the present routine, five different composites can be analysed simultaneously under different loading conditions.

vii) Finally, the computer code NDSANDS has been set up to conduct parametric study. A composite, as already pointed out, is created by choosing constituent materials and by specifying the geometric variables. In this part of the study, the user can change either the material property or the geometry of the composite, and analyse the change in effective properties and stress distribution by inputting five different values for the parameter selected. We have also modified the code to plot the effective properties of the composite selected for analysis as a function of the parameter under consideration so that the influence of the variable could be easily discerned.

5.9 NUMERICAL RESULTS AND DISCUSSION

The second phase of the project was associated with the actual analysis of some of the advanced composite materials available. We were specially interested in analysing composites intended for high temperature applications.

In the general theory developed in first section of this report, the fiber and the coating are transversely isotropic characterized by five independent elastic constants, whereas, the matrix is isotropic in nature, and needs only two constants for material specification. Besides the elastic properties, we are also interested in knowing the hygrothermal properties such as coefficient of thermal expansion, moisture expansion, thermal conductivity, etc., of the constituents to predict the effective thermo-elastic properties of the composite. Finally, in order to calculate the strength ratios and thereby predict the initial or first failure, strength characterization in the longitudinal and transverse directions, both , under tension and compression, as well as the behaviour in shear, is required to be known, for all the concerned phases.

Thus, for a transversely isotropic constituent, we need a total of sixteen properties to carry out the study. An extensive literature survey was therefore undertaken to obtain a complete set of data for each phase. One of the major problems which we encountered while carrying out this survey was how to compile the elastic, thermal and strength properties of different constituents. In most of the reported literature, studies have been undertaken on only one aspect of the problem, say the elastic property, and the remaining two have either been ignored or not mentioned at all.

What follows now is the data that we were able to get together for different phases after an exhaustive search [51 - 77]. It should be pointed out that it is still not complete. This results from a lack of extensive testing of a given material and also from the sensitivity of the properties of different materials to fabrication and test techniques, so that comparison of data from various sources was difficult. This data is intended to be of value primarily in the preliminary selection of materials. It has been compiled to assist the designer in selecting and specifying one or more material that appears to fulfill the requirements of anticipated aerospace applications.

5.5 PROPERTY TABLES

FIBER TABLE - 1

FIBER NAME	:	T300(Gr)	Modmor II	AS4(Carbon)	Boron
PROPERTIES					
ET(Psi)	:	0.3190E+07	0.2170E+07	0.2030E+07	0.6547E+08
EA(Psi)	:	0.3277E+08	0.3370E+08	0.3408E+08	0.5405E+08
NUT	:	0.4200E+00	0.4900E+00	0.2500E+00	0.1210E+00
NUA	:	0.3000E+00	0.2790E+00	0.2000E+00	0.1300E+00
GA(Psi)	:	0.7003E+06	0.3480E+07	0.4008E+07	0.2742E+08
ALFAT(1/°F)	:	0.1500E-04	0.5000E-05	0.1000E-04	0.2700E-05
ALFAA(1/°F)	:	-0.8340E-06	-0.2000E-06	-0.2000E-06	0.2700E-05
BETAT(1/%M)	:	0.0000E+00	0.0000E+00	0.0000E+00	0.0000E+00
BETAA(1/%M)	:	0.0000E+00	0.0000E+00	0.0000E+00	0.0000E+00
MUT(Btu/hr-ft-°F)	:		0.4831E+01	0.3750E+01	
MUA(Btu/hr-ft-°F)	:		0.4831E+02	0.1386E+02	
LULT(Psi)	:	0.4408E+06	0.4250E+06	0.5207E+06	0.4600E+06
LULC(Psi)	:		0.3335E+06	0.3335E+06	0.6000E+06
TULT(Psi)	:		0.4500E+05	0.5076E+05	0.3300E+06
TULC(Psi)	:				0.3000E+05
LS(Psi)	:		0.6000E+04	0.1200E+05	

FIBER TABLE - 2

FIBER NAME	:	E-Glass	AS (Graphite)	S2-Glass	Beryllium
PROPERTIES					
ET(Psi)	:	0.1053E+08	0.2000E+07	0.1250E+08	0.4200E+08
EA(Psi)	:	0.1053E+08	0.3200E+08	0.1250E+08	0.4200E+08
NUT	:	0.2200E+00	0.2500E+00	0.2200E+00	0.3000E-01
NUA	:	0.2200E+00	0.2000E+00	0.2200E+00	0.3000E-01
GA(Psi)	:	0.4316E+07	0.5000E+07	0.5100E+07	0.2040E+08
ALFAT(1/°F)	:	0.2780E-05	0.5000E-05	0.2780E-05	0.6450E-05
ALFAA(1/°F)	:	0.2780E-05	-0.2000E-06	0.2780E-05	0.6450E-05
BETAT(1/%M)	:	0.0000E+00	0.0000E+00	0.0000E+00	0.0000E+00
BETAA(1/%M)	:	0.0000E+00	0.0000E+00	0.0000E+00	0.0000E+00
MUT(Btu/hr-ft-°F)	:	0.6250E+00	0.4831E+01	0.4830E+00	0.8455E+02
MUA(Btu/hr-ft-°F)	:	0.6250E+00	0.4831E+02	0.4830E+00	0.8455E+02
LULT(Psi)	:	0.4979E+06	0.4500E+06	0.7000E+06	0.1300E+06
LULC(Psi)	:	0.7250E+05	0.3335E+06	0.7250E+05	0.1400E+06
TULT(Psi)	:	0.4979E+06	0.5000E+05	0.7000E+06	0.1300E+06
TULC(Psi)	:	0.7250E+05		0.7250E+05	0.1400E+06
LS(Psi)	:	0.2500E+06	0.2500E+05	0.3500E+06	

FIBER TABLE - 3

FIBER NAME	:	Nicalon	AVCO	HM(Carbon)
<hr/>				
PROPERTIES				
ET(Psi)	:	0.2900E+08	0.6000E+08	0.1500E+07
EA(Psi)	:	0.2900E+08	0.6000E+08	0.5200E+08
NUT	:	0.2987E+00	0.2500E+00	0.3600E+00
NUA	:	0.2987E+00	0.2500E+00	0.2600E+00
GA(Psi)	:	0.1117E+08	0.2400E+08	0.2090E+07
ALFAT(1/°F)	:	0.1778E-05	0.2330E-05	0.4390E-05
ALFAA(1/°F)	:	0.1778E-05	0.2330E-05	-0.4230E-06
BETAT(1/%M)	:	0.0000E+00	0.0000E+00	0.0000E+00
BETAA(1/%M)	:	0.0000E+00	0.0000E+00	0.0000E+00
MUT(Btu/hr-ft-°F)	:	0.6710E+01	0.2367E+02	
MUA(Btu/hr-ft-°F)	:	0.6710E+01	0.2367E+02	
LULT(Psi)	:	0.4000E+06	0.5000E+06	0.2700E+06
LULC(Psi)	:	0.2560E+06	0.2559E+06	0.2900E+06
TULT(Psi)	:	0.4000E+06	0.5000E+06	
TULC(Psi)	:	0.2560E+06	0.2559E+06	
LS(Psi)	:			

SHEATH TABLE

SHEATH NAME	:	Ni	SiC	Polyimide	Carbon
PROPERTIES					
ET(Psi)	:	0.3001E+08	0.7003E+08	0.4522E+06	0.1320E+07
EA(Psi)	:	0.3001E+08	0.7003E+08	0.4522E+06	0.1320E+07
NUT	:	0.3100E+00	0.1900E+00	0.3300E+00	0.1100E+00
NUA	:	0.3100E+00	0.1900E+00	0.3300E+00	0.1100E+00
GA(Psi)	:	0.1145E+08	0.2943E+08	0.1700E+06	0.5946E+06
ALFAT(1/°F)	:	0.7390E-05	0.2411E-05	0.3000E-04	0.1220E-05
ALFAA(1/°F)	:	0.7390E-05	0.2411E-05	0.3000E-04	0.1220E-05
BETAT(1/%M)	:	0.0000E+00	0.0000E+00		
BETAA(1/%M)	:	0.0000E+00	0.0000E+00		
MUT(Btu/hr-ft-°F)	:			0.1700E+01	0.1200E+03
MUA(Btu/hr-ft-°F)	:			0.1700E+01	0.1200E+03
LULT(Psi)	:	0.4596E+05	0.8004E+05		0.5600E+04
LULC(Psi)	:				0.7600E+04
TULT(Psi)	:	0.4596E+05	0.8004E+05		0.5600E+04
TULC(Psi)	:				0.7600E+04
LS(Psi)	:				0.2920E+04

MATRIX TABLE

MATRIX NAME	:	EPON 828	H3501-6	X7002-T6(A1)	Graphite
PROPERTIES					
E(Psi)	:	0.4200E+06	0.6200E+06	0.1037E+08	0.1410E+07
G(Psi)	:	0.1560E+06	0.2300E+06	0.3900E+07	0.6350E+06
ALFA(1/°F)	:	0.2667E-04	0.2272E-04	0.1334E-04	0.3340E-05
BETA (1/%M)	:	0.3200E-02	0.3200E-02		
MU(Btu/hr-ft-°F)	:	0.1420E+00	0.1420E+00	0.1280E+03	0.1200E+03
ULT(Psi)	:	0.1025E+05	0.1200E+05	0.5400E+05	0.3000E+04
ULC(Psi)	:	0.2610E+05	0.3000E+05	0.6750E+05	0.7600E+04
S(Psi)	:	0.5125E+04	0.6000E+04	0.3240E+05	0.3000E+04

MATRIX NAME	:	A 277-15(P)	Al 6061	SiC	E-Glass
PROPERTIES					
E(Psi)	:	0.7330E+06	0.9947E+07	0.5600E+08	0.1050E+08
G(Psi)	:	0.3330E+06	0.3698E+07	0.2441E+08	0.4303E+07
ALFA(1/°F)	:		0.1305E-04	0.2500E-05	0.1583E-04
BETA (1/%M)	:				
MU(Btu/hr-ft-°F)	:	0.1200E+03		0.2367E+02	0.2050E+00
ULT(Psi)	:	0.3330E+04	0.4495E+05	0.2250E+05	0.1150E+05
ULC(Psi)	:	0.6670E+04		0.8200E+05	0.3400E+05
S(Psi)	:	0.6010E+04		0.3000E+05	0.5750E+04

MATRIX NAME	:	ATJS(Carbon)	Cer-VIT	Zinc Bromide	Al Oxide
PROPERTIES					
E(Psi)	:	0.1320E+07	0.1340E+08	0.3632E+08	0.4500E+08
G(Psi)	:	0.5946E+06	0.5317E+07	0.1600E+08	0.1800E+08
ALFA(1/°F)	:	0.1220E-05		0.3300E-05	
BETA (1/%M)	:				
MU(Btu/hr-ft-°F)	:	0.1200E+03	0.9670E+00	0.1500E+02	0.1500E+02
ULT(Psi)	:	0.5600E+04	0.1900E+06	0.2250E+05	0.4000E+05
ULC(Psi)	:	0.7600E+04		0.2000E+06	0.3500E+06
S(Psi)	:	0.2920E+04		0.6500E+05	0.4000E+05

MATRIX NAME	:	Titanium	Mg Oxide	LAS III	PMAS III
PROPERTIES					
E(Psi)	:	0.1500E+08	0.2832E+08	0.1276E+08	0.1537E+08
G(Psi)	:	0.5770E+07	0.1200E+08	0.5221E+07	0.6236E+07
ALFA(1/°F)	:	0.5000E-05		0.8334E-06	0.1500E-05
BETA (1/%M)	:				
MU(Btu/hr-ft-°F)	:	0.9660E+01	0.2500E+02		
ULT(Psi)	:	0.1350E+06	0.1400E+05		
ULC(Psi)	:		0.2000E+06		
S(Psi)	:		0.2400E+05		

MATRIX NAME	:	1723 Glass	MAS-LZN	7052 Glass	7050 Glass
-------------	---	------------	---------	------------	------------

PROPERTIES

E(Psi)	:	0.1276E+08	0.1500E+08	0.8200E+07	0.8700E+07
G(Psi)	:	0.5221E+07	0.6250E+07	0.3361E+07	0.3566E+07
ALFA(1/°F)	:	0.2889E-05	0.4300E-05	0.2872E-05	0.2967E-05
BETA (1/%M)	:				
MU(Btu/hr-ft-°F)	:				
ULT(Psi)	:		0.5000E+04		
ULC(Psi)	:		0.1000E+06		
S(Psi)	:				

MATRIX NAME	:	7070 Glass	7740 Glass	1720 Glass	9741 Glass
-------------	---	------------	------------	------------	------------

PROPERTIES

E(Psi)	:	0.7400E+07	0.9100E+07	0.1270E+08	0.7200E+07
G(Psi)	:	0.3033E+07	0.3792E+07	0.5121E+07	0.2927E+07
ALFA(1/°F)	:	0.2167E-05	0.1944E-05	0.2789E-05	0.2722E-05
BETA (1/%M)	:				
MU(Btu/hr-ft-°F)	:				
ULT(Psi)	:				
ULC(Psi)	:				
S(Psi)	:				

MATRIX NAME : CAS I

PROPERTIES

E(Psi) : 0.1276E+08

G(Psi) : 0.5221E+07

ALFA(1/°F) : 0.2777E-05

BETA (1/%M) :

MU(Btu/hr-ft-°F) :

ULT(Psi) :

ULC(Psi) :

S(Psi) :

PARTICLE TABLE

PARTICLE NAME : WC Glass Quartz sand

PROPERTIES

E(Psi) : 0.1020E+09 0.1020E+08 0.1067E+08

G(Psi) : 0.4180E+08 0.4215E+07 0.4269E+07

ALFA(1/°F) :

BETA (1/%M) :

MU(Btu/hr-ft-°F) :

ULT(Psi) :

ULC(Psi) :

S(Psi) :

5.10 ILLUSTRATIVE PROBLEM

We now consider a three-dimensional fibrous composite by arranging six fibers parallel to the six lines joining the opposite vertices of a regular icosahedron. These six axes can be oriented with reference to an orthogonal cartesian coordinate system $x_1 x_2 x_3$ as follows: one pair in the $x_1 x_2$ plane making angles of θ' with the x_1 -axis, one pair in the $x_2 x_3$ plane making angles of θ' with the x_2 -axis, and one pair in the $x_3 x_1$ plane making angles of θ' with the x_3 -axis, where $\theta' = \tan^{-1}(2 \sin 18^\circ) = 31^\circ 43'$.

As shown by Rosen and Shu [77], this type of arrangement gives rise to local isotropy.

The isotropic relation $G = E / [2.0 (1.0 + \nu)]$ can be used as an independent check of the model. In general, this relation is not satisfied exactly in the present analysis, however the error is very small. The results for the Nicalon fiber and BMAS matrix system are shown in table 5.6. Also shown in the table is the effect of different coating thicknesses and coating materials on the effective thermoelastic moduli. The fiber volume fraction was set at 30% but the ratio of coating thickness to the cylinder outer radius, defined as $(r_2 - r_1) / r_3$, was treated as an independent variable.

As seen from table 5.6 below, both carbon and polyimide coatings, because of their lower elastic moduli compared to the BMAS matrix, reduce the effective elastic properties, whereas, nickel, with a higher moduli, adds to the reinforcement. The thermal expansion coefficient of the composite, on the other hand, is influenced more by nickel and polyimide coatings because of the larger degree of mismatch between the constituents.

The microstress distribution within the constituents, for a multidirectional fiber composite, in general, depends both on the type of loading and the fiber orientation. As an approximation, the curing or residual stresses can be estimated by subjecting the composite to a

uniform temperature change. For the specific three-dimensional composite under consideration, the stress distribution remains identical for the six fiber orientations for a unit degree cool down.

In this problem, the only non-zero stress components predicted by the present model are σ_r , σ_θ and σ_z . The stress concentration is a function of both Young's modulus and the thermal expansion coefficient of the coating, besides its thickness. The effect of different coating materials and/or thicknesses on the stress concentrations is quite dramatic. These trends are illustrated in tables 5.7 (a), 5.7 (b) and 5.7 (c) for the components σ_r , σ_θ and σ_z , respectively.

The radial stress component at the interface can be considered as a failure criteria for debonding, e.g., a negative value of σ_r promotes contact between the constituents, whereas, a positive value suggests possible separation and initiation of debonding at the boundary. It is seen that a 'thick' coating of a 'soft' material with a 'low' coefficient of thermal expansion helps in reducing the stress concentration factor at the boundary. Within the coating, the algebraic maximum hoop stress occurs at the fiber-coating interface, whereas, in the matrix, the maximum occurs at the coating-matrix interface. Even though the polyimide coating has a low elastic modulus (3.1 GPa), but because of its high coefficient of thermal expansion ($54 \times 10^{-6}/^\circ\text{C}$), the magnitude of the constituents stress components for the Nicalon/Polyimide/BMAS composite are still large in magnitude for a unit degree cool down.

To conclude, it is apparent that generally a reduction in the stress concentration can be made at the expense of the elastic moduli of the composite. Further, by a proper choice of coating thickness, modulus and coefficient of thermal expansion, the stress component of interest, which is instrumental in causing a specific mode of failure, can be controlled.

TABLE 5.6: Three-dimensional ' isotropic ' composite, effective moduli

<u>Coating thickness</u>	Composite system	E	v	G	α
Cylinder outer radius		(GPa)		(GPa)	(10 ⁻⁶ /°C)
0	Nicalon/BMAS	128.16	0.250	51.25	2.89
0.01	Nicalon/Nickel/ BMAS	129.11	0.251	51.60	3.04
	Nicalon/Carbon/ BMAS	118.06	0.243	47.50	2.88
	Nicalon/Polyimide/ BMAS	106.01	0.249	42.45	3.24
0.10	Nicalon/Nickel/ BMAS	138.72	0.259	55.10	4.45
	Nicalon/Carbon/ BMAS	80.20	0.217	32.94	2.84
	Nicalon/Polyimide/ BMAS	65.93	0.234	26.72	4.76

TABLE 5.7 (a) : Stress component σ_r in the fiber-coating and coating-matrix interface for $\Delta T = -1^\circ \text{C}$

<u>coating thickness</u> cylinder outer radius	Composite system	$(\sigma_r)_{f-c}$ (KPa)	$(\sigma_r)_{c-m}$ (KPa)
0	Nicalon/BMAS	26.4	26.4
0.01	Nicalon/Nickel/ BMAS	-8.98	44.9
	Nicalon/Carbon/ BMAS	22.8	22.3
	Nicalon/Polyimide/ BMAS	104.0	107.0
0.10	Nicalon/Nickel/ BMAS	-290.0	140.0
	Nicalon/Carbon/ BMAS	8.54	5.95
	Nicalon/Polyimide/ BMAS	293.0	306.0

TABLE 5.7 (b) : Stress component σ_θ (algebraic maximum) in the fiber, coating and matrix for $\Delta T = -1^\circ \text{C}$

<u>coating thickness</u> cylinder outer radius	Composite system	$(\sigma_\theta)_f$ (KPa)	$(\sigma_\theta)_c$ (KPa)	$(\sigma_\theta)_m$ (KPa)
0	Nicalon/BMAS	26.4	-	-55.6
0.01	Nicalon/Nickel/ BMAS	-8.98	3020.0	-97.5
	Nicalon/Carbon/ BMAS	22.8	-7.46	-50.7
	Nicalon/Polyimide/ BMAS	104.0	289.0	-163.0
0.10	Nicalon/Nickel/ BMAS	-290.0	2720.0	-407.0
	Nicalon/Carbon/ BMAS	8.54	-9.63	-32.0
	Nicalon/Polyimide/ BMAS	293.0	383.0	-494.0

TABLE 5.7 (c): Stress component σ_z in the fiber, coating and matrix for $\Delta T = -1^\circ\text{C}$

<u>coating thickness</u> cylinder outer radius	Composite system	$(\sigma_z)_f$ (KPa)	$(\sigma_z)_c$ (KPa)	$(\sigma_z)_m$ (KPa)
0	Nicalon/BMAS	77.9	-	-26.9
0.01	Nicalon/Nickel/ BMAS	26.3	3060.0	-48.4
	Nicalon/Carbon/ BMAS	77.9	-4.52	-25.5
	Nicalon/Polyimide/ BMAS	54.9	288.0	-69.7
0.10	Nicalon/Nickel/ BMAS	-424.0	2590.0	-248.0
	Nicalon/Carbon/ BMAS	76.9	-5.99	-21.0
	Nicalon/Polyimide/ BMAS	-136.0	377.0	-262.0

5.11 CONCLUDING REMARKS

In summary, we have developed a first order ideal material model to approximate the elastic response of a composite body reinforced by coated fibers oriented in various directions. The coating can either be applied intentionally to achieve the desirable composite properties or it can occur due to the processing conditions involved in the composite manufacture. We have further demonstrated, through a parametric study, how an applied coating modifies the micro stress distribution and the elastic properties of a three-dimensional Nicalon/BMAS system. The model can be used to provide material guidance to control the micromechanical failure modes. In conjunction with a disciplined experimental program, studies such as those conducted here, can be employed to direct further improvements in the model, such as the capability to handle discontinuity of some of the traction and /or displacement components at the boundary. This formulation will be the subject of future work to be undertaken.

REFERENCES

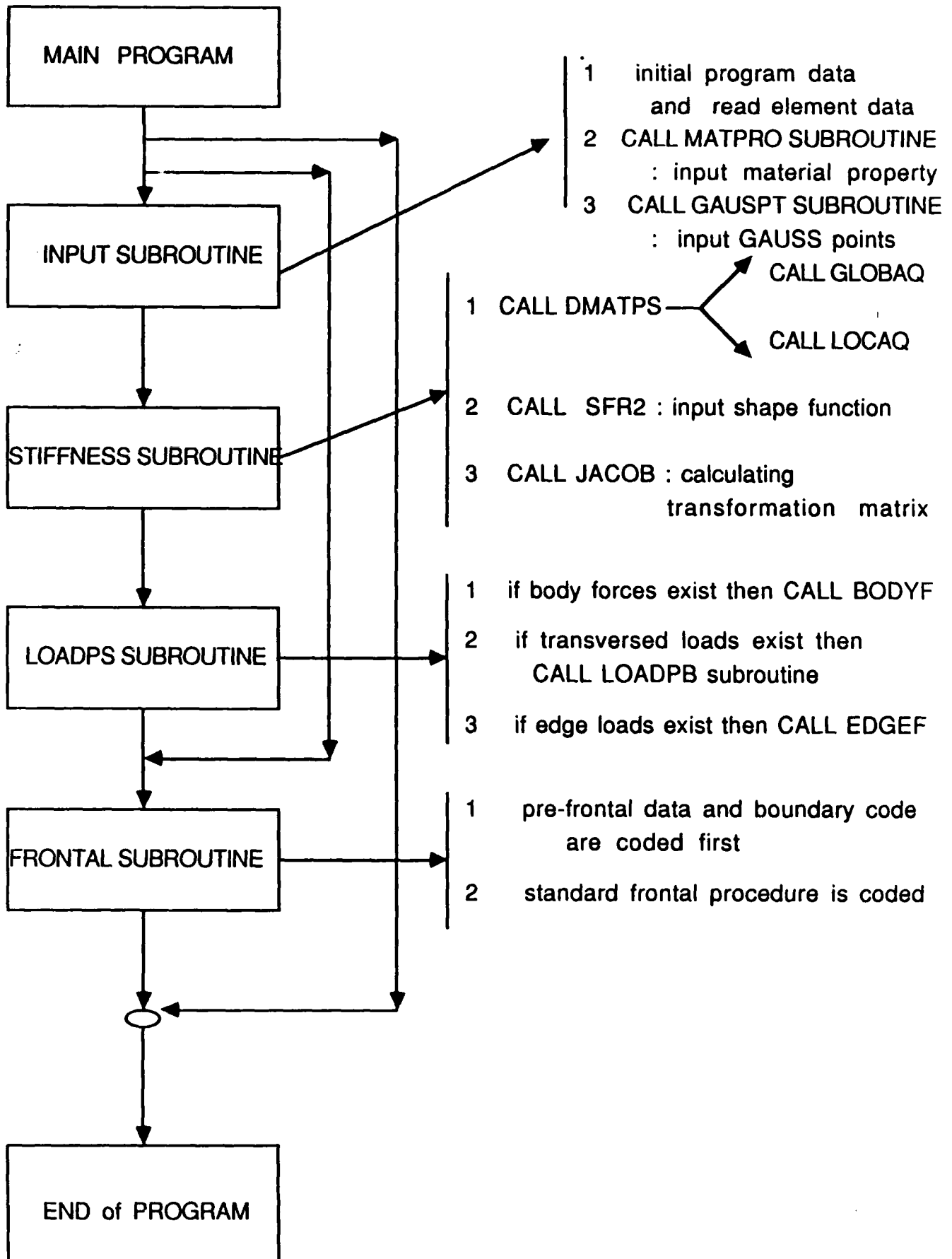
1. N. J. Pagano and R.B. Pipes, "Some Observations on the Interlaminar Strength of Composite Laminates", *Int. J. Mech. Sci.*, Vol. 15, p. 679, 1973.
2. L. B. Greszczuk, "Failure Mechanics of Composites Subjected to Compressive Loading", *AFML-TR-72-107*, Air Force Material Laboratory Report V, 1973.
3. S. V. Kulkarni, J.S. Rice, and B.W. Rosen, "An Investigation of the Compressive Strength of PRD-49-III/Epoxy Composites", *NASA CR-112334*, 1975.
4. F. H. Chang, D.E. Gordon, B.T. Rodini, R. H. McDaniel, "Real Time Characterization of Damage Growth in Graphite/Epoxy Laminates", *J. Comp. Mat.*, Vol. 10, p. 182, 1976.
5. *Composite Design*, Ed: S.W. Tsai, 4th Edition, Dayton, Ohio, 1988.
6. P. C. Yang, C.H. Norris, and Y. Stavsky, "Elastic Wave Propagation in Heterogeneous Plates", *Int. J. Sol. Struct.*, Vol.2, p. 665, 1966.
7. N. J. Pagano, "Exact Solutions for Rectangular Bidirectional Composites and Sandwich Plates", *J. Comp. Mat.*, Vol. 4, p. 20, 1970.
8. J. M. Whitney and N. J. Pagano, "Shear Deformation in Heterogeneous Anisotropic Plates", *J. Appl. Mech.*, Vol. 37, p. 1031, 1970.
9. J. M. Whitney and C. T. Sun, "A Higher Order Theory for Extensional Motion of Laminated Composites", *J. Sound Vib.*, Vol. 30, p. 85, 1973.
10. N. J. Pagano, "On the Calculation of Interlaminar Normal Stress in Composite Laminates", *J. Comp. Mat.*, Vol.8, p. 65, 1974.
11. T. Hayashi, "Analytical Study of Interlaminar Shear Stresses in a Laminate Composite Plate", *Trans. Japan Society for Aeronautics and Space Sciences*, Vol. 10, No. 17 (1967). pp. 43-48.
12. R. L. Foye and D. J. Baker, "Design of Orthotropic Laminates", 11th Annual AIAA structural Dynamics and Materials Conference, Denver, Colorado, April 1970.
13. R. B. Pipes and N.J. Pagano, "Interlaminar Stress in Composite Laminates under Uniform Axial Extension", *J. Comp. Mat.*, Vol. 4, p. 538, 1970.
14. A.S.D.Wang and F.W. Crossman, "Some New Results on Edge Effect in Symmetric Composite Laminate", *J. Comp., Mat.*, Vol. 11, p. 92, 1977.
15. E.L. Stanton, L.M. Crain and T.L. Neu, "A Parametric Cubic Modeling System for General Solids of Composite Material", *Int. J. Num. Meth. Eng.*, Vol. 11, p. 653, 1977.
16. A. Harris, O. Orringer and E.A. Whitmer, "A Multilayer, Traction-Free-Edge, Quadrilateral Warping Element for the Stress Analysis of Composite Plates and Shell", *MIT-ASRL-TR-193-1*, 1979.
17. R. L. Spilker and S. C. Chou, "Edge Effects in Symmetric Composite Laminates: Importance of Satisfying the Traction-Free Edge Condition", *J. Comp. Mat.*, Vol. 14, p. 2, 1980.

18. S.S. Wang and F.K. Yuan, "A Singular Hybrid Finite Element in Composite Laminates", *Int. J. Solids Struct.*, Vol. 19, p. 825, 1983.
19. R. L. Spilker and T.C.T. Ting, "Stress Analysis of Composites", Army Materials and Mechanics Research Center, Watertown, Mass. Tech. Rep. AMMRC-TR-81-5, 1981.
20. I.S. Raju, J.D. Whitcomb and J.G. Goree, "A New Look at Numerical Analyses of Free Edge Stress in Composite Laminates", *NASA Tech. Paper 1751*, 1981.
21. E. Altus, A. Rotem and M. Schmueli, "Free Edge Effect in Angle-Ply Laminates: A New Three-Dimensional Finite Difference Solution", *J. Comp. Mat.*, Vol. 14, p. 21, 1980.
22. P.W. Hsu and C.T. Herakovich, "Edge Effects in Angle-ply Composite Laminates", *J. Comp. Mat.*, Vol. 11, p. 422, 1977.
23. J.T.S. Wang and J.N. Dickson, "Interlaminar Stress in Symmetric Composite Laminates", *J. Comp. Mat.*, Vol. 12, p. 390, 1978.
24. N. J. Pagano, "Stress Fields in Composite Laminates", *Technical Report*, AFML-TR-77-114, Wright Patterson AFB, 1977. Also *Int. J. Solids Struct.*, Vol. 14, p. 385, 1978.
25. N.J. Pagano and S.R. Soni, "Global-local Laminate Variational Model", *Int. J. Solids Struct.*, Vol. 19, p. 207, 1983.
26. N. J. Pagano, "Free Edge Stresses in Composite Laminates", *Technical Report*, AFML-TR-77-113, Wright Patterson AFB, 1977.
27. G. A. Cooper and A. Kelly, "Role of the Interface in the Fracture of Fiber-Composite Materials", *ASTM STP-452*, p. 90, 1969.
28. D. F. Adams, "A Micromechanical Analysis of the Influence of the Interface on the Performance of Polymer-Matrix Composites", *Proc. Amer. Soc. Comp.*, First Technical Conference, p. 207, 1986.
29. L. T. Drzal, "Composite Interphase Characterization", *SAMPE J.*, Vol. 19, No. 5, p. 7, 1983.
30. T. Ishikawa, K. Koyama and S. Kobayashi, "Thermal Expansion Coefficients of Unidirectional Composites", *J. Comp. Mat.*, Vol. 12, p. 153, 1978.
31. D. Iesan, "Thermal Stresses in Composite Cylinders", *J. Thermal Stresses*, Vol. 3, p. 495, 1980.
32. R. M. Christensen and H. Lo, "Solutions for Effective Shear Properties in Three-Phase Sphere and Cylinder Models", *J. Mech. Phys. Solids*, Vol. 27, p. 315, 1979.
33. Z. Hashin and B. W. Rosen, "The Elastic Moduli of Fiber-Reinforced Materials", *J. Appl. Mech.*, Vol. 31, p. 223, 1964.
34. Y. Takeuchi, T. Furukawa and Y. Tanigawa, "The Effect of Thermoelastic Coupling for Transient Thermal Stresses in a Composite Cylinder", *ASME, WAM, DE - 2*, 1983.
35. Y. Mikata and M. Taya, "Stress Field in a Coated Continuous Fiber Composite Subjected to Thermo-Mechanical Loadings", *J. Comp. Mat.*, Vol. 19, p. 554, 1985.

36. N.J. Pagano and L.E. Whitford, "On the Solution for the Elastic Response of Involute Bodies", *Comp. Sci. Tech.*, Vol. 22, p. 295, 1985.
37. N.J. Pagano, "Refined Solutions for the Elastic Response of Involute Bodies", *Comp. Sci. Tech.* Vol. 25, p. 251, 1986.
38. O.C. Zienkiewicz, "*The Finite Element Method*", McGraw-Hill Book Co., UK, 1979.
39. R.H. Gallagher, "*Finite Element Analysis-Fundamentals*", Prentice Hall Inc., USA, 1975.
40. T.H.H. Pian and P. Tong, "Basis of Finite Element Methods for Solid Continua", *Int. J. Num. Meth. Eng.*, Vol. 1, p. 3, 1969.
41. A.K. Noor and M.D. Mathers, "Finite Element Analysis of Anisotropic Plates", *Int. J. Num. Meth. Eng.*, Vol. 11, p. 289, 1977.
42. B.M. Irons, "A Frontal Solution Program", *Int. J. Num. Meth. Eng.*, Vol. 2, p. 532, 1970.
43. Hashin, Z., "Theory of Mechanical Behaviour of Heterogeneous Media", *Applied Mechanics Reviews*, Vol.17, p. 1, 1964.
44. Hill, R., "Elastic Properties of Reinforced Solids: Some Theoretical Principles", *J. Mech. Phys. Solids*, Vol. 11, p. 357, 1963.
45. N. J. Pagano, "The Stress Field in a Cylindrically Anisotropic Body under Two-Dimensional Surface Traction", *J. Appl. Mech.*, Vol. 38, p. 1, 1971.
46. G. P. Tandon and N. J. Pagano, "Thermo-Elastic Characterization of Coated Fiber Composites: Traction Formulation", manuscript in preparation.
47. N. J. Pagano and G. P. Tandon, "Elastic Response of Multidirectional Coated Fiber Composites", *Comp. Sci. and Tech.* , Vol. 31, p. 273, 1988.
48. Hashin, Z., "Analysis of Properties of Fiber Composites with Anisotropic Constituents", *J. Appl. Mech.*, Vol. 46, p. 543, 1979.
49. Edwards, R.H., "Stress Concentration around Spheroidal Inclusions and Cavities", *J. Appl. Mech.*, Vol. 18, p. 19, 1951.
50. R. M. Jones, *Mechanics of Composite Materials* , McGraw-Hill Book Company, New York pp. 37-45, 1975.
51. Composite Materials: Testing and Design, 2nd Conference, *ASTM STP 497*, 1972.
52. Composite Materials: Testing and Design, 4th Conference, *ASTM STP 617*, 1976.
53. Advanced Fibrous Reinforced Composites, 10th National SAMPE Symposium, Vol. 10, 1966.
54. Advances in Structural Composites, 12th National SAMPE Symposium, Vol. 12, 1967.
55. *Proceedings of the International Conference on SiC*, ed: H.K. Henisch and R. Roy, 1968.
56. *Proceedings of the American Society for Composites*, 1st Technical Conference, 1986.
57. *Proceedings of International Symposium of Composite Materials and Structures*, ed: T.T. Loo and C.T. Sun, 1986.

58. *Handbook of Composites*, ed: George Lubin, Van Nostrand Reinhold Co.
59. *Encyclopedia of Composite Materials and Components*, ed: Martin Grayson.
60. *Thermomechanical Behavior of High Temperature Composites*, ed: J. Jortner, ASME, New York.
61. *Fiberglass Reinforced Plastics Deskbook*, ed: Nicholas P. Cheremisinoff and Paul N. Cheremisinoff., Ann Arbor Science Publishers Inc., 1979
62. *Environmental Effects on Composite Materials*, Vol. 2, ed: George S. Springer, Technomic Publishing Co. Inc., 1984.
63. *Primer on Composite Materials: Analysis*, ed: J.C. Halpin, Technomic Publishing Co., Inc., 1984.
64. "Refractory Ceramics of Interest in Aerospace Structural Applications - A Materials Selection Handbook", ASD - TDR 63-4102, 1963.
65. D.E. Walrath and D.F. Adams, "Finite Element Micromechanics and Minimechanics Modeling of Three-Dimensional Carbon-Carbon Composite Materials", *Report UWME-DR-501-106-1*, December, 1985.
66. K.M. Prewo, "Elevated Temperature Performance of SiC Fiber Reinforced Glass Ceramics", *ONR Contract N 00014--81-C-0571*.
67. *Hercules Product Data Sheet No. 847-3: Magnamite Graphite Fiber Type AS4*, Hercules Inc., Magna, Utah (1981).
68. *Textile fibers for Industry*, Owens-Corning Fiberglas Corp., Toledo, Ohio , 1971.
69. *3-M Product Data Center*, Ceramic Materials Department, St. Paul, Minnesota.
70. *Dow Corning Product Data Center*, Dow Corning Corporation, Midland, Michigan.
71. R.E. Smith, "Ultrasonic Elastic Constants of Carbon Fibers and Their Composites", *J. Appl. Phys.*, Vol. 43, No. 6, p. 2555, 1972.
72. I.M. Kowalski, "Determination of the Transverse Modulus of Carbon Fibers", *SAMPE Journal*, Vol. 22, No. 4, p. 38, 1986.
73. R.D. Kriz and W.W. Stinchomb, "Elastic Moduli of Transversely Isotropic Graphite Fibers and Their Composites", *Experimental Mechanics*, p. 41, 1979.
74. C.H. Anderson and R. Warren, "Silicon Carbide Fibres and Their Potential for Use in Composite Materials, Part I ", *Composites*, Vol. 15, No. 1, p. 11, 1984.
75. S.K. Datta and H.M. Ledbetter, "Elastic Constants of Fiber Reinforced Boron-Al: Observation and Theory ", *Int. J. Solids and Structures*, Vol. 19, No. 10, p. 885, 1983.
76. H.M. Hawthorne and E. Teghtsoonian, "Axial Compression Fracture in Carbon Fibres", *J. Mat. Sci.*, Vol. 10, p. 41, 1975.
77. B. W. Rosen and L. S. Shu , "On Some Symmetry Conditions for Three-Dimensional Fibrous Composites", *J. Comp. Mat.*, Vol. 5, p. 279, 1971.

APPENDIX A



DEFINITION OF THE NOTATION

NFIA, NFIB	:	input files unit
NFOA, NFOB NFOC, NFOD	:	output files unit
MELEM	:	maximum element number per layer
MPOIN	:	maximum node number per layer
MPLY	:	total number of plies
MDIME	:	maximum number of dimension
NDOFP	:	maximum degree of freedom per node at local region.
MGASP	:	maximum number of Gauss Integral points
MEVAB	:	maximum dimension of stiffness matrix in element level
MFRON	:	maximum frontal size
MTOTV	:	total maximum variable number
MNODE	:	maximum number of nodes per element

DATA FROM UNIT = NFIA

BLOCK A
VARIABLE =

XL	XY	NX	NY	NARIDX	NGRZDY	IDGL	KSTRAN
----	----	----	----	--------	--------	------	--------

This block read grid data and number of plies of the structure.

XL	:	X coordinate
YL	:	Y coordinate
NX	:	number of nodes per side in X direction
NY	:	number of grids per side in Y direction
NGRIDX	:	number of grid in X direction
NGRIDY	:	number of grid in Y direction
IDGL	:	total number of plies of the structure
KSTRAN	:	

BLOCK B
VARIABLE =

JLIPA INCT

This block data use to determine the shape function is linear or parabolic function.

JLIPA : 1 linear shape function
2 quadratic shape function
INCT : increment

BLOCK C
VARIABLE =

NVFIX NCASE NTYPE NNODE NDOFN NMATS
NPROP NGAUS NDIME NSTRE

This block read some control data including material, dimension, ingeration, boundary and load control data.

NVFIX : total number of boundary points
NCASE : number of load case
NTYPE : parameter for output
NNODE : number of nodes per element
NDOFN : total degree of freedom per element
NMATS : parameter for different material region
NPROP : number of material properties
NGAUS : number of gauss point
NDIME : number of dimension
NSTRE : dimension of stress vector

BLOCK D
VARIABLE =

NUMEL MATNO LNDDS

This block read material ID and element connectivity.

NUMEL : element number

MATNO : region ID

LNDDS : element connectivity vector

BLOCK E
VARIABLE =

I LPSN

This block read element ID and element connectivity for linear case

I : element ID

LPSN : element connectivity vector

BLOCK F
VARIABLE =

IPOIN COORD

This block read nodes coordinates

IPOIN : node ID

COORD : node coordinates vector

BLOCK G
VARIABLE =

NOFIX IFPRE PRESE KODE

This read general boundary condition code

NOFIX : node number

IFPRE : prescribed code

 1 : prescribed displacement or load

 2 : not prescribed

PRESC : prescribed value

KODE : index of node

 1 : 1 degree of freedom per that node

 3 : 3 degree of freedom per that node

 6 : 6 degree of freedom per that node

BLOCK H
VARIABLE =

NOEND KJEND ENDPS KCOD

This block read boundary code for last plies or last layer of symetry structure

NOEND : index number

KJEND : prescribed code

 1 : prescribed displacement or load

 0 : not prescribed

ENDPS : prescribed value of displacement or load

KCOD : index of node

 1 : 1 degree of freedom of that node

 3 : 3 degree of freedom of that node

 6 : 6 degree of freedom of that node

DATA FROM UNIT = NFIB

BLOCK I
VARIABLE =

NPLY NGROPG NGROPL NINDEX

This block read group data

NPLY : total number of group
NGROPG : total number of global group
NGROPL : total number of local group
NINDEX :

BLOCK J
VARIABLE =

NGS NGE NLSE

This block read control data for global and local region

NGS : starting layer number of global vector
NGE : ending lay number of global vector
NLSE : starting layer number of local vector

BLOCK K
VARIABLE =

JPLY IGLCOD PROPS

This bolock read ply geometry and properties

JPLY : ply ID
IGLCOD : region ID
PROPS : material properties vector including angle, thickness, modulus poisson ration
 shear modulus

LIST OF FIGURES

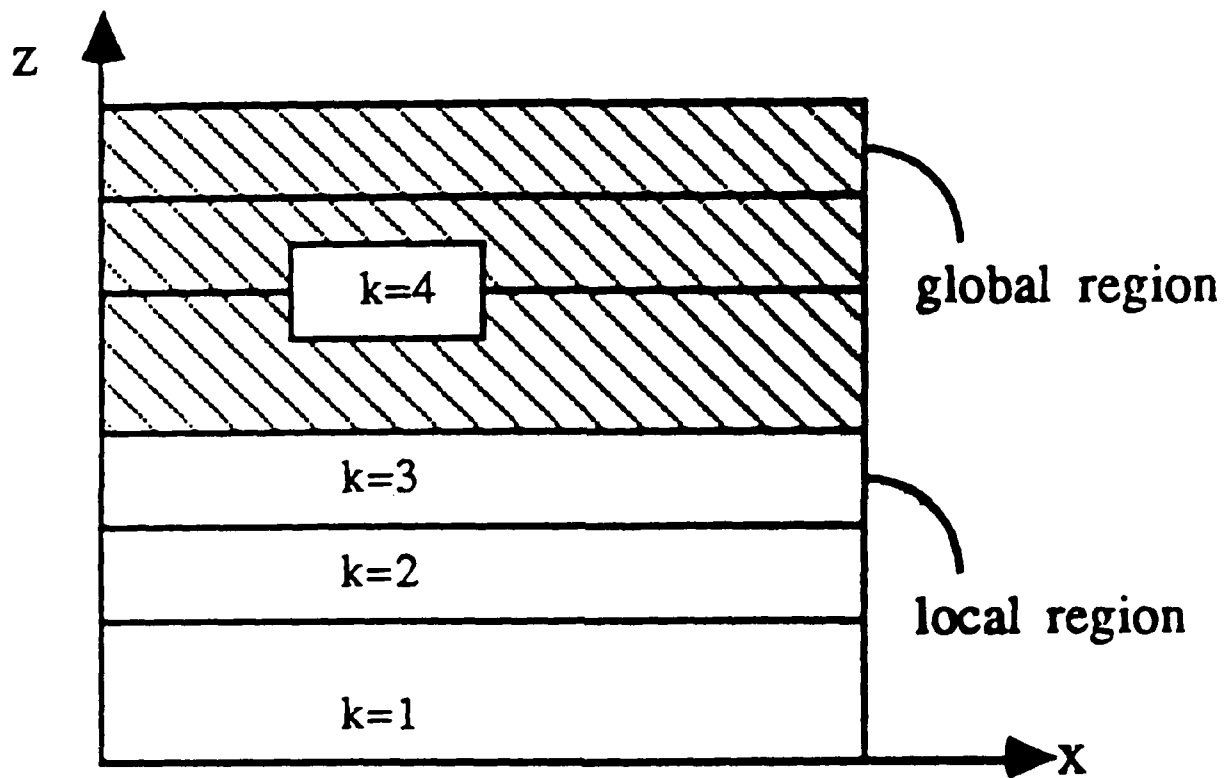


Figure 1. Global and Local Regions of Laminate

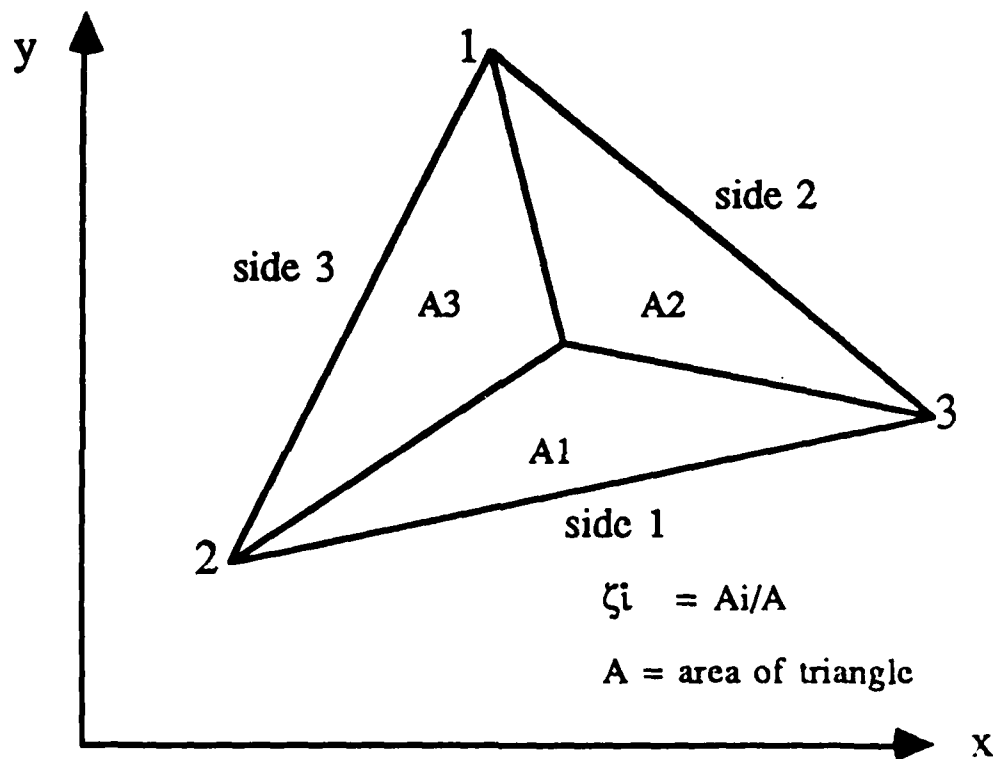


Figure 2. Triangular (Area) Coordinates

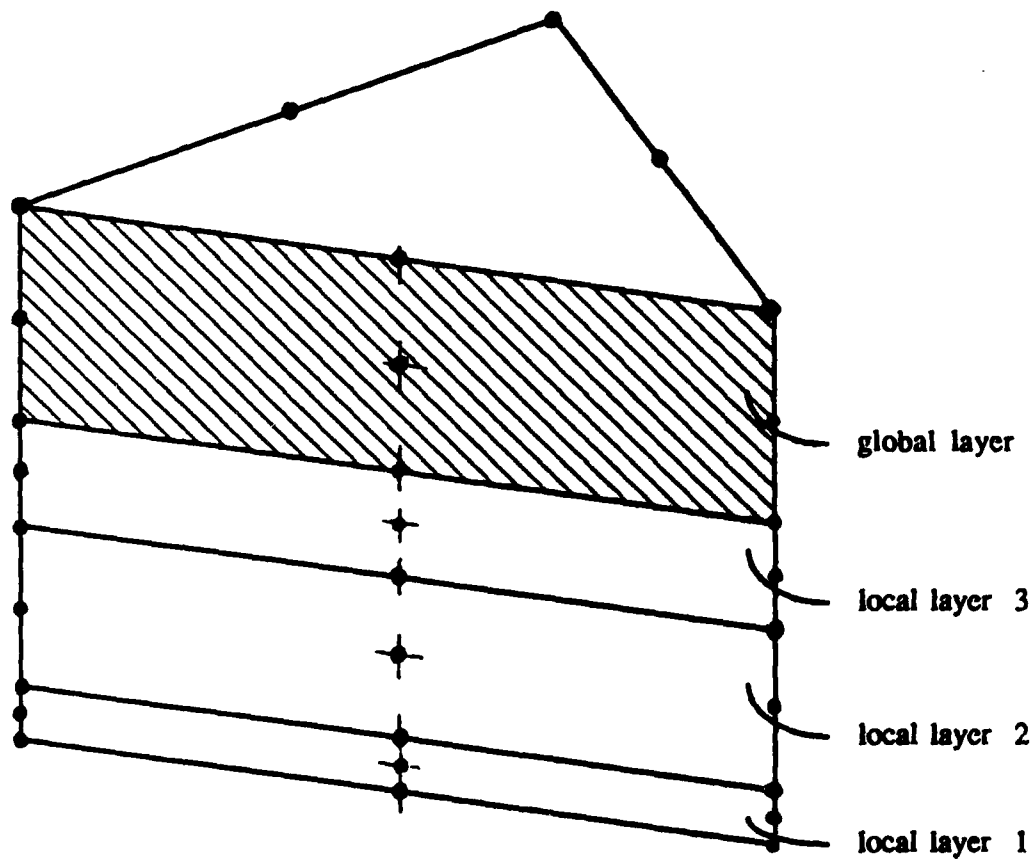


Figure 3. Composite Element with Global and Local Layers

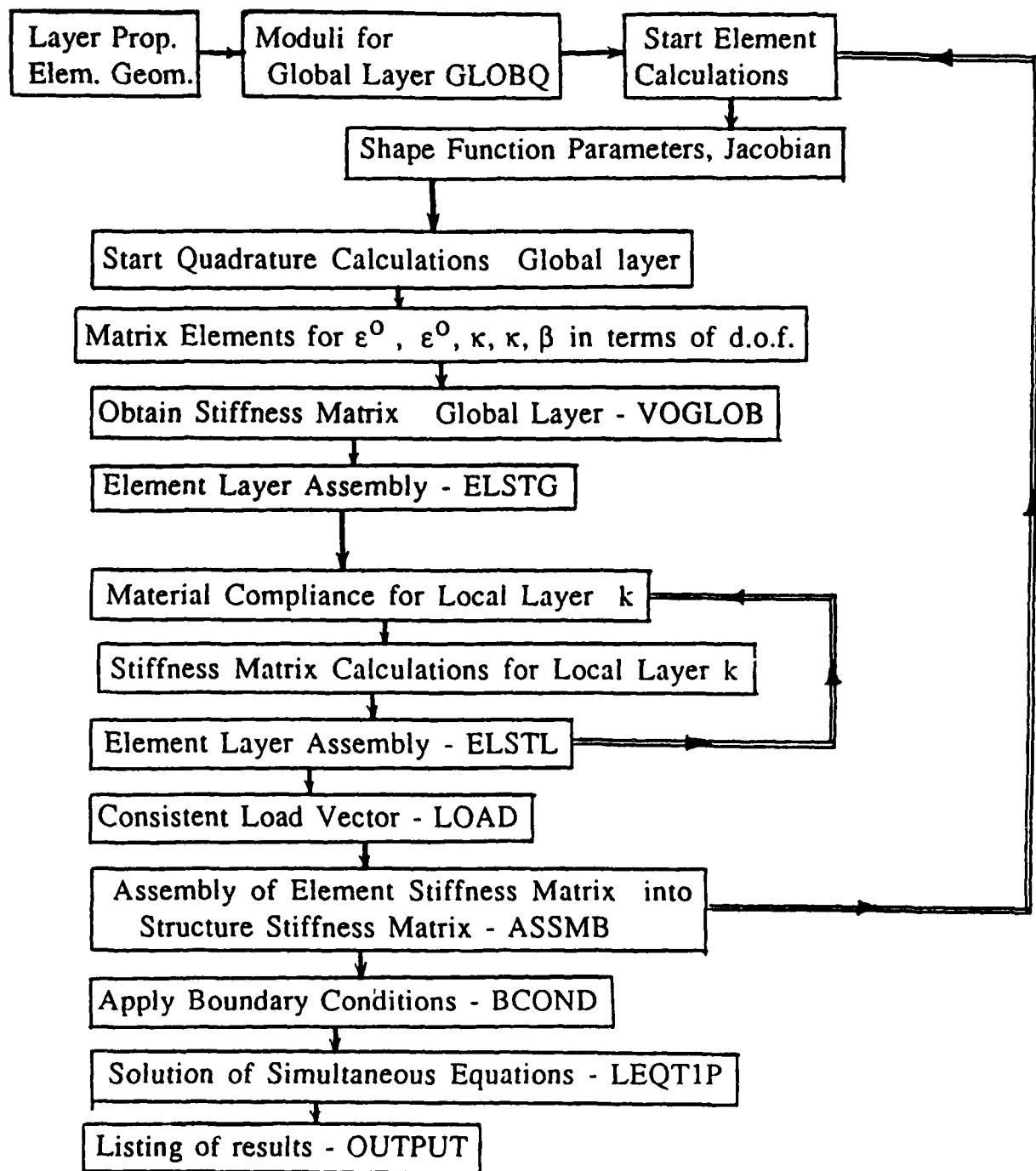
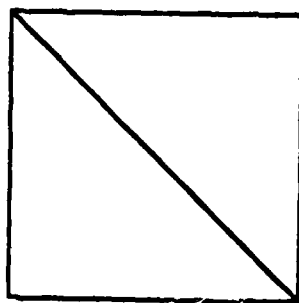
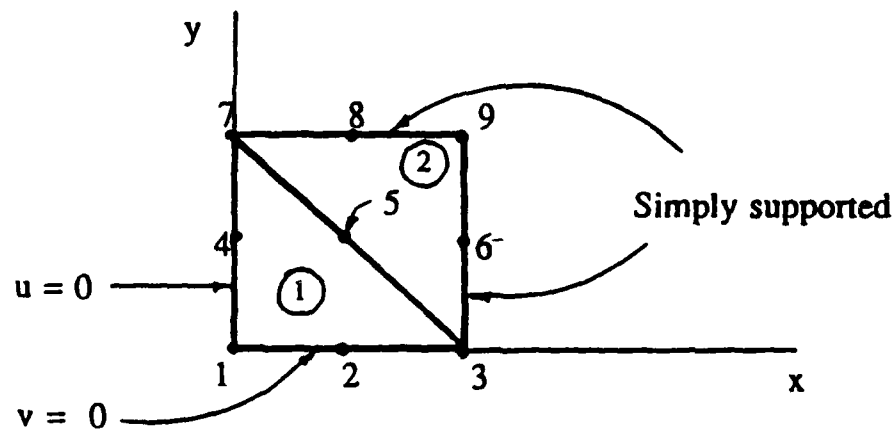
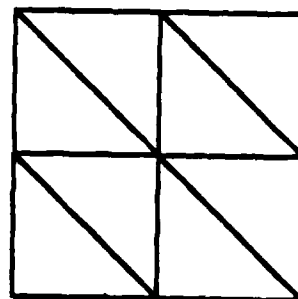


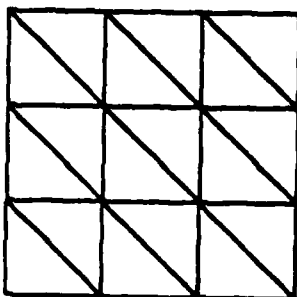
Figure 4. Flow Chart for Stiffness Finite Element Method with Global and Local Layers



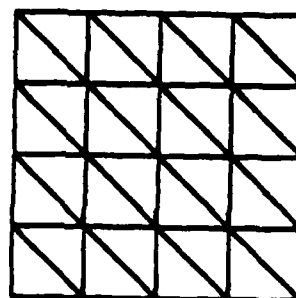
GRID 1



GRID 2



GRID 3



GRID 4

Figure 5. Finite Element Grid Pattern for Square Plate

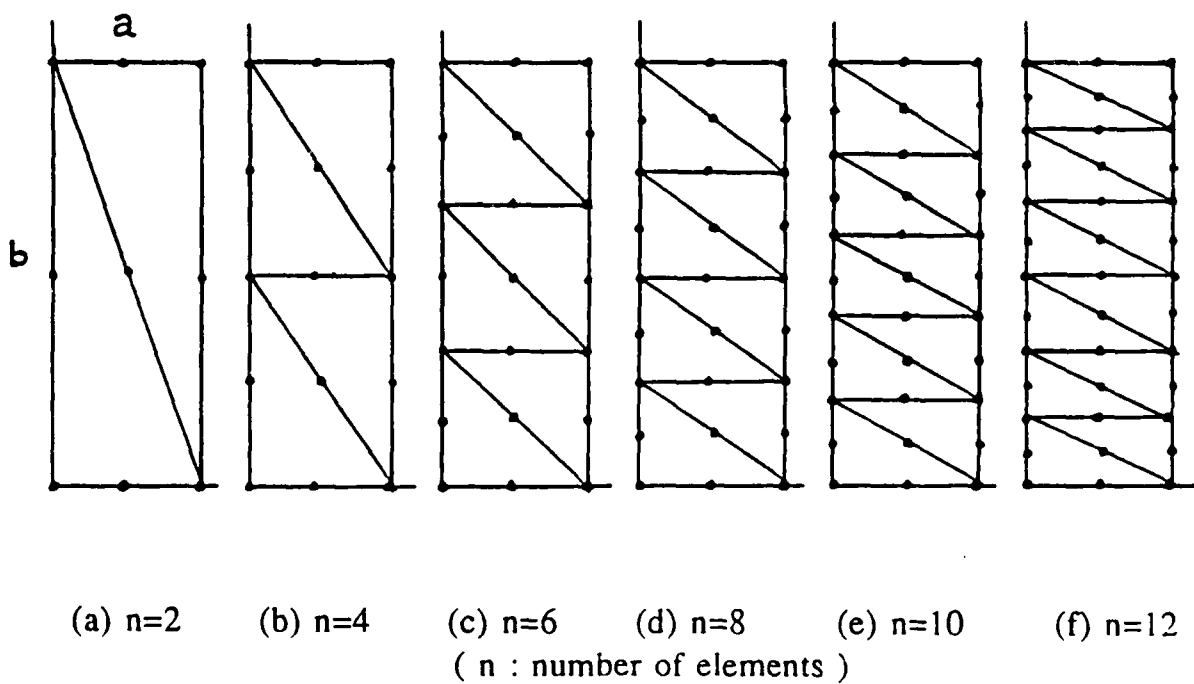
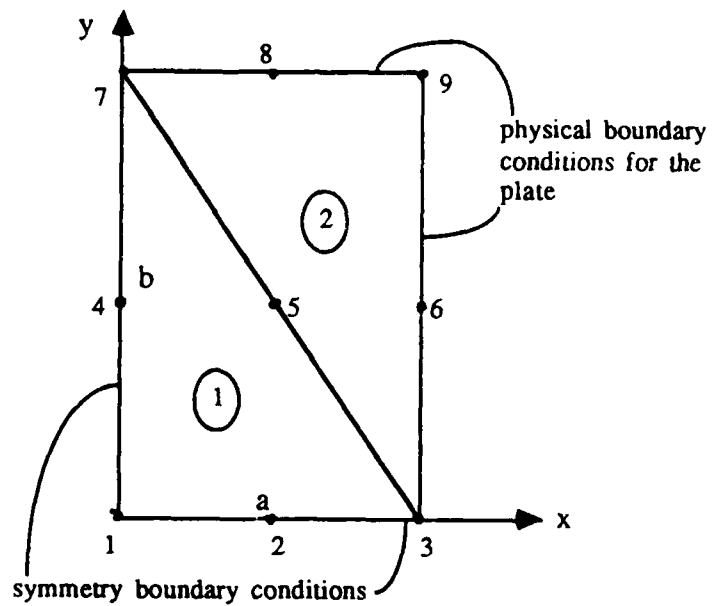


Figure 6. Finite Element Grid Pattern for Rectangular Plate

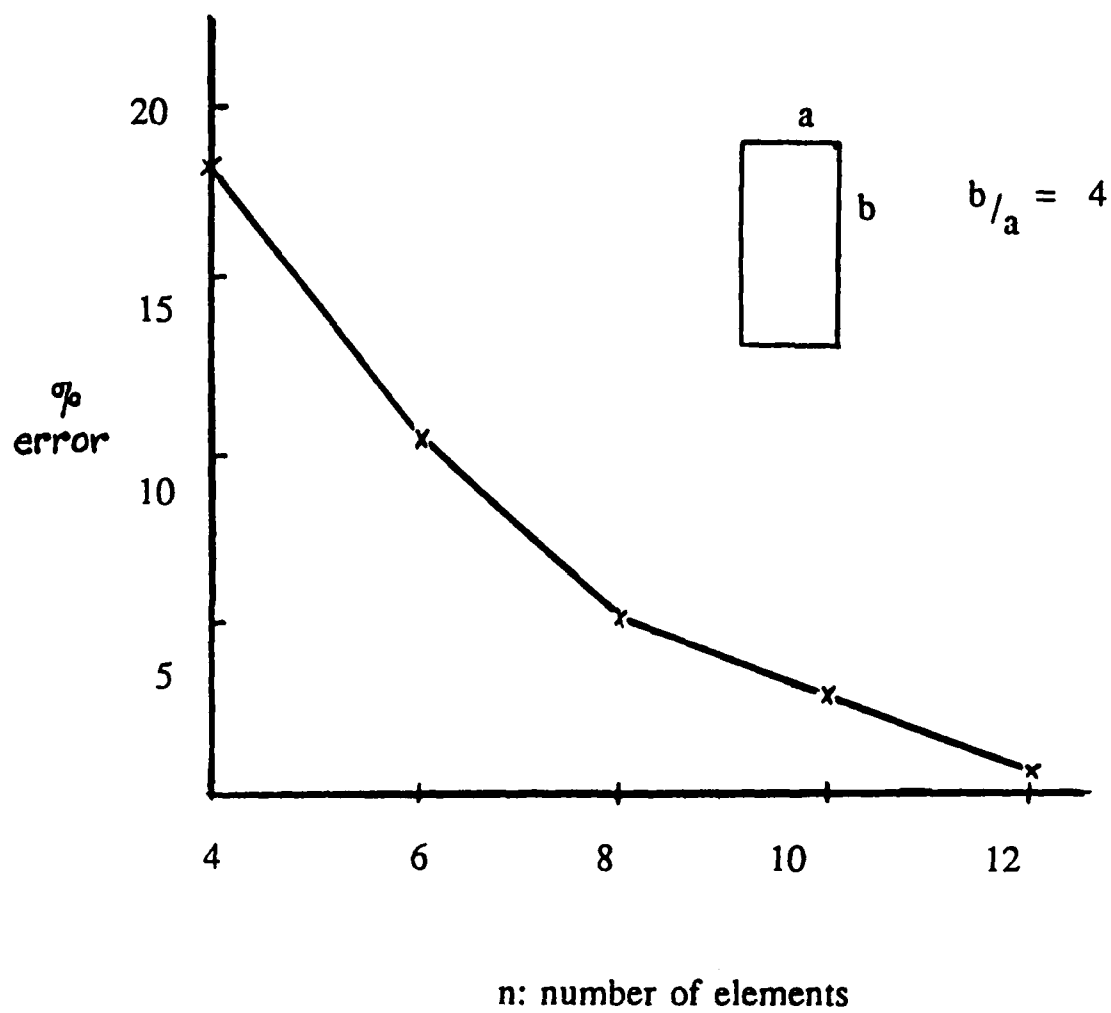


Figure 7. Convergence Study for Stiffness Finite Element Method

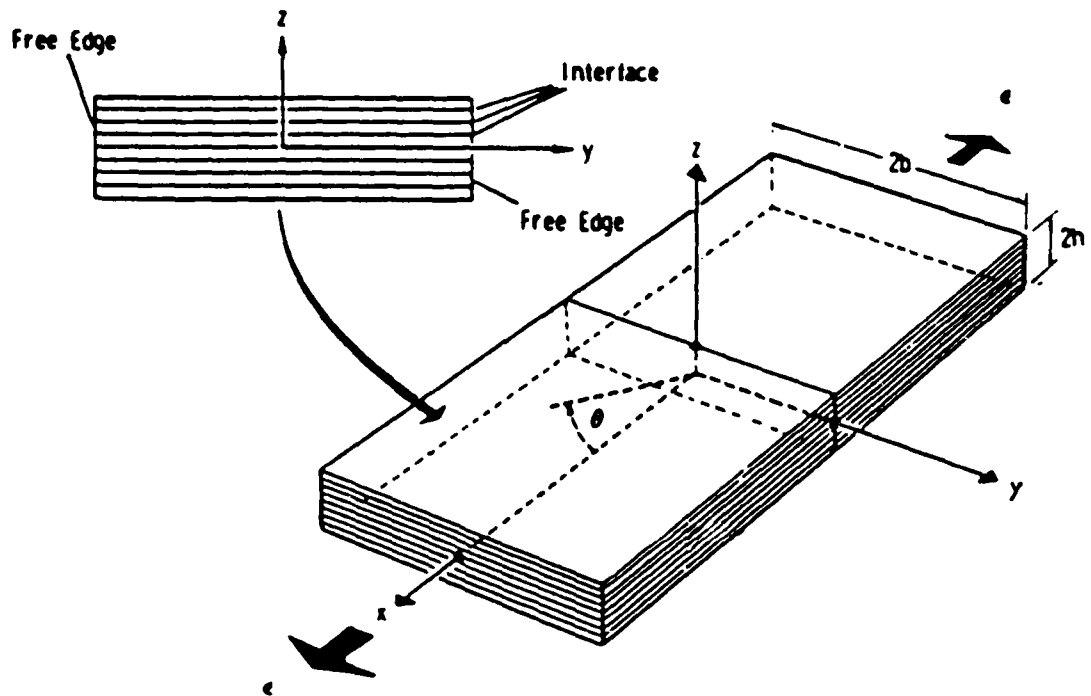


Figure 8. Laminate Geometry for Free Edge Problem

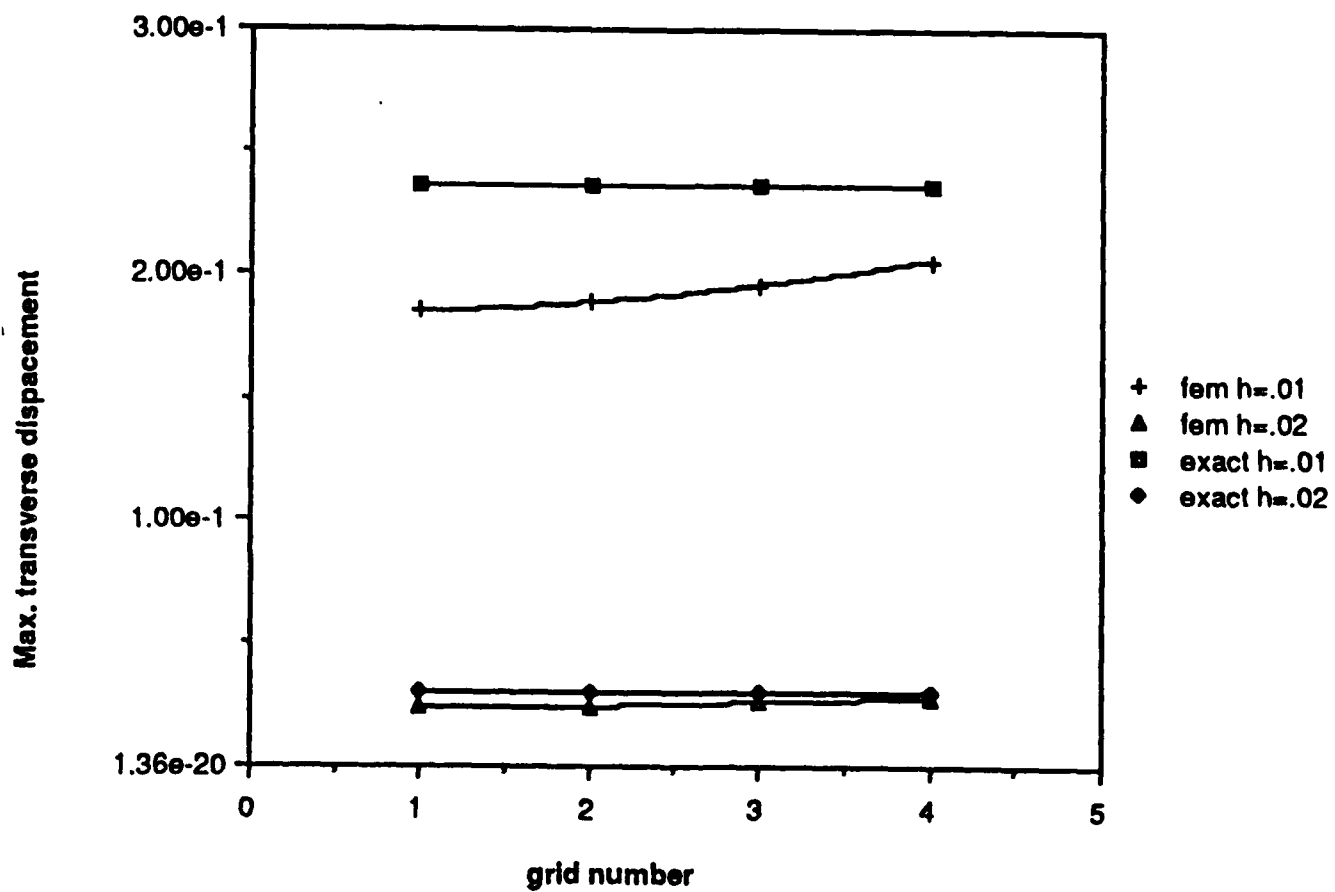


Figure 9. Convergence Study of Transverse Displacement for Rectangular Plate

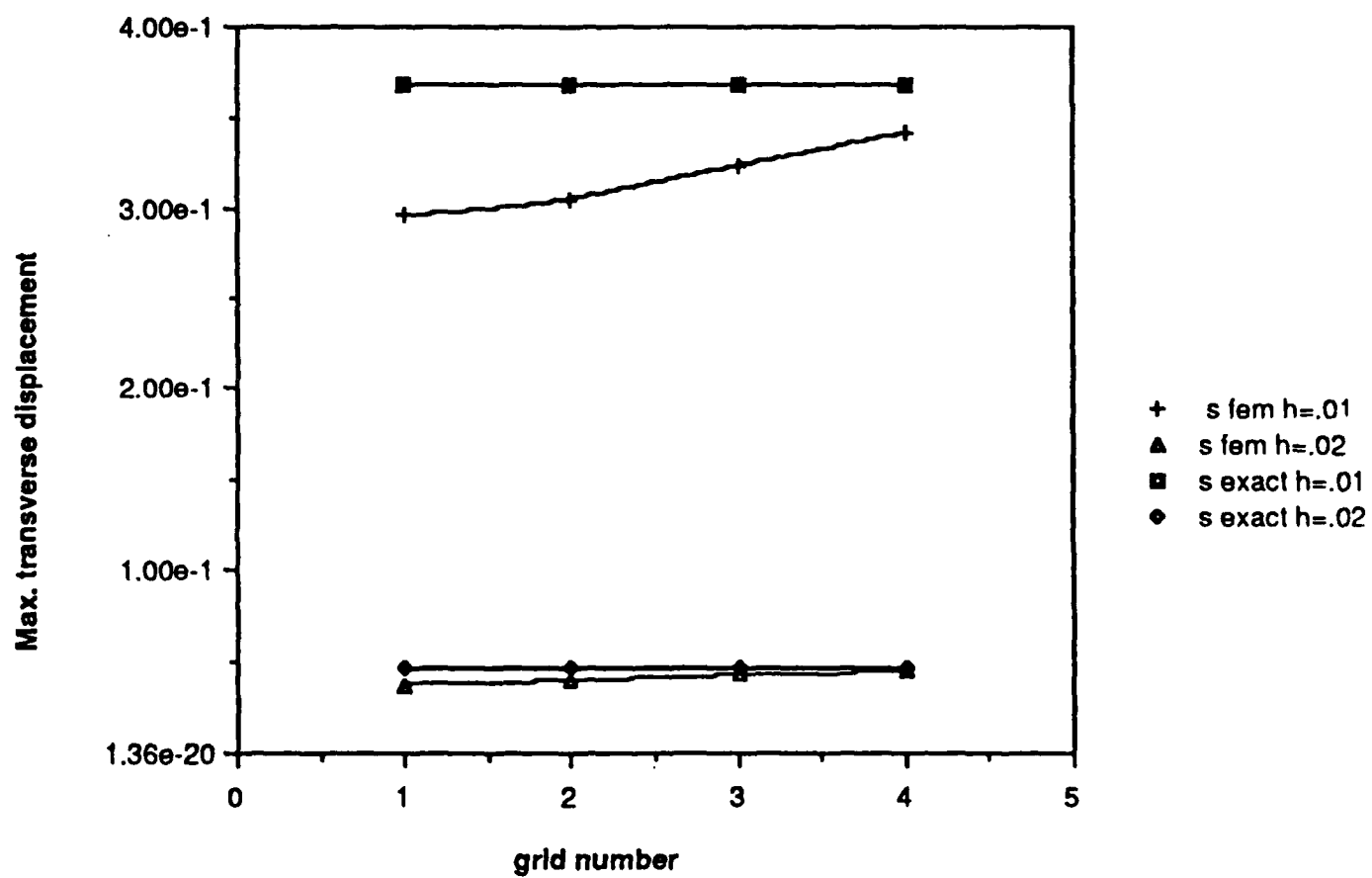


Figure 10. Convergence Study of Transverse Displacement for Square Plate

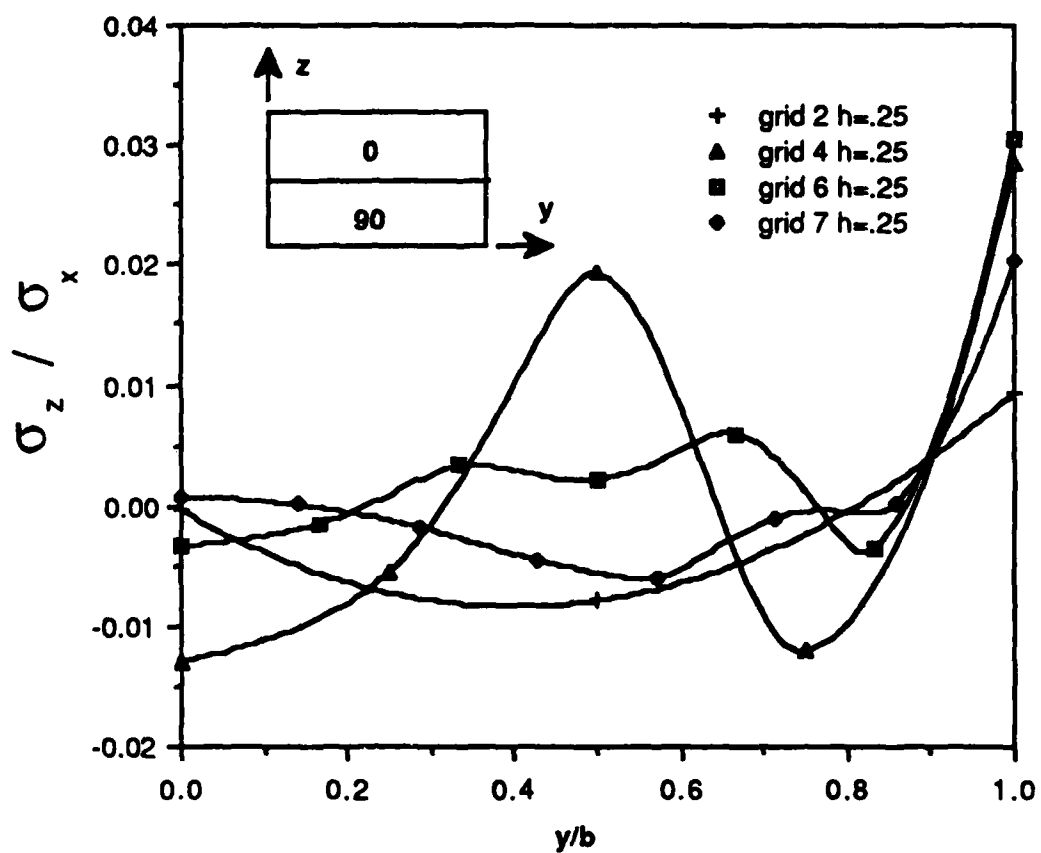


Fig. 6 Convergence study of normal stress at mid-surface for tensile load

Figure 11. Convergence Study of Normal Stress at Mid-surface for Tensile Load

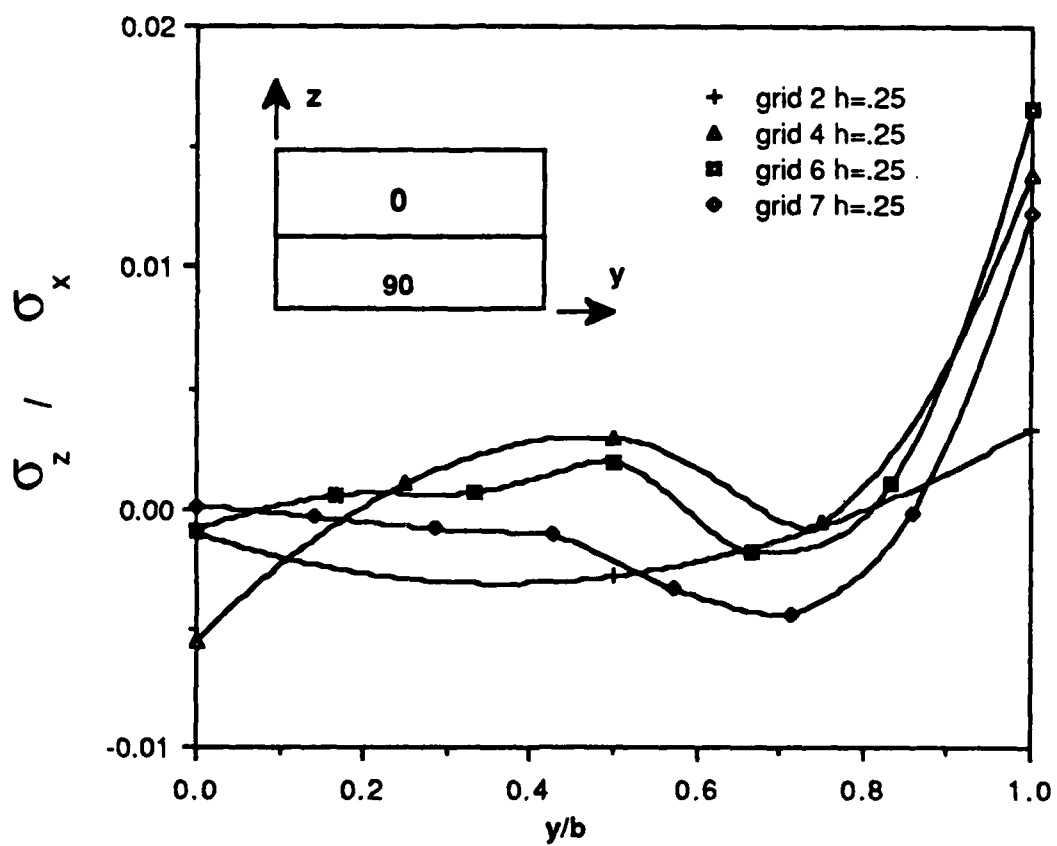


Figure 12. Convergence Study of Normal Stress at 0/90 Interface for Tensile Load

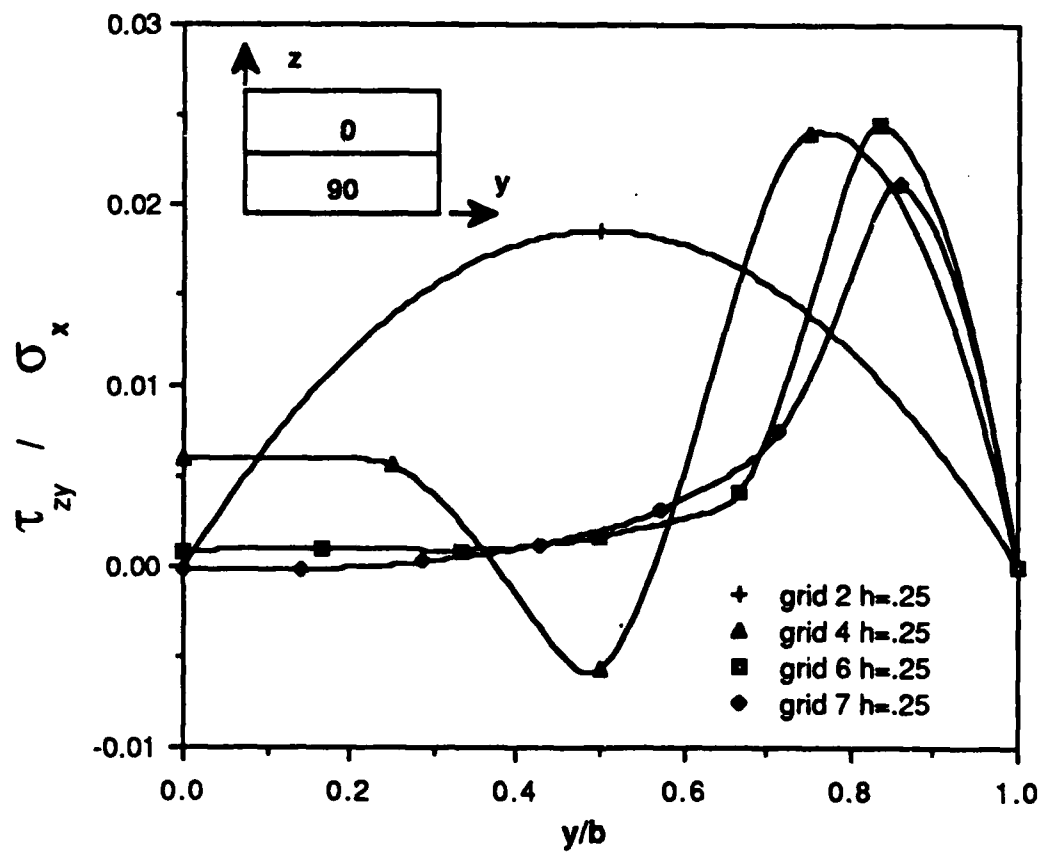


Figure 13. Convergence Study of Shear Stress in z-y Plane at 0/90 Interface for Tensile Load

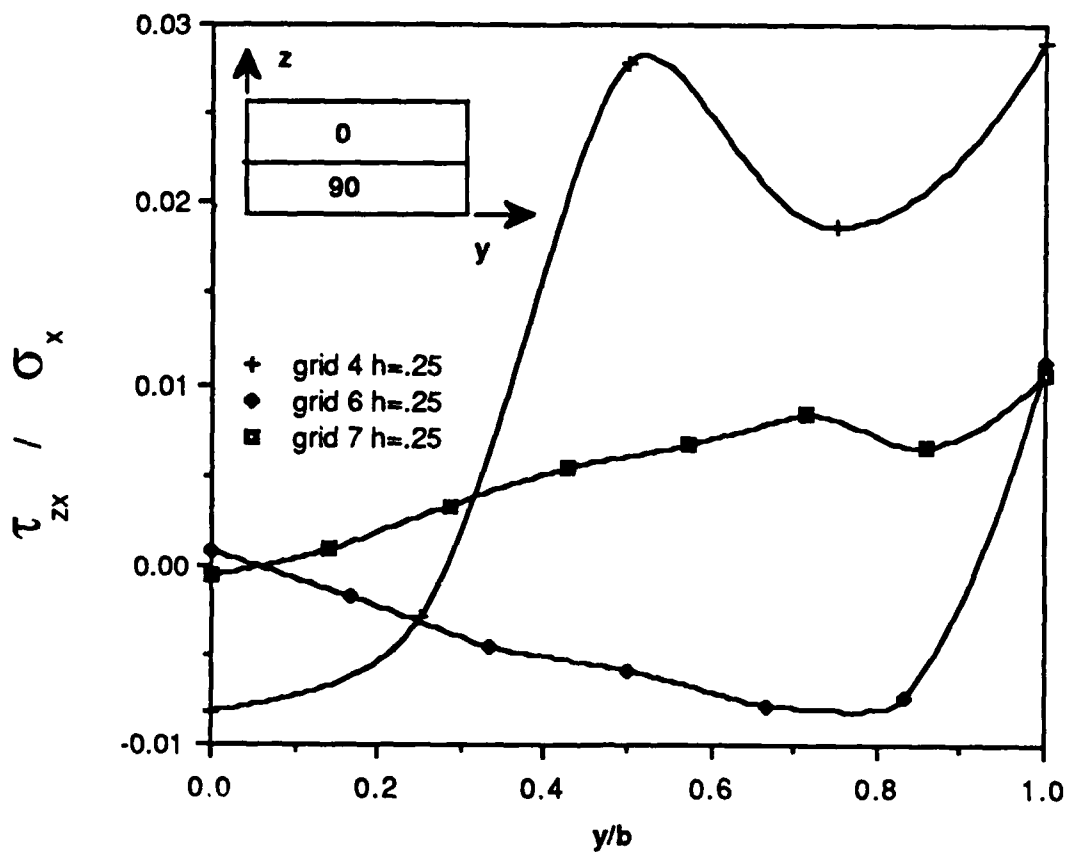


Figure 14. Convergence Study of Shear Stress in z-x Plane at 0/90 Interface for Tensile Load

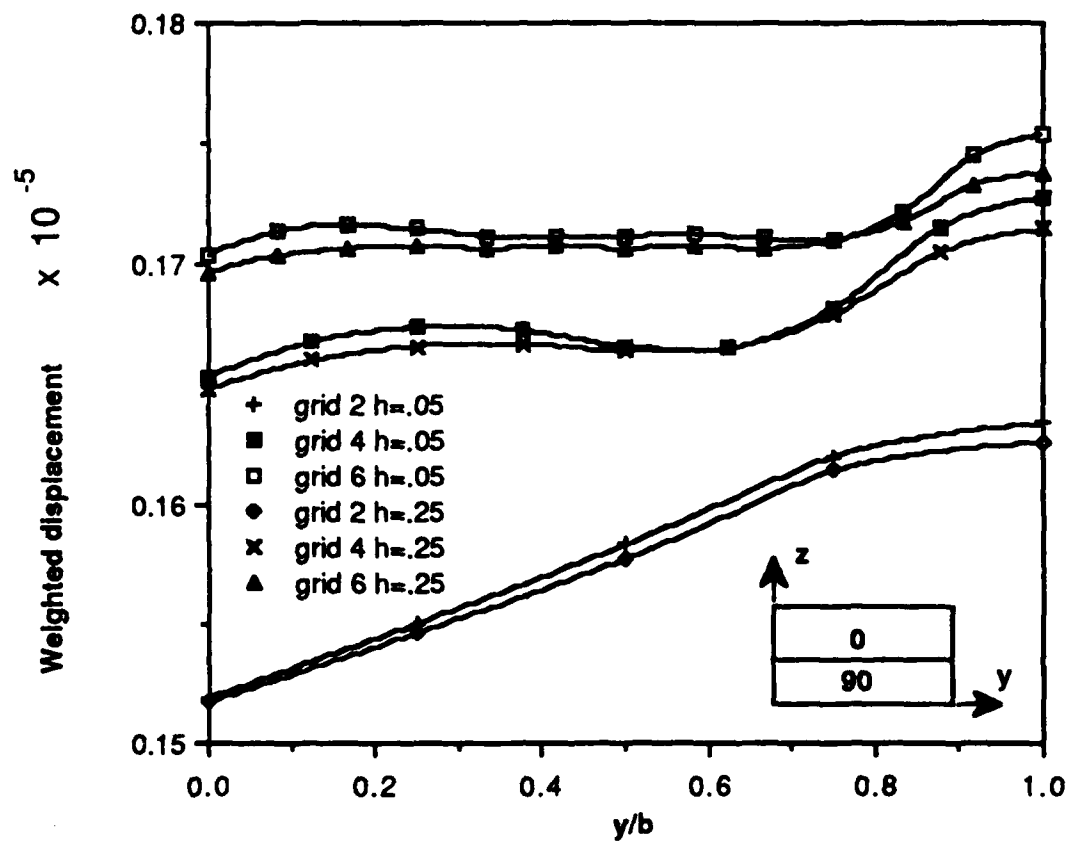


Figure 15. Convergence Study of Weighted Displacement across Top Surface for Tensile Load

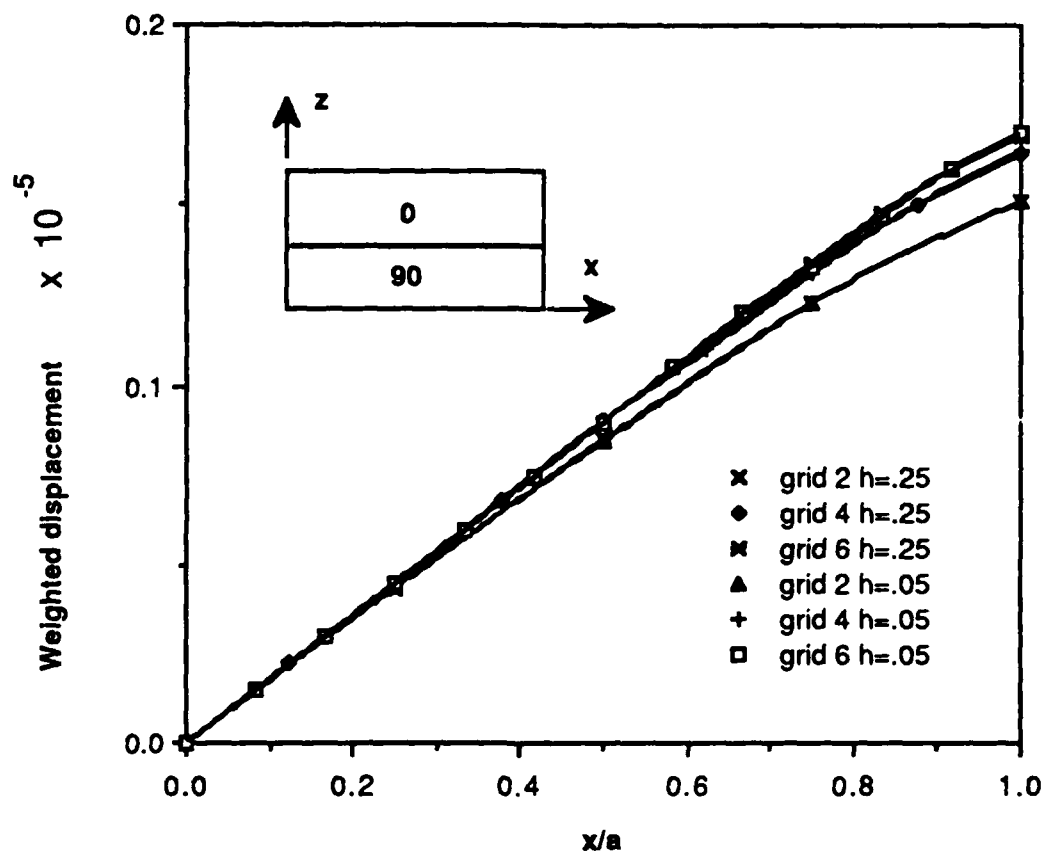


Figure 16. Convergence Study of Weighted Displacement across Top Surface for Tensile Load

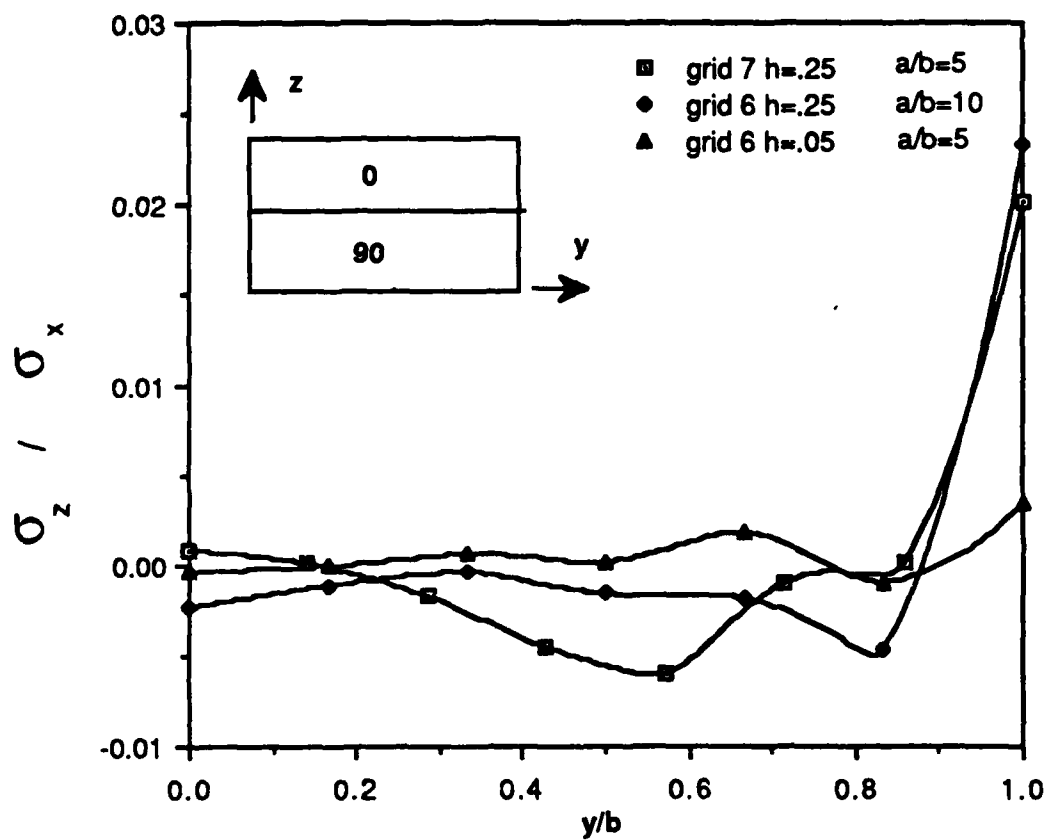


Figure 17. Comparing Normal Stress (Mid-surface) of Different Geometry Parameter for Tensile Load

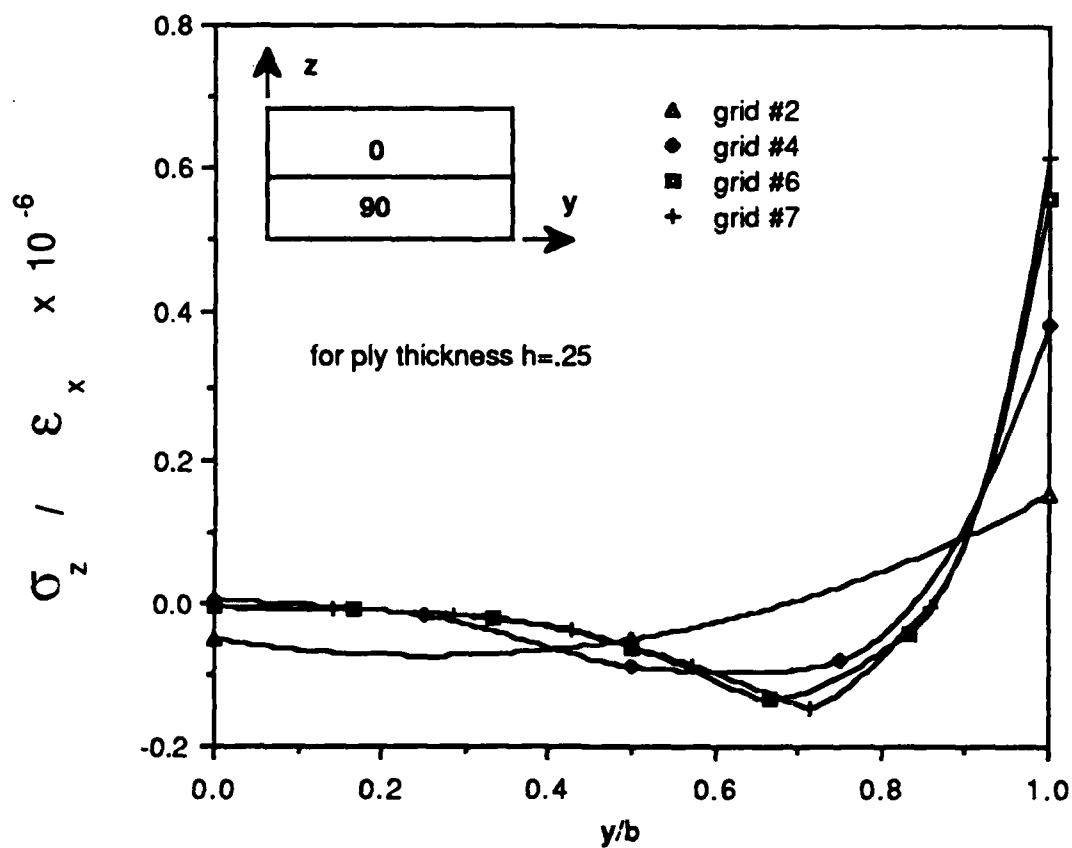


Figure 18. Convergence Study of Normal Stress at Mid-surface
for Stretch Load

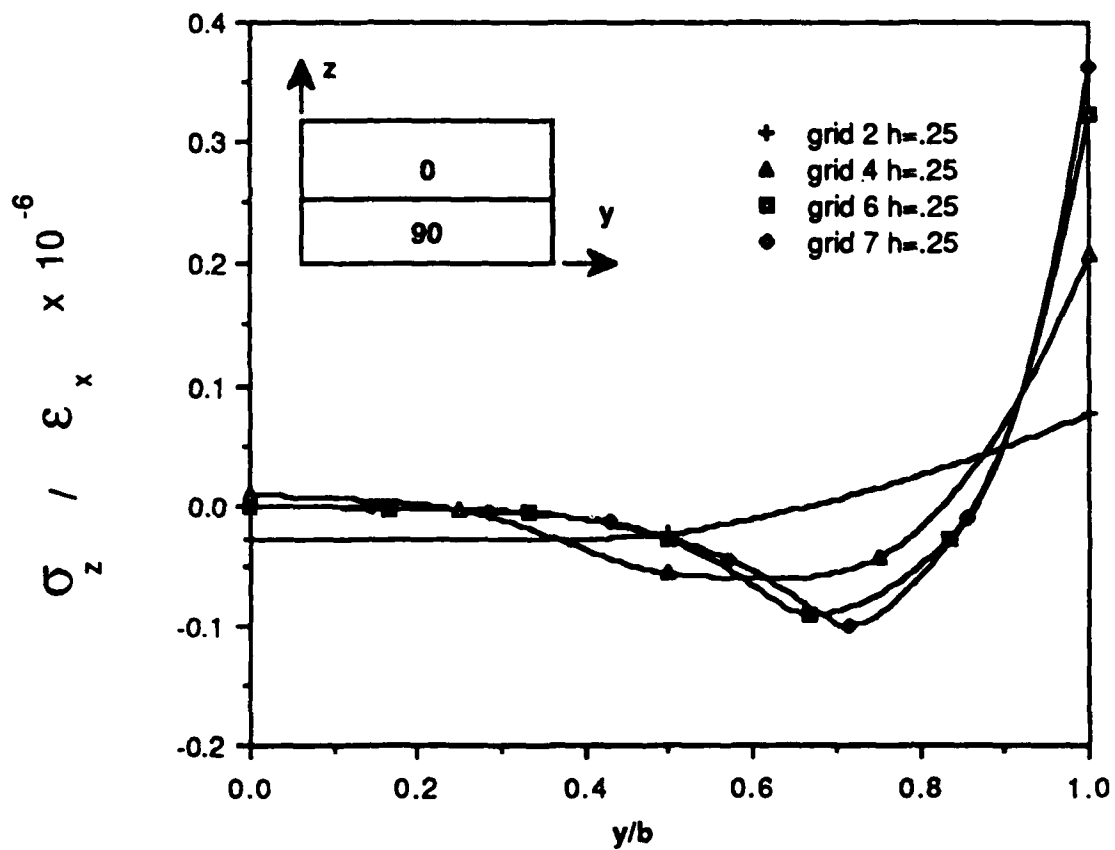


Figure 19. Convergence Study of Normal Stress at 0/90 Interface for Stretch Load

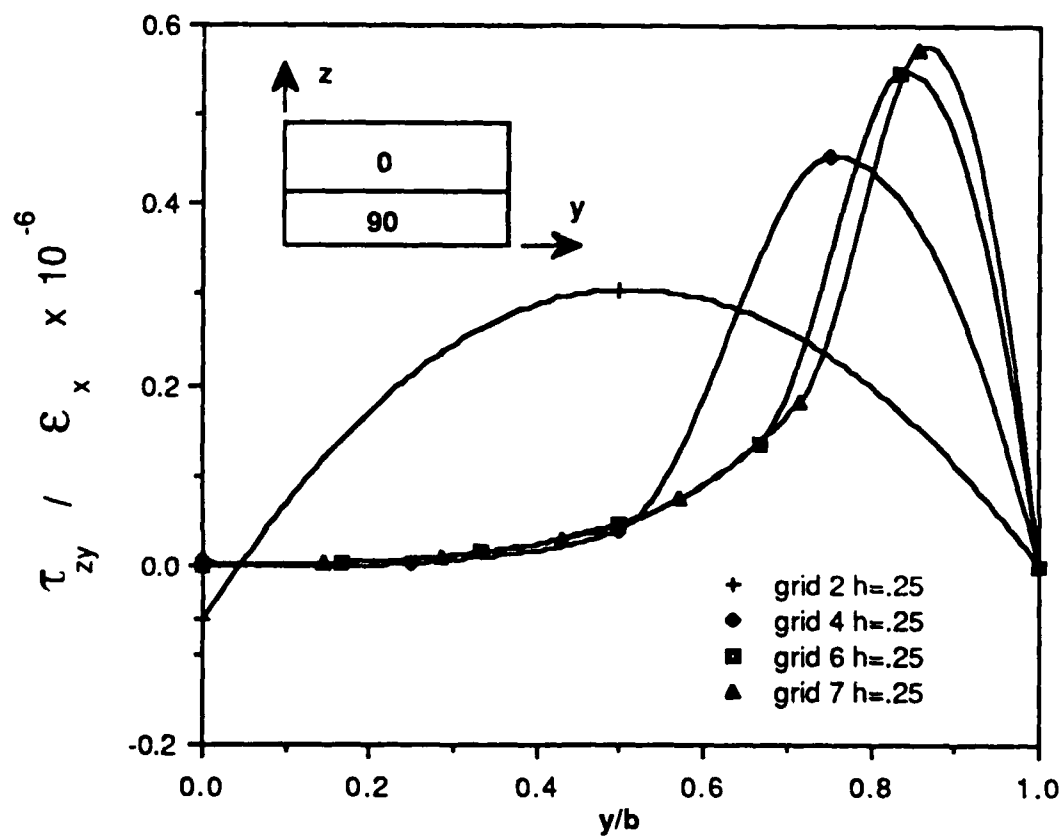


Figure 20. Convergence Study of Shear Stress in z-y Plane at 0/90 Interface for Stretch Load

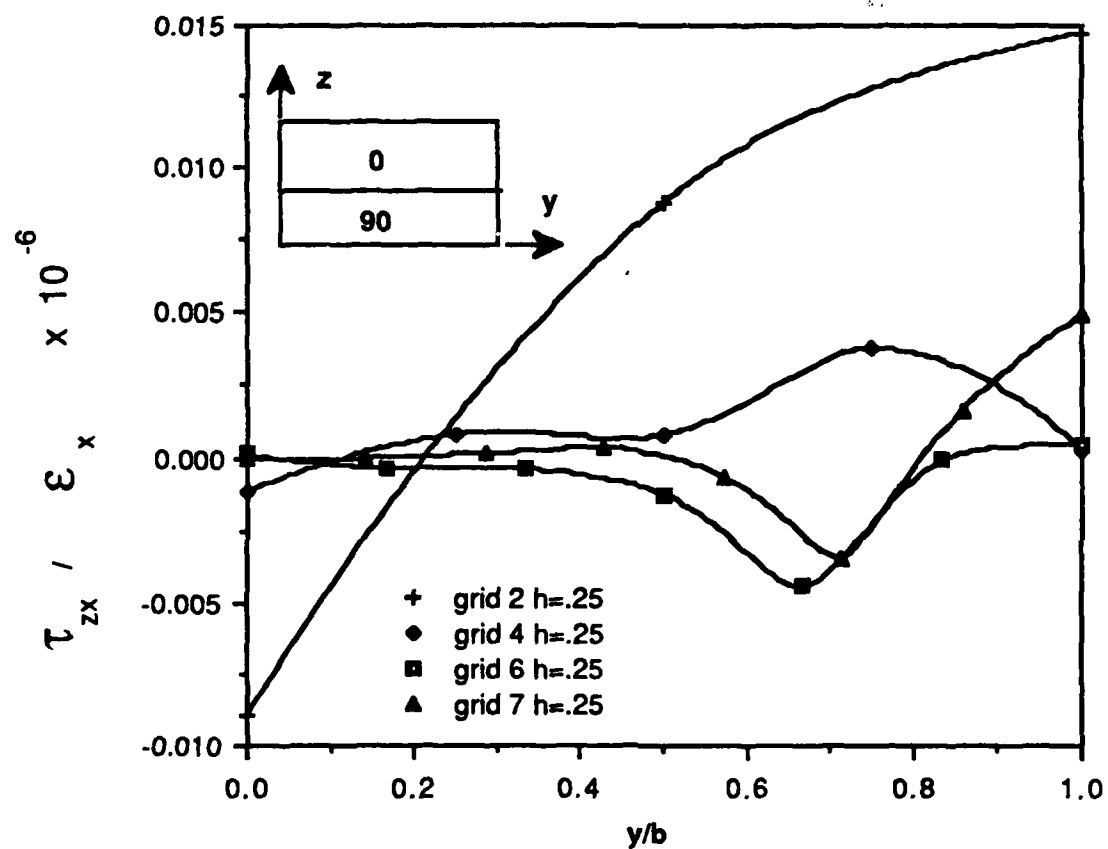


Figure 21. Convergence Study of Shear Stress in z-x Plane at 0/90 Interface for Stretch Load

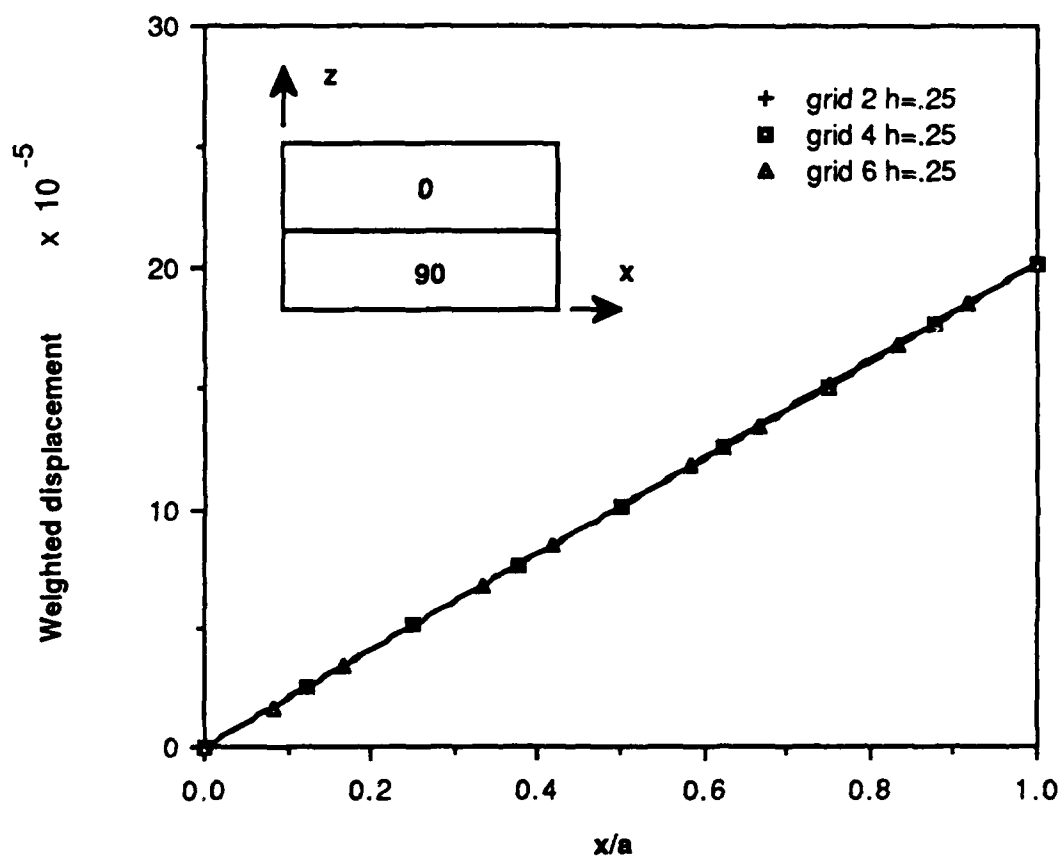


Figure 22. Convergence Study of Weighted Displacement across Top Surface for Stretch Load

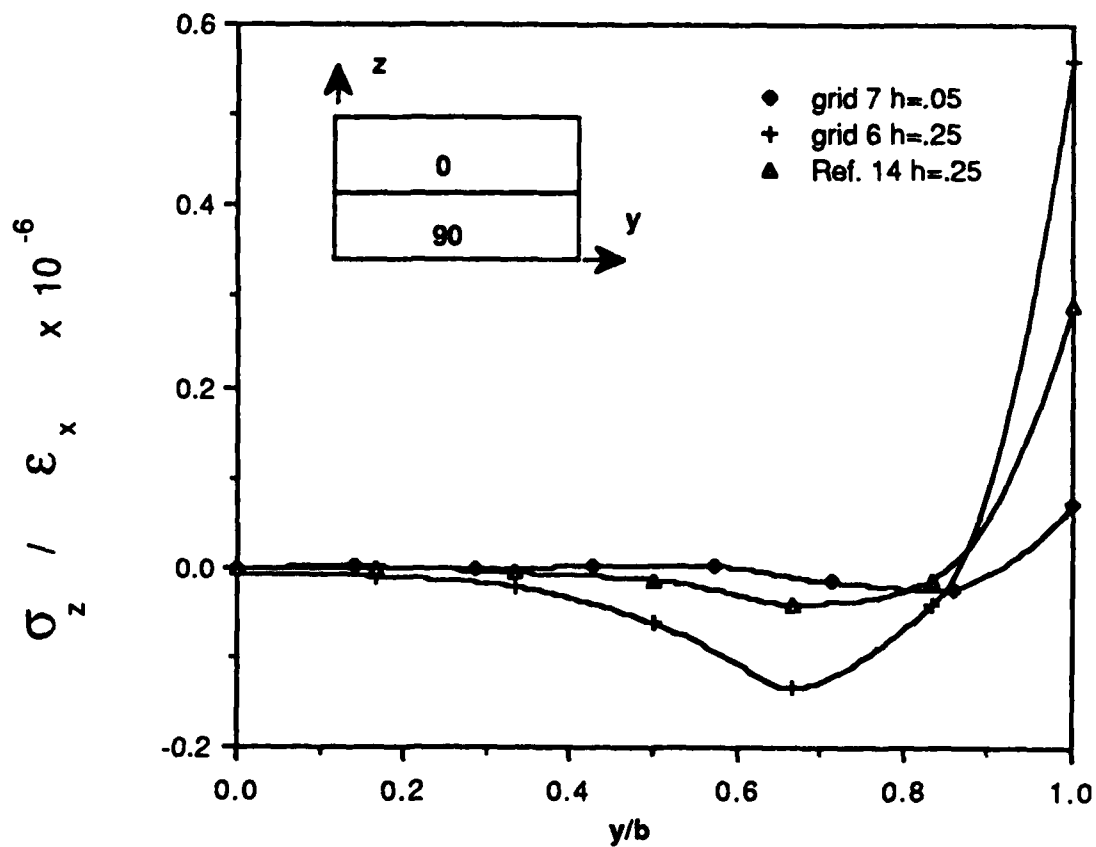


Figure 23. Comparing Normal Stress (at Mid-surface) of Different Geometry Parameter for Stretch Load

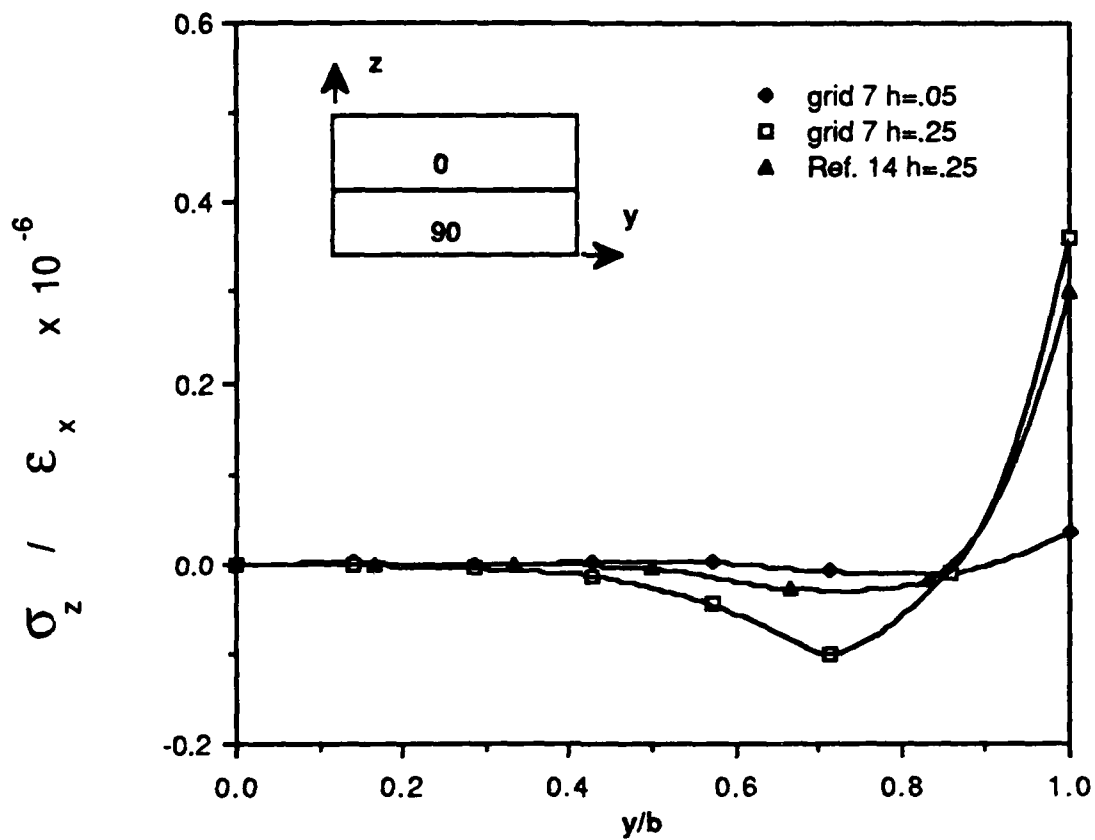


Figure 24. Comparing Normal Stress (at 0/90 Interface) of Different Geometry Parameter for Stretch Load

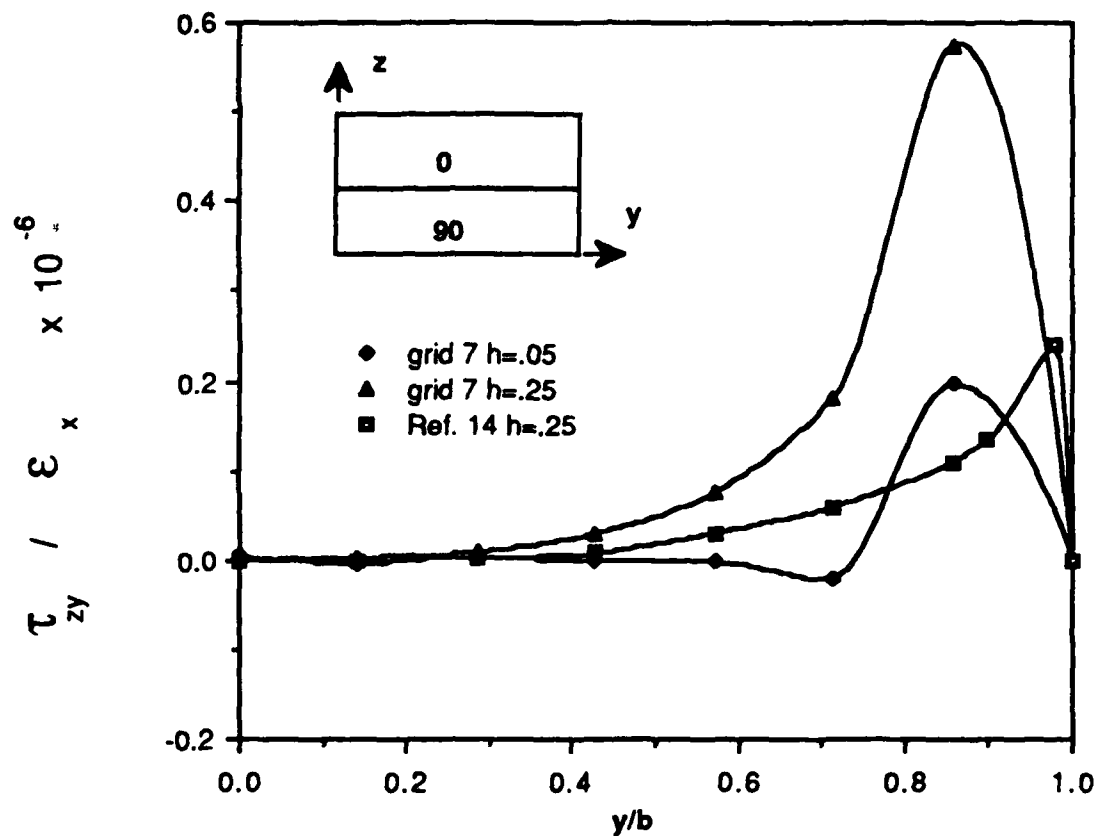


Figure 25. Comparing Shear Stress (at 0/90 Interface) of Different Geometry Parameter for Stretch Load

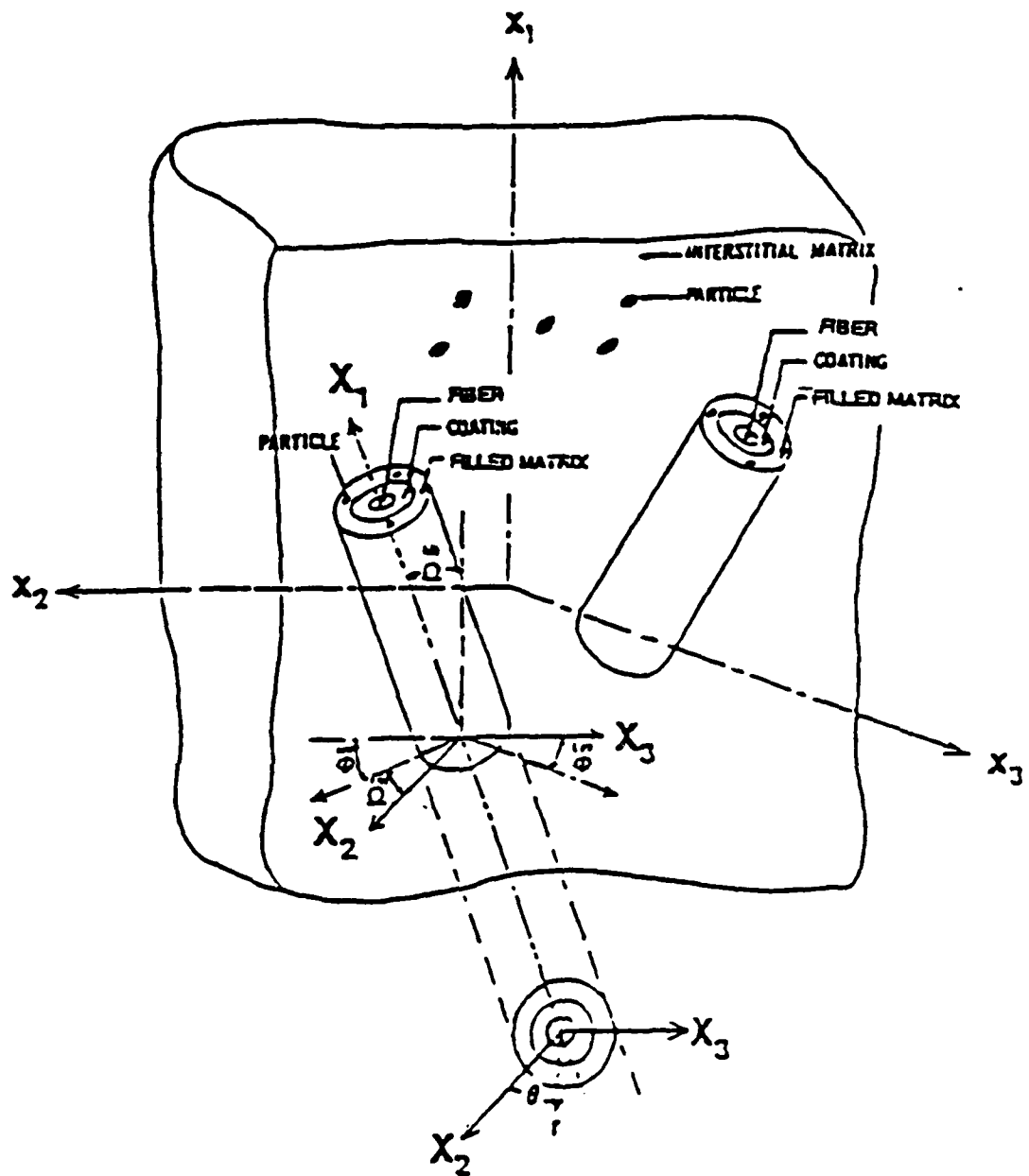
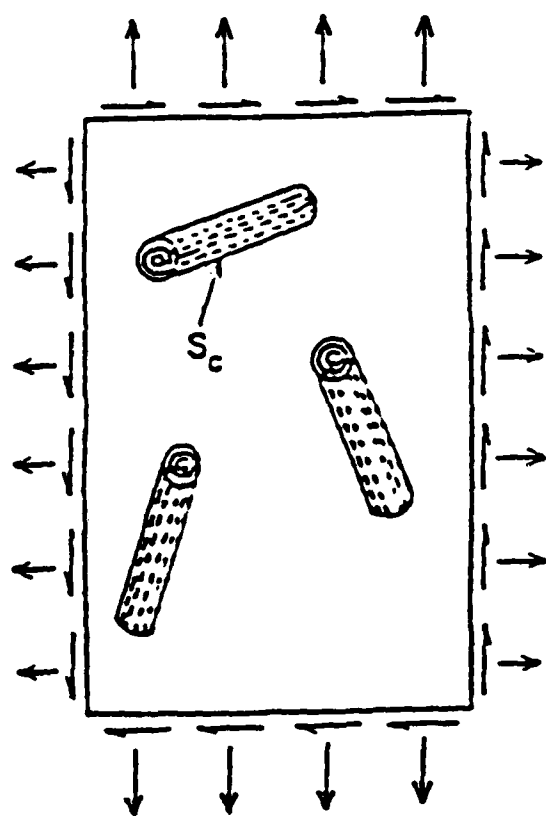
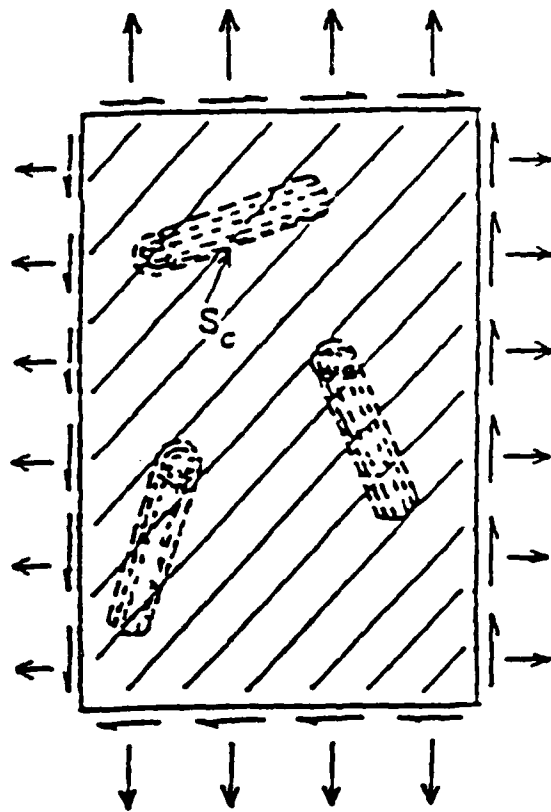


Figure 26. Theoretical Micro-mechanics Model



COMPOSITE



"EQUIVALENT HOMOGENEOUS BODY"

Figure 27. Composite and Equivalent Body Characterization

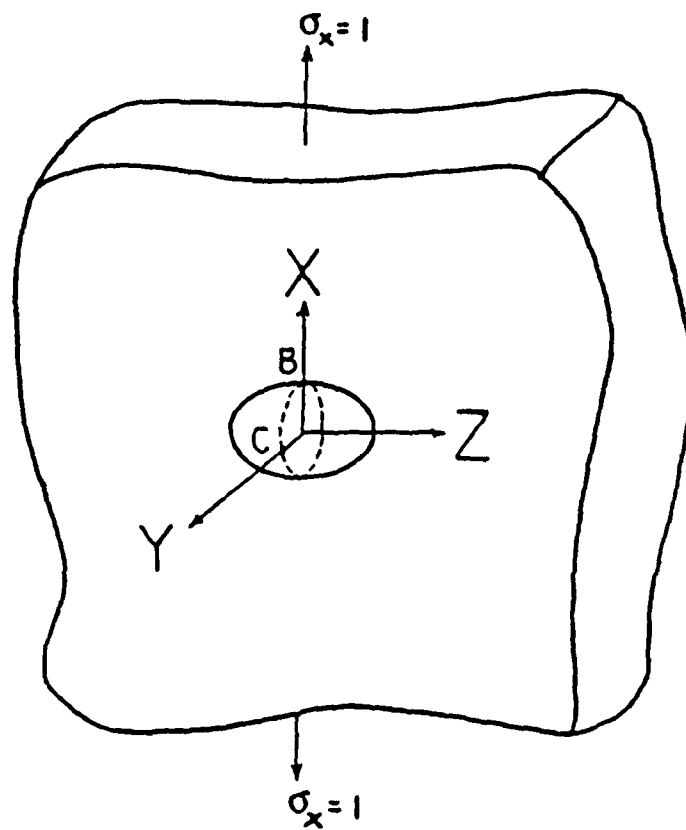


Figure 28. Case of Uniaxial Tension

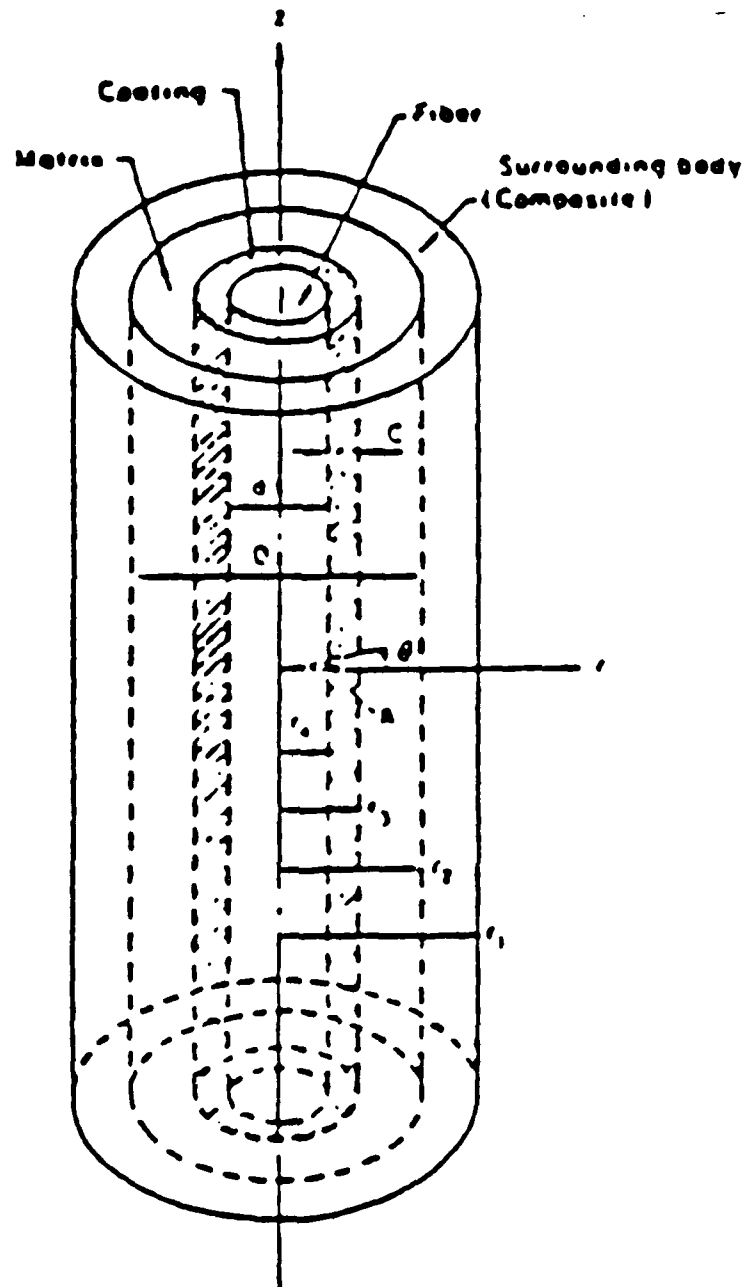


Figure 29. Four Phase Model

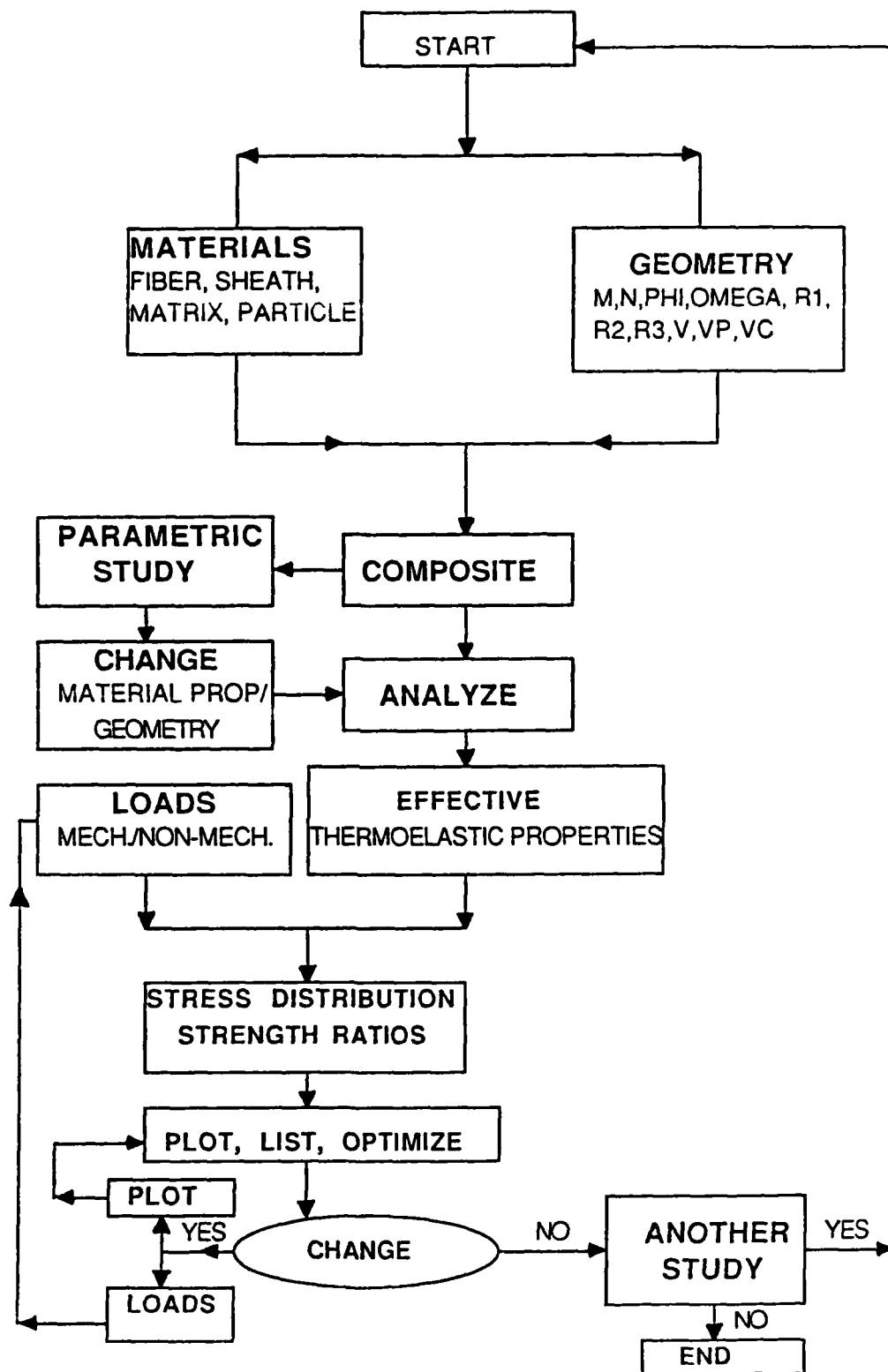


Figure 30. Flow Chart for Micro-mechanics Calculations